NASA CR-54148
TRW ER-6291

INVESTIGATION, TESTING, AND DEVELOPMENT OF THE ION ENGINE SYSTEM

By
A. C. ECKERT
R. J. COERDT
M. B. MOFFETT
M. W. MUELLER

Prepared for
NATIONAL AERONAUTICS AND SPACE ADMINISTRATION
CONTRACT NAS3-5745

NEW PRODUCT RESEARCH DEPARTMENT
THOMPSON RAMO WOOLDRIDGE INC.
23555 EUCLID AVENUE
CLEVELAND, OHIO

NOTICE

This report was prepared as an account of Government sponsored work. Neither the United States, nor the National Aeronautics and Space Administration (NASA), nor any person acting on behalf of NASA:

A.) Makes any warranty or representation, expressed or implied, with respect to the accuracy, completeness, or usefulness of the information contained in this report, or that the use of any information, apparatus, method, or process disclosed in this report may not infringe privately owned rights; or

B.) Assumes any liabilities with respect to the use of, or for damages resulting from the use of any information, apparatus, method or process disclosed in this report.

As used above, "person acting on behalf of NASA" includes any employee or contractor of NASA, or employee of such contractor, to the extent that such employee or contractor of NASA, or employee or such contractor prepares, disseminates, or provides access to, any information pursuant to his employment or contract with NASA, or his employment with such contractor.

Request for copies of this report should be referred to

National Aeronautics and Space Administration
Office of Scientific and Technical Information
Attention: AFSS-A
Washington, D. C. 20546

NASA CR-54148
TRW ER-6291

FINAL REPORT

INVESTIGATION, TESTING, AND DEVELOPMENT OF AN ELECTRON-BOMBARDMENT ION ENGINE SYSTEM

By

A. C. ECKERT
R. J. COERDT
M. B. MOFFETT
M. W. MUELLER

Prepared for
NATIONAL AERONAUTICS AND SPACE ADMINISTRATION
DECEMBER 15, 1964

CONTRACT NAS3-5745

Technical Management
NASA Lewis Research Center
Cleveland, Ohio
Spacecraft Technology Division
Sanford G. Jones

NEW PRODUCT RESEARCH DEPARTMENT
THOMPSON RAMO WOOLDRIDGE INC.
23555 EUCLID AVENUE
CLEVELAND, OHIO

ABSTRACT

22975

An applied research program of investigation, testing and development of an electron-bombardment, mercury-fueled ion engine system is reported. Ion source performance data are presented for a wide range of conditions of operation, employing electromagnets and a laboratory feed system. Supplementary efforts to develop long-life, efficient, porous-nickel-matrix cathodes are described. Extended tests of over 500 hours on ion engine systems utilizing permanent magnets are reported and system lifetime estimates based thereon are presented. The associated facility for automatic engine testing is described in detail.

Author

TABLE OF CONTENTS

LIST OF SYMBOLS

CS	Width of Cathode slit, mm
I_A	Arc current, amperes
I_{Acc}	Accel electrode drain current, ma
I_B	Beam current, ma $\left[I_B = I_S - (I_{Acc} + I_{Dec})\right]$
I_C	Cathode heater current, amperes
I_{Dec}	Decel electrode drain current, ma
I_F	Feed rate, ma; the equivalent Hg^+ current for $\eta_M = 100\%$
I_M	Magnet current, amperes
I_S	Source current, ma
I_{SP}	Specific impulse, seconds
I_T	Target current, ma
J	Approximate cathode current density, amperes/cm^2
"n" x "m" anode	Anode dimensions, when "n" is the anode width (mm) at the exit aperture, "m" is the anode length (mm)
p	Testing tank pressure with engine running, torr
P_A	Arc power, watts
P_{Acc}	Accel electrode power drain, watts ($P_{Acc} = V_{Acc}\ I_{Acc}$)
P_B	Beam power, watts ($P_B = V_{Dec}\ I_B$)
P_C	Cathode heater power, watts ($P_C = I_C V_C$)
P_{Dec}	Decel electrode power drain, watts ($P_{Dec} = V_{Dec}\ I_{Dec}$)
P_M	Magnet power, watts
T	Lifetime, hours
T_C	Cathode temperature, °C
V_A	Arc voltage, volts
V_{Acc}	Potential of accel electrode relative to engine frame, kv

List of Symbols (cont.)

V_C	Cathode heater voltage, volts
V_{Dec}	Potential of decel electrode relative to engine frame, kv
η_A	Arc power inefficiency, ev/ion ($\eta_A = I_A V_A / I_S$)
η_C	Cathode power inefficiency, ev/ion ($\eta_C = I_C V_C / I_S$)
η_M	Mass utilization, per cent ($\eta_M \equiv I_S / I_F$)
η_P	Engine power efficiency, per cent $\left[\eta_P = P_B/(P_B + P_A + P_C + P_{Acc} + P_{Dec})\right]$
η_R	Rocket (thrustor) efficiency, per cent ($\eta_R = \eta_P \eta_M$)

LIST OF FIGURES

List of Figures (cont.)

LIST OF TABLES

SUMMARY

The applied research and development efforts described herein constitute the summary report for the period March 3, 1964 through December 14, 1964 of the work performed under Contract NAS3-5745, "Investigation, Testing, and Development of an Electron-Bombardment Ion Engine System". The scope of this program included the investigation, extended testing, and developmental modification and analysis of electron bombardment ion engines having accel-decel extraction systems, permanent magnets, nickel matrix cathodes, and employing mercury as the propellant. The goals of the program were to develop an ion engine system, utilizing a laboratory feed system, with an engine power efficiency exceeding 85 per cent at a specific impulse of 7500 seconds, a propellant utilization efficiency exceeding 95 per cent, a beam current exceeding 60 milliamperes, a specific impulse range from 4500 to 7500 seconds, and a demonstrated lifetime exceeding 500 hours. To help attain these goals, work was prescribed in several general areas, including source optimization, cathode studies, extraction and neutralization efforts, system tests, and reliability activities.

The source optimization studies were conducted making use of a variable geometry source. Use of this source enabled geometric variations during source operation. Using this variability the geometry which yielded high performance was readily determined. The conditions for high performance included, however, the requirement of arc voltage exceeding the cathode sputtering threshold. Because of the necessary high arc voltage several cathode geometries including the cavity cathode were investigated. The results of the cavity cathode investigation, however, were inconclusive. A permanent magnet engine, based on the geometry established with the variable geometry source and suitable for extended testing, was fabricated. Two extended tests were performed, one of erosion rates were used to predict the extraction system lifetime. No prediction of the cathode lifetime could be made.

1.0 INTRODUCTION

The work reported herein was performed under Contract NAS3-5745, administered by the National Aeronautics and Space Administration, Lewis Research Center. The program consisted initially of ion source and cathode investigations, supplemented with ion extraction and neutralization efforts; subsequent portions of the program included a series of extended tests. Before describing in detail the activities and results of this program, it is appropriate to give some background of prior work by TRW Inc. in this area, so that the work to be reported may be put into proper perspective. This section, therefore, will include a brief review of previous work, will describe the goals of the program to be reported, and will outline the organization of the report.

1.1 Previous Work

Experience at TRW in the area of electron bombardment ion engines dates back some five years, to the time when the limitations on power efficiency of cesium-fueled contact ion engines had become apparent. At that time it was postulated that gas discharge (bombardment) ion sources could be operated at substantially improved power efficiencies while maintaining good propellant utilizations and without sacrificing engine lifetime because of sputtering damage to acceleration electrodes. The concept proposed by TRW consisted of a bombardment engine based on a slit aperture geometry. This approach was shown to favor a single aperture per ionization chamber, yielding considerable design latitude (particularly in acceleration electrode shaping); the result was an ion source of relatively high ion current density per unit of total area subtended by the engine.

The basic ion source utilizes an axial field electron trap in which electrons are confined axially by electrostatic forces and laterally by magnetic forces. (Reference 1) Electrons from a cathode are injected into the trap and accelerated axially toward the anode region. Being constrained from direct travel toward the anode by a magnetic field, these electrons pass through the (hollow) anode region and reflect from the meniscus between the plasma and the ion beam. After reflection, the electrons return through the anode channel, and must return again after reflecting from sheaths in the vicinity of the cathode. A

multiple reflection and anode traversal situation is generated extending the electron path length such that a high probability for an ionizing collision with a gas (propellant) atom results. Preliminary experimental work, performed under company sponsorship, established the feasibility of the source design, showed that a cathode could be made to operate under the conditions required by the source, and upheld the promise for the attainment of high power efficiencies. On the strength of this work, NASA provided support for continued development of the concept under Contract NAS8-42.

Under the above contract, various electron trapping techniques were investigated so that an efficient ionization chamber could be designed. A number of ion sources were constructed, employing both electromagnets and permanent magnets to supply the necessary magnetic trapping fields. The former were considerably more flexible experimentally, particularly in the early stages of source testing. Again, for expediency, much of the initial work was done using argon for the propellant, and tungsten-filament cathodes. A variety of internal source geometries were studied; variables included magnetic field strength and shape, anode width and length, cathode slit length and width, source aperture width, etc. The details of this optimization constituted a significant fraction of the total effort under NAS8-42. The result was 84 per cent (argon) propellant utilization at an arc input of about 450 electron volts (ev) per ion. (Reference 1).

Source operation with mercury propellant was the next effort in the program. Mercury was ultimately selected as the most logical propellant for use with the source for a variety of reasons including its ease of handling, storage, metering, and vaporizing, its high mass per particle, and its apparent ability to provide ionizing discharges of high efficiency at arc voltages compatible with sufficient cathode lifetimes. A mercury feed system and porous-plug vaporizer were used in conjunction with tungsten-filament cathodes. Satisfactory source performance required that some changes be made in the mode of propellant feed to the ionization chamber.

A portion of the program was devoted to finding suitable cathodes for use in the source. The tungsten-filament cathodes were adequate for experimental work, but were unacceptable for space applications because of their short life and high power demands. The cathode effort centered about the development of a sintered

nickel-matrix cathode containing commercial barium-strontium oxide emitting compounds. Suitable dispenser cathodes were made. Subsequent testing of these cathodes in the ion source and measurements of the energy distribution of the electrons emitted necessitated some further slight changes in geometry; the ultimate result was an indicated arc power efficiency of about 450 ev/ion at or near ninety per cent propellant utilization. Near the end of work under Contract NAS8-42, a permanent magnet source was built and preliminary data was obtained which upheld the original promises of both good propellant utilization and arc power efficiency.

It was subsequently decided that further efforts were desirable and support for such work was afforded under Contract NAS3-2522. The goals of this program include (1) further testing of the permanent magnet source, (2) extraction system studies, both experimental and theoretical, (3) optimization of the source under extraction conditions, (4) extended tests of the extraction system, and (5) additional cathode development. The accomplishments in each of these areas have been reported in detail (Reference 2); a brief summary follows.

Ion source studies were conducted concurrently with two engines, differing somewhat in their internal magnetic field geometries. A variety of source configurations were investigated, including internal geometries and spacings, and magnetic field variations (both strength and shaping). The replacement of the porous-plug vaporizer with a capillary-tube unit aided considerably in assuring that reliable and reproducible data was obtained; the new design substantially reduced the waiting time for the vaporizer to reach equilibrium for a fixed propellant feed rate. Subsequent source experimentation with this redesigned vaporizer, however, indicated somewhat higher arc losses than had been measured previously.

Extraction studies were carried out with a variety of accel-decel geometries. Initially these geometries were fitted to sources whose magnetic fields were provided by electromagnets, thus affording experimental latitude in that the magnetic field strength could be varied and the field distribution could be symmetrized.

The mutual interactions between ion source and extraction system were studied and the effects of various accel-decel geometries and voltages, cathode location,

etc. were established. Later extraction studies with a permanent magnet ion source yielded substantially the same low electrode current drains and good beam focusing without a sacrifice in source power or propellant efficiency.

The experimental extraction efforts were supplemented by an analytical (digital computer) effort. The result of this work was the prediction of charge-exchange rates, resulting electrode impingement areas, and a predicted erosion pattern for an extraction geometry similar to that which evolved as a result of the experimentation.

Neutralization efforts succeeded in producing current neutralization, although neutralizer currents typically exceeded the total beam current. Efforts to improve the neutralizer-to-beam coupling were deliberately limited in favor of additional effort in other areas of the program.

The low electrode interceptions obtained as a result of the extraction system studies led to the initiation of extended testing of the permanent magnet engine system utilizing a laboratory propellant feed system. Near the end of the program, two such extended tests were performed. The first, of seventy hours duration, was deliberately terminated when the engine performance had become influenced by aluminum sputtered back from the beam target. The second test proceeded to completion and was terminated after about 104 hours of operation. These extended tests showed very little evidence of wear in the critical (focusing) regions of the extraction system and provided experimental evidence in support of the theoretical prediction of long system lifetimes. The principal result of contract NAS3-2522 was the experimental demonstration that long extraction electrode lifetimes could be obtained in high-current-density electron bombardment engines.

This brief survey of prior contractual efforts is intended to serve as a background for the work to be reported in the following pages. Contract NAS3-5745 constitutes a logical extension to this previous work as will be seen below.

1.2 Program Goals

The apparent solution to the extraction system lifetime question permitted attention one more to be directed to the demonstration of high overall engine propulsive efficiency. The attainment of such high efficiencies while

maintaining good lifetime on all components of the ion source and extraction systems was the primary objective of the Contract NAS3-5745 which is reported herein. This program consisted initially of source and cathode investigations which subsequently were supplemented with ion extraction and beam neutralization efforts. The final portion of the program was a series of lifetime tests to validate the performance levels obtained.

The specific goals of the program were to develop an ion engine system, utilizing a laboratory feed system, with an engine power efficiency exceeding 85 per cent at a specific impulse of 7500 seconds, a propellant utilization efficiency exceeding 95 per cent, a beam current exceeding 60 milliamperes, a specific impulse range from 4500 to 7500 seconds, and a demonstrated lifetime exceeding 500 hours. Mercury propellant, nickel-matrix cathodes, permanent magnets, and accel-decel extraction systems were to be employed.

Progress toward these goals was to proceed through concentrated effort in each of several specific areas, including source (and cathode) studies, extraction system and neutralizer studies, and system tests. In each of these areas specific tasks were defined. For example, efforts under "source studies" were to include considerations of improved cathode heat shielding and support, reduction of radiated power from the cathode, improved propellant introduction techniques, reduction of wall losses within the source, and additional cathode work. Furthermore, the desired improvements in engine performance were to be verified in several "extended tests" of the entire system; these tests were to be conducted under carefully specified and controlled conditions so as to insure the validity of the results obtained.

1.3 Organization of Report

On the basis of unity and coherence, the efforts of the program naturally divide into three separate categories: engine design optimization, cathode studies, and extended testing. Although work in all three areas was often concurrent, this breakdown also will serve to indicate, to some degree, the chronological development which evolved. Section 2 of this report, therefore, will discuss the optimization of the engine design; this section will include a description of the experimental ion source, its test facility, the resulting data, and the conclusions drawn. Section 3 will describe the cathode studies,

including the testing apparatus, test results, and conclusions. Presented in Section 4 will be the extended testing portion of the program, including details of the test facility (vacuum facility, beam target, feed system, power supplies, and automatic control system), preliminary engine data, extended testing results and the conclusions drawn (including some predictions of system lifetimes). Finally Section 5 of this report will summarize the results of the program.

2.0 ENGINE DESIGN OPTIMIZATION

2.1 Introduction

At the conclusion of work under Contract NAS3-2522, the performance of the permanent magnet source had been reproducibly measured at 600-700 arc ev/ion for ninety per cent propellant utilization. From the point of view of engine power efficiency, these arc losses were somewhat high. The associated arc voltage, furthermore, was higher than desirable from the standpoint of cathode sensitivity to sputtering and the consequent cathode lifetime limitation. As a result, it was decided to examine critically the ionization process in an attempt to improve the ionization efficiency (i.e., decrease the arc ev/ion) without sacrifice of propellant utilization and to accomplish this at a lower arc voltage, if at all possible.

The power efficiency of an ion engine may be written

$$\eta_P = \frac{P_B}{P_B + \left[P_A + P_C + P_{Acc} + P_{Dec}\right]}$$

where the symbols are defined in the List of Symbols. The terms in brackets represent engine inefficiencies or losses which must be minimized to achieve maximum power efficiency. The terms P_{Acc} and P_{Dec} may be regarded as constants of the extraction system, at least for a fixed extraction geometry and beam current, and thus may be interpreted as fixed losses.

The extent of the problem can best be exemplified numerically, using the performance goals of the program. For a mercury engine delivering a 60 ma beam at a specific impulse of 7500 seconds (V_{Dec} = 5.6 kv), the beam power P_B, is 336 watts.

For an engine power efficiency of 85 per cent, the bracketed terms may not exceed 60 watts, or 1000 ev/ion. Assuming, for the moment, that by proper design the extraction system losses can be held to about 6 watts (100 ev/ion), about 54 watts remain to provide power for cathode heating and propellant ionization. An arc power efficiency of 600 ev/ion, however, represents 36 watts, leaving only 26 watts for cathode heating. Prior to work under the present contract, it had been observed that cathode powers typically ran higher, about 40 to 50 watts.

It was obvious that efficiency gains were essential, both in ionization and in cathodes. It was decided initially to attack these two problems separately, recognizing, of course, that ultimately good ionization and cathode performance would have to be achieved simultaneously. The cathode matter, to some extent at least, was not considered to be a problem. It was recognized that the cathode power losses could be substantially reduced by improved radiation shielding techniques and by additional attention to the manner in which the cathodes were supported in the engine. Nonetheless, efforts were initiated to produce cathodes of increased electron emission capability (see Section 3).

A large portion of the work under this program was directed toward the problems of increasing the ionization efficiency. The arc losses of 600-700 ev/ion mentioned above were for mass utilizations of 90 per cent. Utilizations of 95 per cent, one of the program goals, required arc losses of 700-800 ev/ion. It was felt that the best approach to the problem was experimental, to perform a series of tests in which one parameter was varied at a time, and some "optimum" performance converged upon.

To some degree this had been done in previous work. That is, a large number of source tests had already been performed, under various conditions of propellant flow, internal source geometry, magnetic field strength, and so forth. Most of these prior tests, unfortunately, were made with source configurations such that a significant change of an important parameter (e.g., anode length) required cooling the engine, venting the vacuum system, decoupling the feed system, removing the engine, disassembling the engine, making the desired change, rebuilding the engine, etc. The result was simply that one could never be sure that only the desired change was made and that a change in some other factor (either in the engine itself or in the environmental conditions) had not been inadvertently made also. Furthermore, not all of the prior data was self-consistent in terms of testing tank pressure, extraction voltage, propellant feed equilibrium, etc. As a consequence, it became highly desirable to "repeat" some of the earlier work under more rigorously controlled test conditions. It was, therefore, decided to design and fabricate an experimental ion source capable of having its geometry varied during operation.

2.2 The Variable Geometry Ion Source

The basic device employed in the program to achieve an optimum source design was the variable geometry ion source (VGS) shown in cross-section in Figure 2.2-1. The parameters that could be independently varied were:

1. the distance of the cathode behind the cathode slit.
2. the cathode slit width.
3. the anode chamber width.
4. the anode chamber length.
5. the spacial distribution of input mercury vapor to the anode chamber.

It was anticipated that the ability to vary the distance between the cathode and the cathode slit would probably yield no new information since this parameter had been variable during previous experimental testing. The previous results had indicated that the closer the cathode was to the cathode slit, the better the source performance. Since this feature had already been incroporated into the engine design it was felt that it should be retained on the chance that variation of the other source parameters might affect the previously obtained conclusion.

Previous data obtained for several values of slit width had indicated that as the ratio of cathode slit width to anode chamber width was reduced the arc performance improved. The arc improvement was obtained, however, at the expense of cathode power; as the cathode slit width was reduced, the effective cathode emission area was reduced. Hence to maintain a constant value of emission current, the emission current density had to increase requiring an increase in cathode temperature. This was equivalent to requiring an increased cathode power input. In order to maintain a small value of cathode slit width relative to the anode chamber width for good arc performance and simultaneously obtain acceptable cathode power requirements, it was, therefore, necessary to expand the width of both the anode chamber and the cathode slit maintaining the minimum possible ratio of the two widths. This had been done previously with encouraging results. It was expected that the cathode slit and anode chamber width variations incorporated into the variable geometry source would be suitable to explore a significantly larger range of configurations.

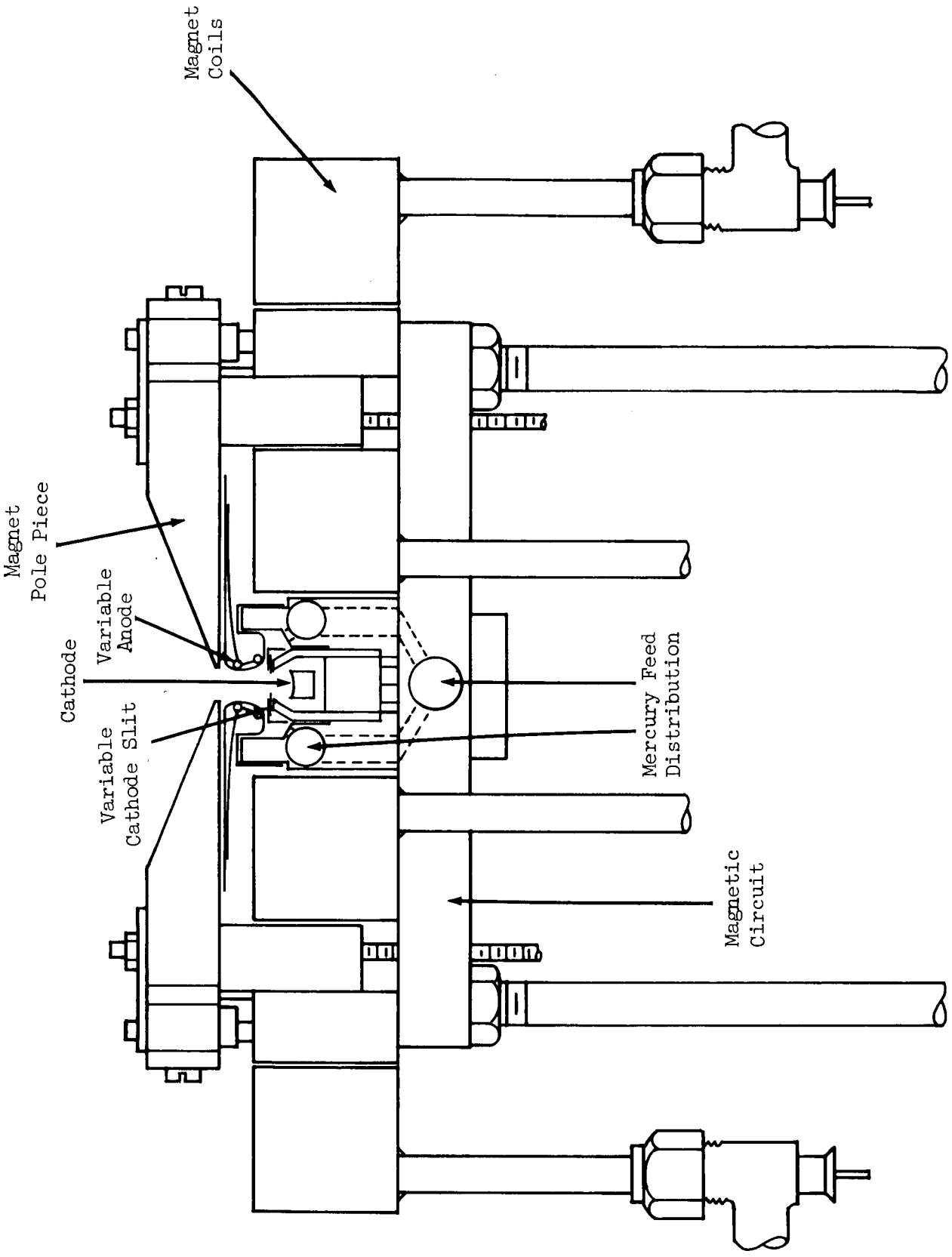

Figure 2.2-1

Cross Section of the Variable Geometry Ion Source

As the anode chamber width is increased, maintaining a constant mercury feed rate, the atom number density in the anode chamber decreases reducing the probability of the atom being ionized before escaping from the anode region. The ionization probability can be increased, however, by lengthening the anode chamber region maintaining constant magnetic field strength. Thus, as the anode chamber is widened, it should be lengthened to maintain a high ionization probability. The ability to vary the anode region length was, therefore, included in the source design.

The source design employed electromagnets to provide the necessary trapping field. The ability to provide more or less magnet coil current was highly desirable in the search for optimum source performance. Furthermore, the ability to vary the anode length (essentially the magnet gap) virtually demanded that electromagnets be used to insure completeness of data. The electromagnets were arranged so that either could be controlled independently for field strength and balance.

The final variable parameter was the input vapor distribution. Previous results had indicated a possible beam nonuniformity with maximum current density occurring at the center and falling off towards either end of the slit. The possibility of producing a more uniform beam density by inserting relatively more vapor near the ends than at the center could be explored. The input distribution could vary from all entering at the ends, to a uniform distribution, to all entering at the center. Thus, the effect of input distribution for a wide range of conditions could be studied.

Testing of the variable geometry source was to be performed using a positive-displacement driven capillary vaporizer (Reference 2). To provide good visibility to all parts of the engine, operation was to be in a glass vacuum system. (The test facility will be described in greater detail in Section 2.3). All operation was to be under high voltage extraction conditions.

The completed source, including its extraction system, vaporizer, and base plate is shown in Figures 2.2-2 and 2.2-3. The graduated scales evident in these pictures are position indicators for the various variable geometric parameters. The calibration accuracy of these indicators was within 0.2 mm. All variations were made externally, through rotating mechanical seals in the engine

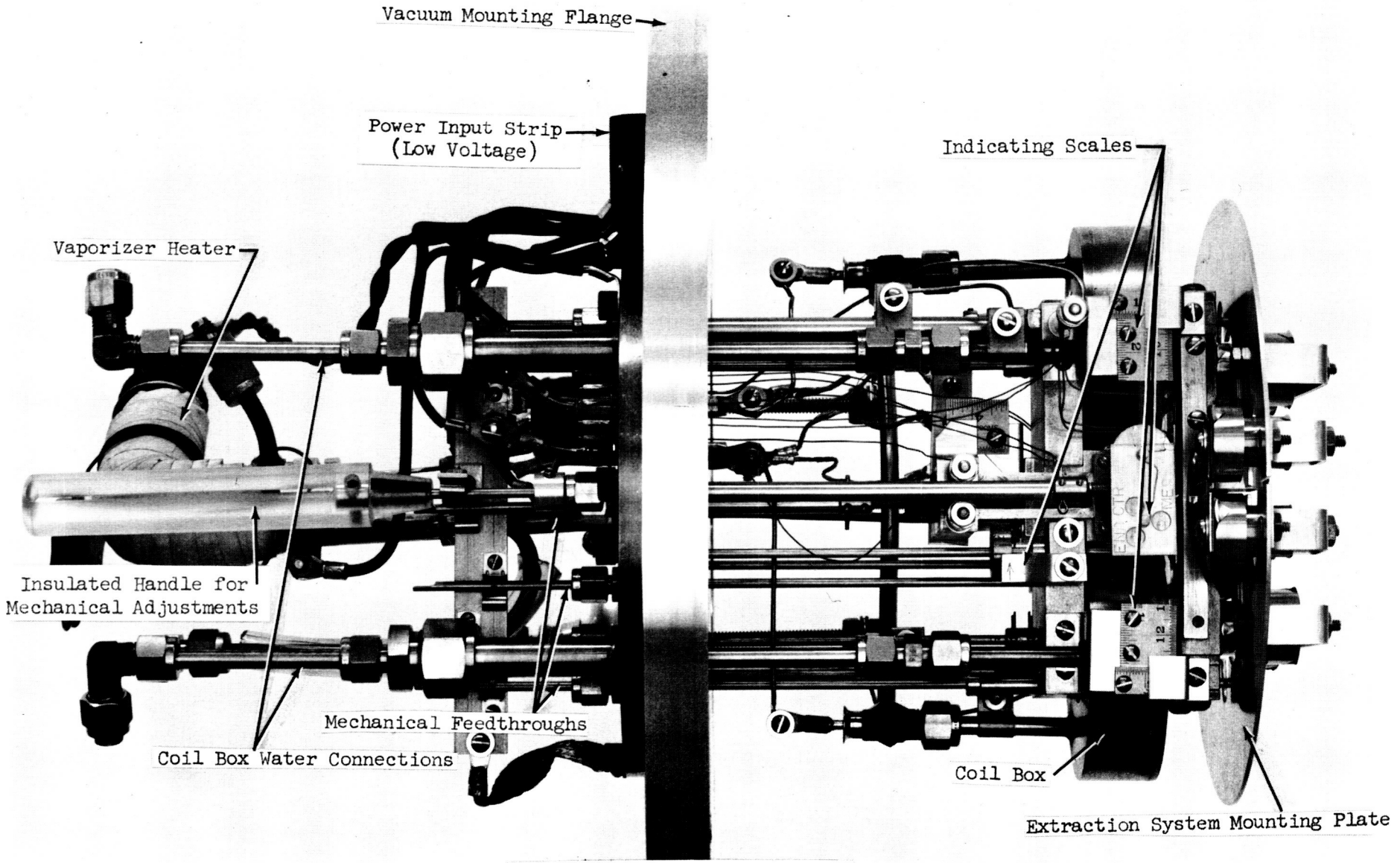

Figure 2.2-2

Variable Geometry Ion Source

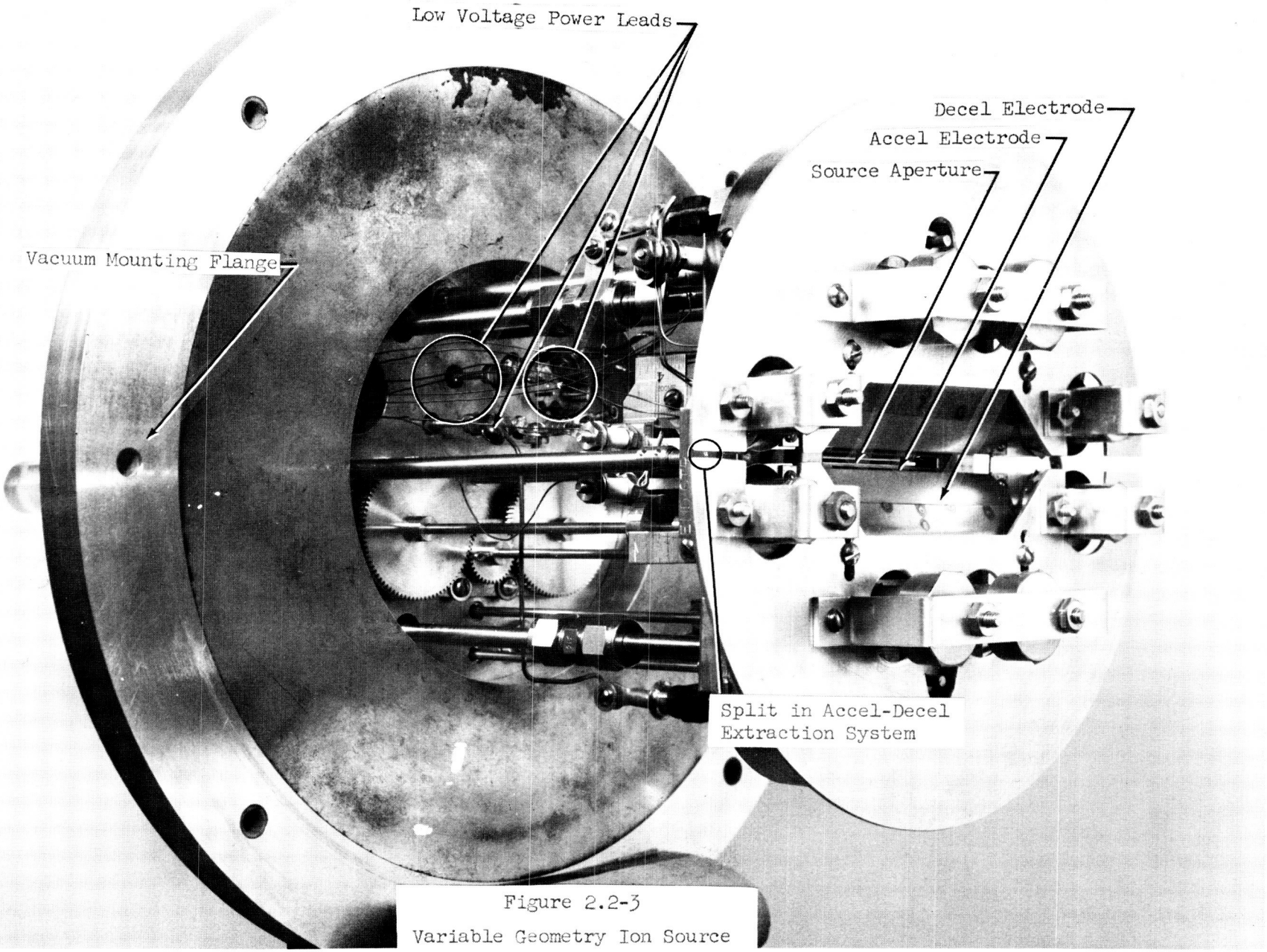

Figure 2.2-3

Variable Geometry Ion Source

mounting plate. These seals were Swagelok fittings, using teflon ferrules, around a 1/8 inch diameter stainless steel rod; periodic tightening of the fitting was all that was necessary to prevent leaks.

Figure 2.2-4 shows the source with coil boxes, anode and extraction assemblies removed. Some of the gear mechanisms used to achieve the geometrical variations can be seen. Figure 2.2-5 shows the variable cathode slit as well as the propellant entry ducts. It can be seen that some of these are open, some partially open, and some closed. The lateral distribution of open and closed propellant feed ducts could be externally controlled.

Into the "ionization chamber" of Figure 2.2-4 was placed the anode assembly. This was made in two identical halves, so that the anode wall separation (width) could be varied. Each anode half was connected to half of a "split" accel/decel extraction system, so that the anode and extractors moved laterally as a unit. This insured constant spacing of the accel and decel electrodes relative to each other and to the anode structure. The anode structures were made in a "hinged" fashion (see Figure 2.2-1) so the anode channel length could be increased in the axial direction simply by "stretching the spring". In practice, the downstream end of the anode was moved outward (further downstream), and the half of the extraction system to which it was connected simply moved with it. The spring employed was a leaf arrangement, so that in cross-section the anode channel was tapered, as shown in Figure 2.2-1. Balance, of course, demanded that both halves of this split anode-accel/decel system be displaced symmetrically (either in the axial or lateral directions, or both) before measurements were made.

2.3 Testing Facility

Experimentation with the variable geometry ion source was conducted in the facility pictured in Figure 2.3-1. This testing facility was arranged for maximum convenience and ease of usage, based on experience in engine testing under contracts NAS8-42 and NAS3-2522.

The variable geometry ion source in Figure 2.3-1 was operated in a nominal 18-inch diameter, 24-inch long Pyrex bell jar which rested on a stainless steel base plate. The glass bell jar afforded visual observation of the

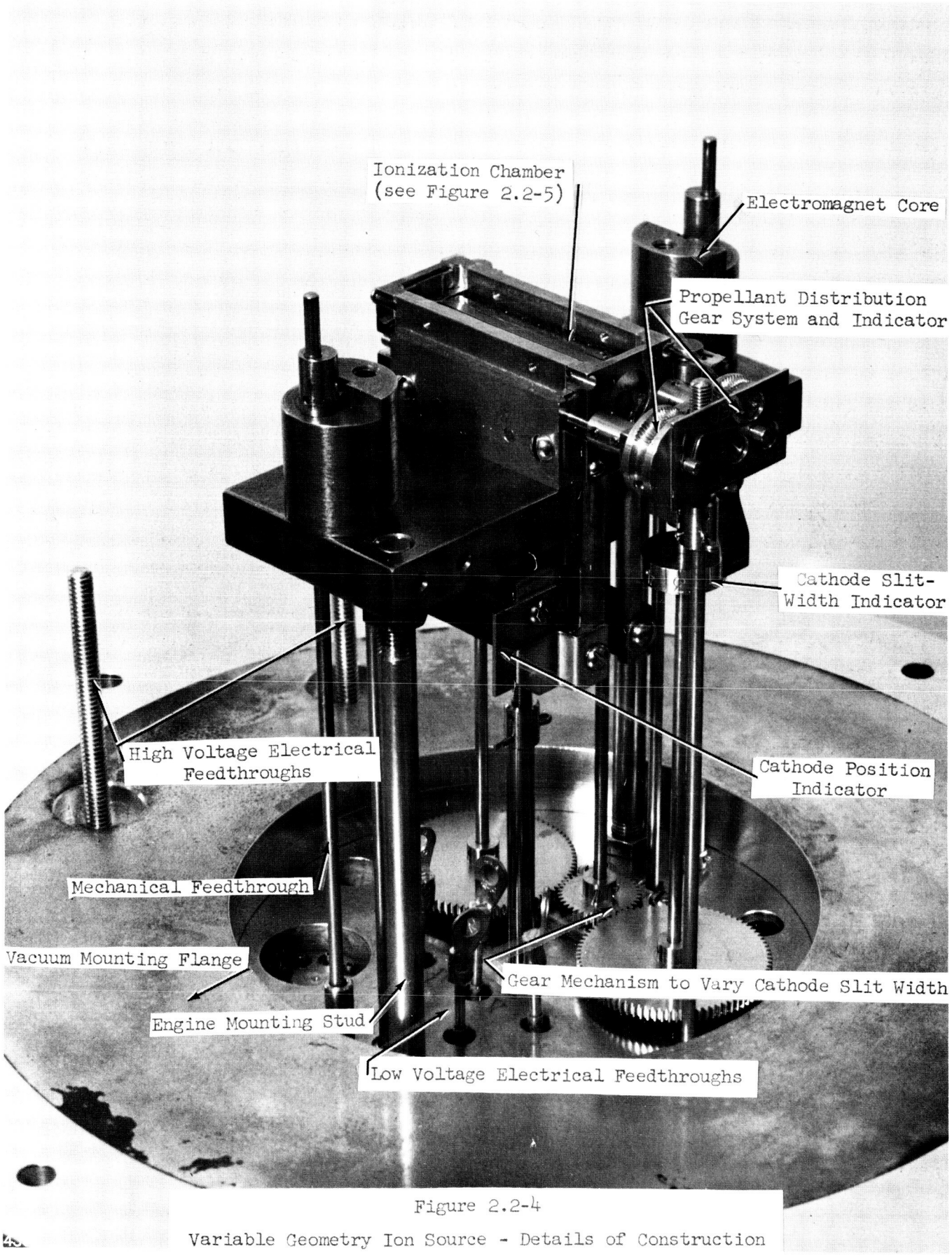

Figure 2.2-4

Variable Geometry Ion Source - Details of Construction

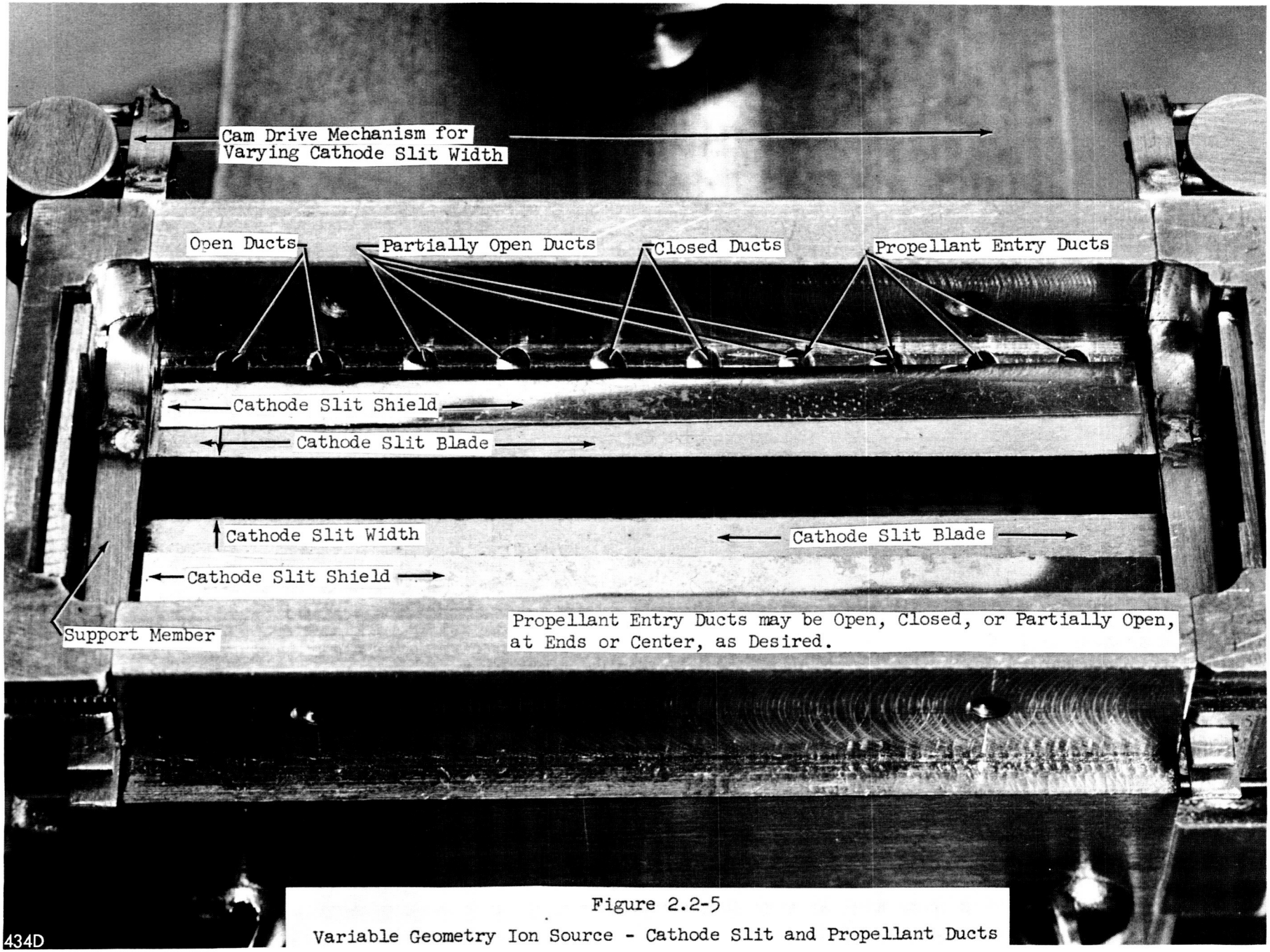

Figure 2.2-5

Variable Geometry Ion Source - Cathode Slit and Propellant Ducts

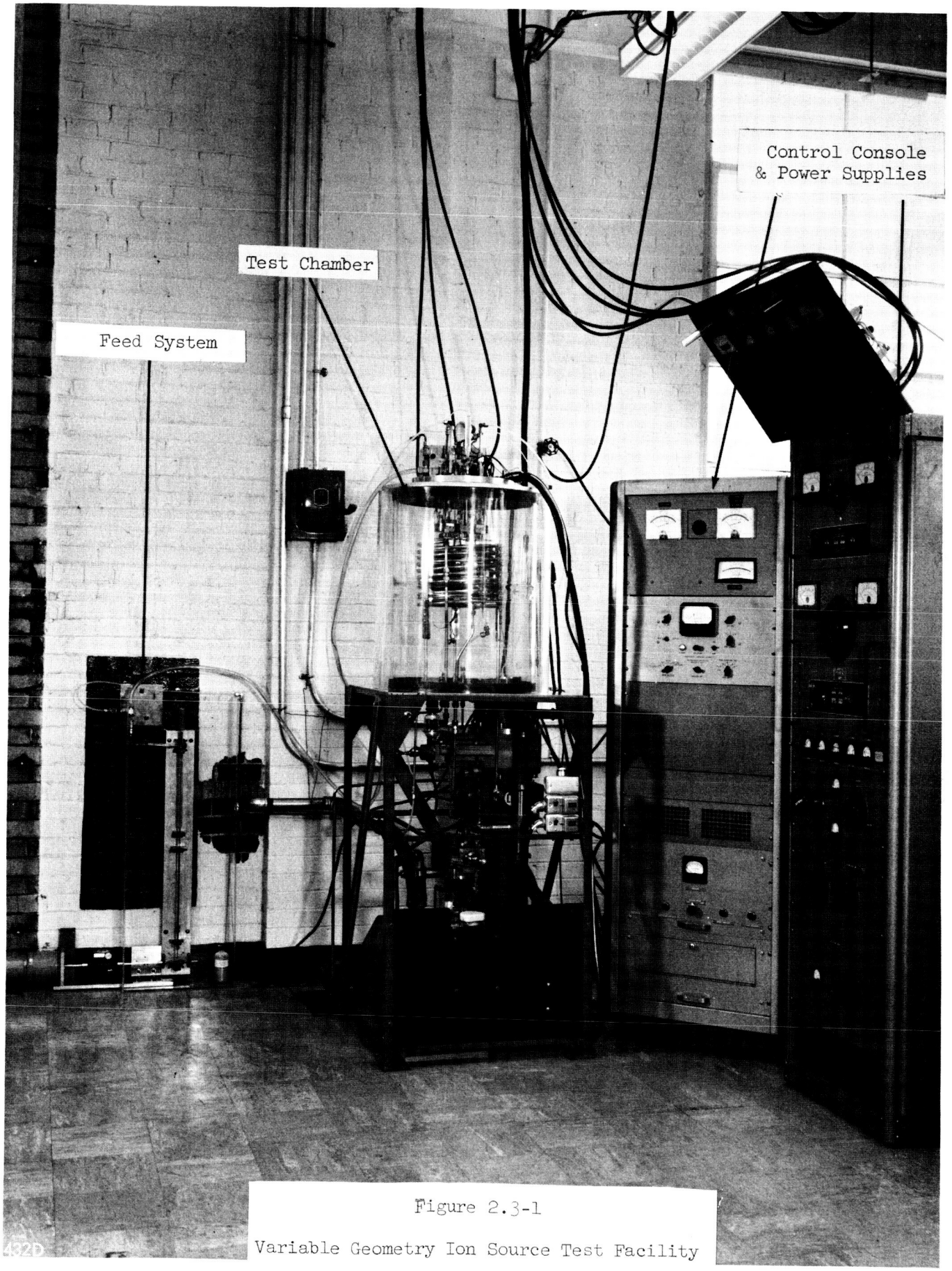

Figure 2.3-1

Variable Geometry Ion Source Test Facility

engine at all times and permitted direct readings to be made of the calibrated scales indicating the geometric parameters of the source. The Pyrex bell jar was surrounded by a 3/4-inch thick Lucite implosion shield for safety.

The ion beam was directed into a cooled cylindrical target operated at high voltage; the target sides were coiled stainless steel tubing and the bottom was an aluminum plate, cooled on the underside. Sufficient vacuum pumping capability was assured by maintaining a separation of about one tubing diameter between adjacent turns of the coil. Initial testing was conducted with the target air-cooled through "Nylaflow" feed-tubing sections which served to insulate the high voltage target from the base-plate. It was found that prolonged source operation under high voltage extraction conditions led to excessive target temperatures and subsequent softening of the teflon ferrules in the tubing joints, resulting ultimately in vacuum leaks. The target cooling arrangement subsequently was modified to permit tap water cooling; Nylaflow feed-tubing was again employed, but the length was increased so that the leakage current from the target through the water circuit to ground was about 0.2 ma/kv.

Surrounding the beam target was a liquid-nitrogen cold trap which was used to help maintain high vacuum and to condense mercury vapor. This trap was simply a coil of stainless steel tubing, insulated electrically and thermally from the beam target. Both the liquid-nitrogen to the cryo-trap and the water (or air) to the beam target were supplied through high vacuum feed-thrus in the base plate. A CEC type PMC-721 oil diffusion pump yielded typical pressures of about 5×10^{-5} torr without cold trapping and less than 10^{-6} torr with liquid nitrogen.

At the left of Figure 2.3-1 is shown the propellant feed system which served to deliver liquid mercury to the vaporizer at a constant metered rate. A positive-displacement liquid mercury driver was employed which consisted essentially of a plunger pushing into a precision-bore glass capillary which was filled with mercury. The displacement rate of the plunger was controlled by a synchronous motor, variable-speed transmission permitted the selection of mercury flow rates ranging from about 5 to 90 milliamperes. The precision-bore capillary tubing was joined to a three-position glass stop cock which

in turn could be connected to a mercury reservoir for refilling purposes or to the liquid transfer line. The latter was water-jacketed to eliminate thermal expansions and/or contractions of the liquid mercury in the transfer line induced by room-temperature fluctuations. The glass capillary, mercury plunger, and mercury reservoir were enclosed in a Lucite box to minimize the effects of drafts upon these components of the system. The known plunger displacement speed and capillary bore size permitted the calculation of the liquid mercury delivery rate to the vaporizer. This rate was periodically verified by feed system calibrations in which the vaporizer was disconnected and the liquid mercury displaced during a known time collected and weighed.

The vaporizer employed was a "capillary" vaporizer (Reference 2), and consisted basically of a length of thick-wall stainless steel tubing, heated at one end, cooled at the other, with liquid mercury driven into the cooled end. At equilibrium mercury vaporization occurred somewhere between the hot and cold ends, such that mercury vapor exited from the hot end at the same rate at which liquid mercury was driven into the cold end. The capillary bore size and temperature gradient were selected to yield the response time desired (Reference 2); careful temperature-gradient control assured the maintenance of a constant vapor delivery rate.

The propellant vapor was ducted from the vaporizer to the engine through an electrically-heated stainless steel tube whose temperature could be varied; in practice the temperature of this "transfer tube" was kept just below the point at which it began to glow red, thus assuring that mercury vapor condensation could not occur within this tube.

Within the engine body itself were several small propellant flow passages which served to duct the mercury vapor from the transfer tube to the ionization chamber. To prevent mercury condensation in these passages, the engine was operated at a relatively high temperature. The mechanisms of engine heating were several and included the absorption of power radiated from the cathode, conductive heat transfer from the propellant transfer tube, and conductive heat transfer from ionization chamber walls. Temperatures representative of what were expected to be maximum and minimum values at locations near the mercury vapor flow paths were monitored during source testing. In practice the engine

structure was permitted to heat for an hour or more, with the cathode hot and the arc struck, until the "engine base" temperature (the expected minimum) approached the temperature of the heated end of the capillary vaporizer. Since mercury vaporization at a considerably lower temperature was a virtual certainty, this precaution obviated the possibility of propellant condensation in the engine passages.

An additional precaution against propellant condensation was afforded by the "hot" operation of the magnet coil boxes. This was accomplished through a recirculating, electrically-heated, thermostatically-controlled, hot-water system which continually pumped distilled water near 100°C through the magnet coil boxes. In this manner the magnet coil windings were held at a temperature sufficiently cool to prevent burnout, yet hot enough to prevent mercury vapor condensation on the outer (vacuum) side of the coil cans. A 2 kw thermostatically-controlled heater (not visible in Figure 2.3-1) and a centrifugal pump served to deliver about 1/2 gpm of water at 100°C through the system. The magnet coil boxes were thermally insulated from the remainder of the ion source (so as not to cool those portions designed to operate hotter) and the exit temperature of the water monitored.

The remainder of the items in Figure 2.3-1 consist primarily of low voltage power supplies and metering equipment. These included a 50 volt, 25 ampere DC electromagnet power supply, a 150 volt, 25 amper DC arc power supply, a cathode heating power control, a vaporizer heater control, arc and cathode voltages and current meters, a magnetic field balancing rheostat which permitted more or less current to be supplied to either coil and individually measured. Cathode temperature was measured with a thermocouple or optical pyrometer; vacuum tank pressures were read with an ionization gauge. Not visible in the figures are the accel and decel high voltage DC power supplied; the former was rated at 50 kv, 0.1 ampere, the latter at 6 kv, 0.5 ampere. The high voltage power was brought to the engine through high voltage cables and the appropriate voltages and currents metered; insulated switches were provided to select meters of increased sensitivity to read accel and decel electrode current drains.

2.4 Experimental Results

During the course of the program, thirty-one different tests were conducted on the variable geometry source (VGS). These tests, referenced as VGS-1 through VGS-31, established the source performance under a wide variety of conditions. A "test", as used here, is defined to be the totality of source operation during the course of one calendar day. In many instances, however, a single such "test" included data obtained at several input feed rates, cathode powers, etc. since such rapid data acquisition was, in fact, the purpose of the variable geometry source. In this section, no attempt will be made to provide all the data obtained. Instead the emphasis will be upon the major results and conclusions obtained. Sufficient supporting data will be provided.

The first tests with the variable geometry source were exploratory in nature and used cathode stock made under a previous program (NAS3-2522). As a result, the cathode powers were somewhat high, but interest at the time was centered upon the arc characteristics in terms of ionization efficiency. The very first run, VGS-1, yielded but 25.5 per cent mass utilization (I_F = 100 ma) for a 14 volt, 0.86 ampere arc (η_A = 472 ev/ion) despite a cathode temperature in excess of 2100°F ($P_C \approx$ 75 watts). A reduction in the propellant input rate to 69 equivalent milliamperes yielded 72.5 per cent mass utilization (for a 27.5 volt, 1.41 ampere arc) at 715 arc ev/ion for about the same cathode conditions. It should be emphasized that all VGS data was obtained under conditions of high voltage extraction; the electrode voltages and drain currents will be reported for later tests.

Tests VGS-2 and VGS-3 employed the same cathode ($T_C > 2100$°F, $P_C \approx$ 60-70 watts) and sought to determine the effect of varying the cathode slit width (from 1.0 to 4.0 mm) for a constant anode geometry, 3 mm wide by 6 mm long. This effect was largely overshadowed by the relatively inefficient operation of the source, some 1300-1400 arc ev/ion being necessary for 90 per cent mass utilization (I_F = 56 ma). These data runs were characterized by unduly high arc currents, the result of the cathode being positioned too far back from the cathode slit (0.7 and 1.3 mm).

Somewhat improved performance was observed during VGS-4, in which the same cathode was employed but the cathode to cathode-slit distance was reduced to

about 0.5 mm. For a constant anode geometry 3 mm wide and 5 mm long, the arc losses ranged from about 350 to 1200 ev/ion at 95 per cent mass utilization, for cathode slit widths ranging from 1.0 to 2.5 mm; the mercury input was about 65 equivalent milliamperes. The most efficient arc performance was obtained with the narrowest (1.0 mm) cathode slit width, but required an arc voltage of 50 volts. Subsequent operation at an increased feed rate (I_F = 82.5 ma) improved matters, yielding about 350-500 arc ev/ion near 97 per cent mass utilization for arc voltages of about forty volts.

By this time it had become clear that, from the standpoint of arc power efficiency, it was advantageous to have the cathode as close as possible to the cathode slit, without electrical or thermal shorting. This is shown in Figure 2.4-1 which summarizes the results of VGS-5. Curves 1 and 2 were obtained for all conditions identical except for a reduced cathode to cathode slit distance for 2. In curves 2 through 5 this distance was constant and the effect of varying some of the other geometrical parameters of the source can be seen. The data shown was obtained under the condition of high voltage extraction although no particular effort was made to optimize the extraction system since the primary interest of the experimentation was centered on the source performance. The accel electrode interception was, however, one per cent or less for propellant utilization values greater than 70 per cent.

All the data shown in Figure 2.4-1 was obtained for the same distribution of propellant input. It will be recalled (Section 2.2, particularly Figure 2.2-5) that the variable geometry ion source provided for control and variation of the lateral distribution of input propellant vapor. At one time it had been hoped that this feature might prove to be the most important single factor in establishing optimum source performance. As it turned out, however, such was not the case. Propellant distribution was found to have a relatively minor effect upon engine performance.

Data similar to that shown in Figure 2.4-1 was obtained in VGS-6; the arc losses ranged from about 325 to 500 ev/ion for 97 per cent utilization. High cathode powers ($>$70 watts) were still required, however, since the same cathodes had been used in VGS-1 through VGS-6. Furthermore, in virtually all data runs, mass utilization near 95 per cent at reasonable arc power efficiencies (say 600 ev/ion or less) required arc voltages of forty volts, if not more.

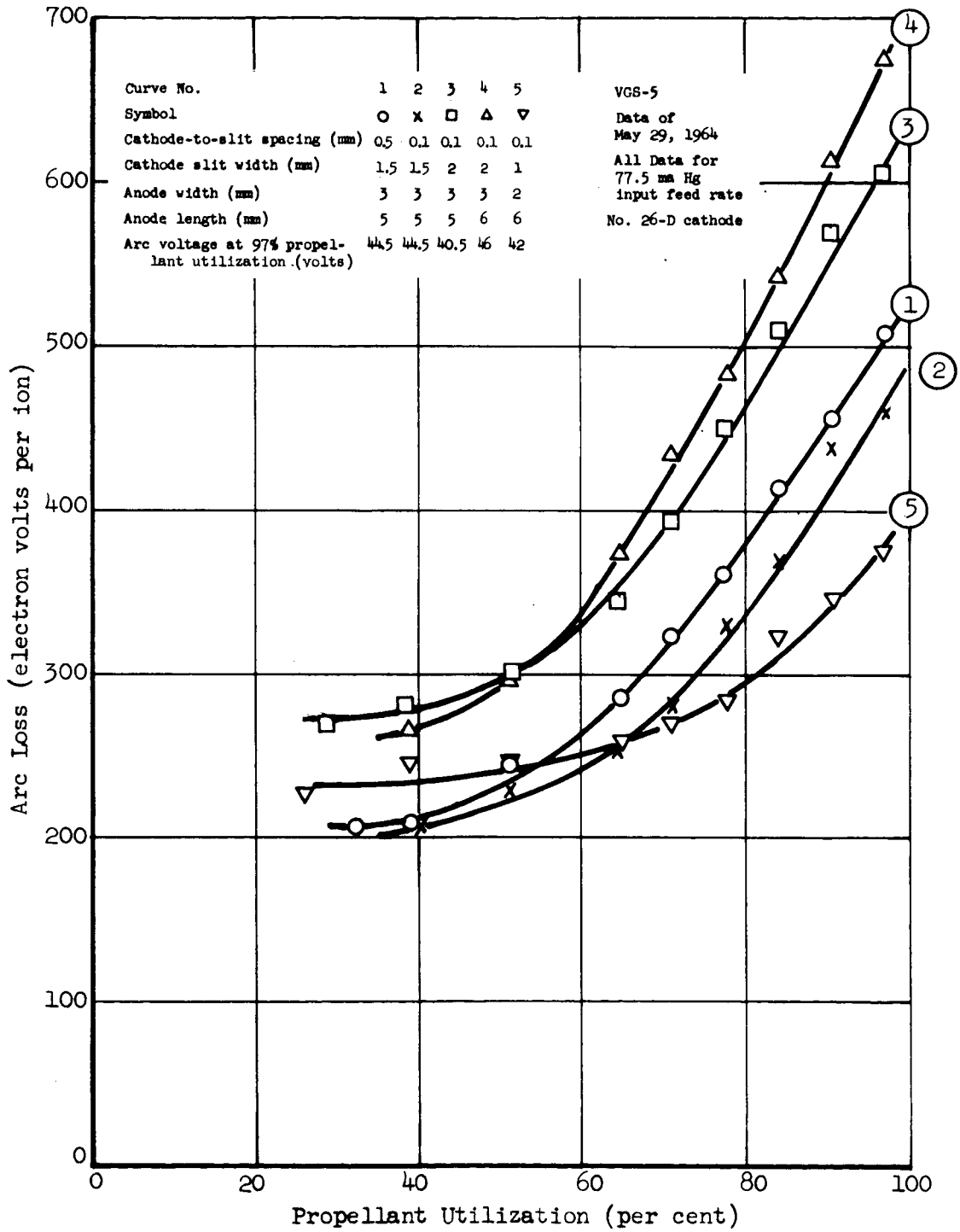

Figure 2.4-1

Ion Generation Characteristics of Variable Geometry Source (VGS-5)

Such high arc voltages not only lead to cathode sputtering but also introduce the possibility of double ionization. The effect of double ionization on the measured source performance has been estimated using the data of Reference 3. The results are shown in Figure 2.4-2. The solid curve is a replot of curve 5 of Figure 2.4-1; the dashed-curve resulted from correcting the data points for double ionization. It is seen that the corrections reduce the measured values of propellant utilization as well as increase the values of the measured ionization losses. Unless otherwise specified, all data contained herein will be uncorrected for double ionization.

The next test employed a new cathode, made from stock fabricated under the program. Cathode performance was, in general, somewhat better in that comparable arc performance characteristics could be obtained at somewhat lower cathode temperatures (about 1900-1960°F) and reduced heater powers ($\sim$60 watts). The first test with the new cathode (VGS-7) essentially was a repetition of the previous two. The purpose of this test was, basically, to verify that the good ionization efficiencies previously obtained could be obtained with the new cathode also. Typical data from this test are shown in Figure 2.4-3. All data was obtained under conditions of high voltage extraction (16.5-19 kv accel, 7.5-10.5 kv decel). No particular effort was made initially to optimize the extraction system or to operate at low specific impulse since the primary interest was still the arc performance of the source. Presented in Figure 2.4-3 are ionization losses (arc ev/ion) vs. propellant utilization curves for several anode configurations at two propellant input feed rates. It would appear from this data that an anode 3 mm wide and 7 mm long is preferable to the other sizes tested with some slight additional advantage to be gained by operating at higher flow rates. The 4 mm x 7 mm anode showed excessive atc losses (and arc voltages) at the propellant utilizations of interest and, furthermore, required 19.2 kv accel and 10.5 kv decel potentials for any reasonable sort of beam focusing. Run 1 and Run 2 for each flow rate were conducted for identical experimental conditions. The differences which are evident in Figure 2.4-3 suggest cathode deterioration.

These first seven tests with the variable geometry source served to establish that acceptable arc ionization characteristics could be achieved. The requisite cathode heater powers, however, still remained high, compared to the anticipated radiative power for the cathode temperatures measured. This discrepency indicated

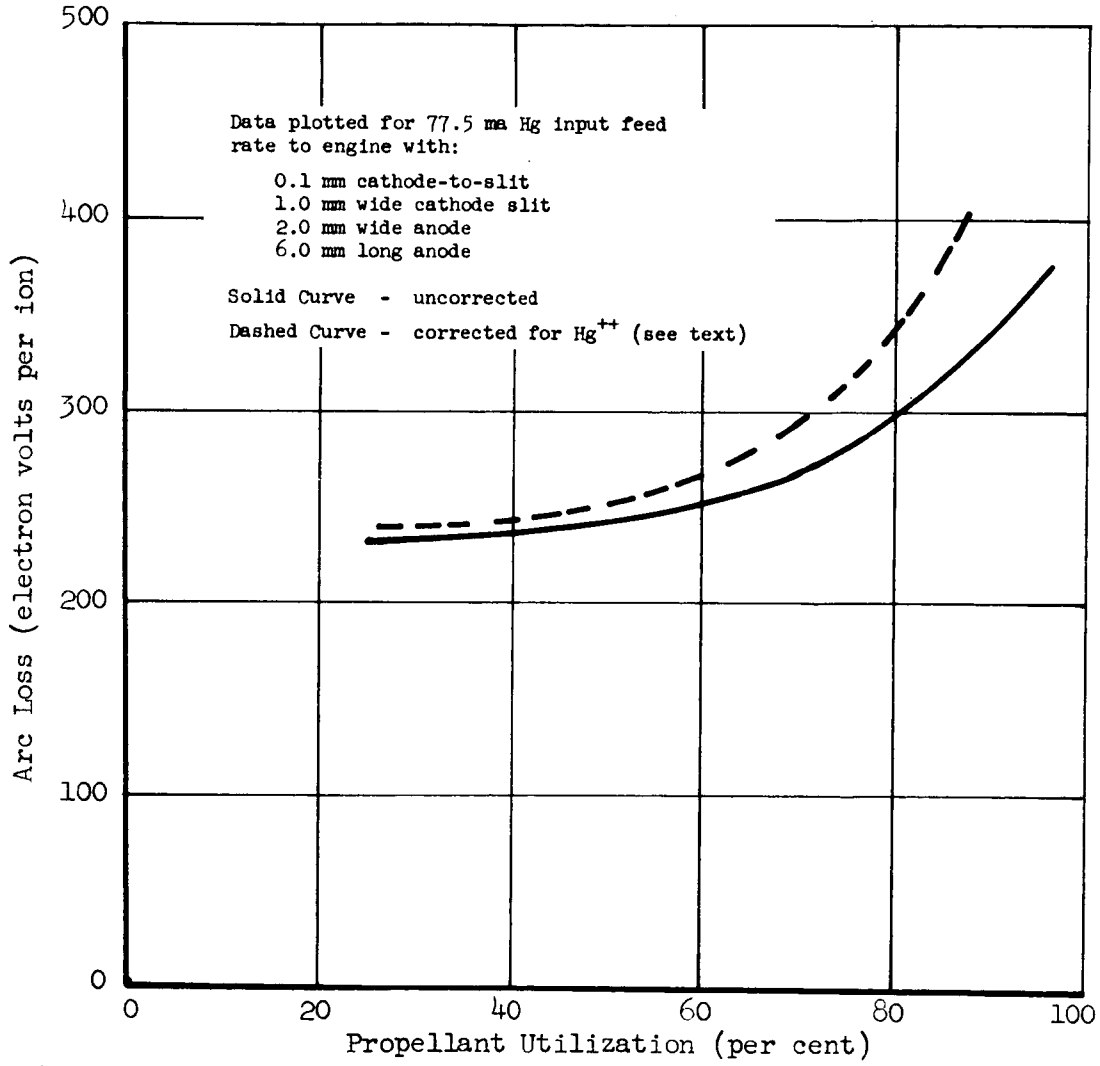

Figure 2.4-2

Estimated Effect of Double Ionization

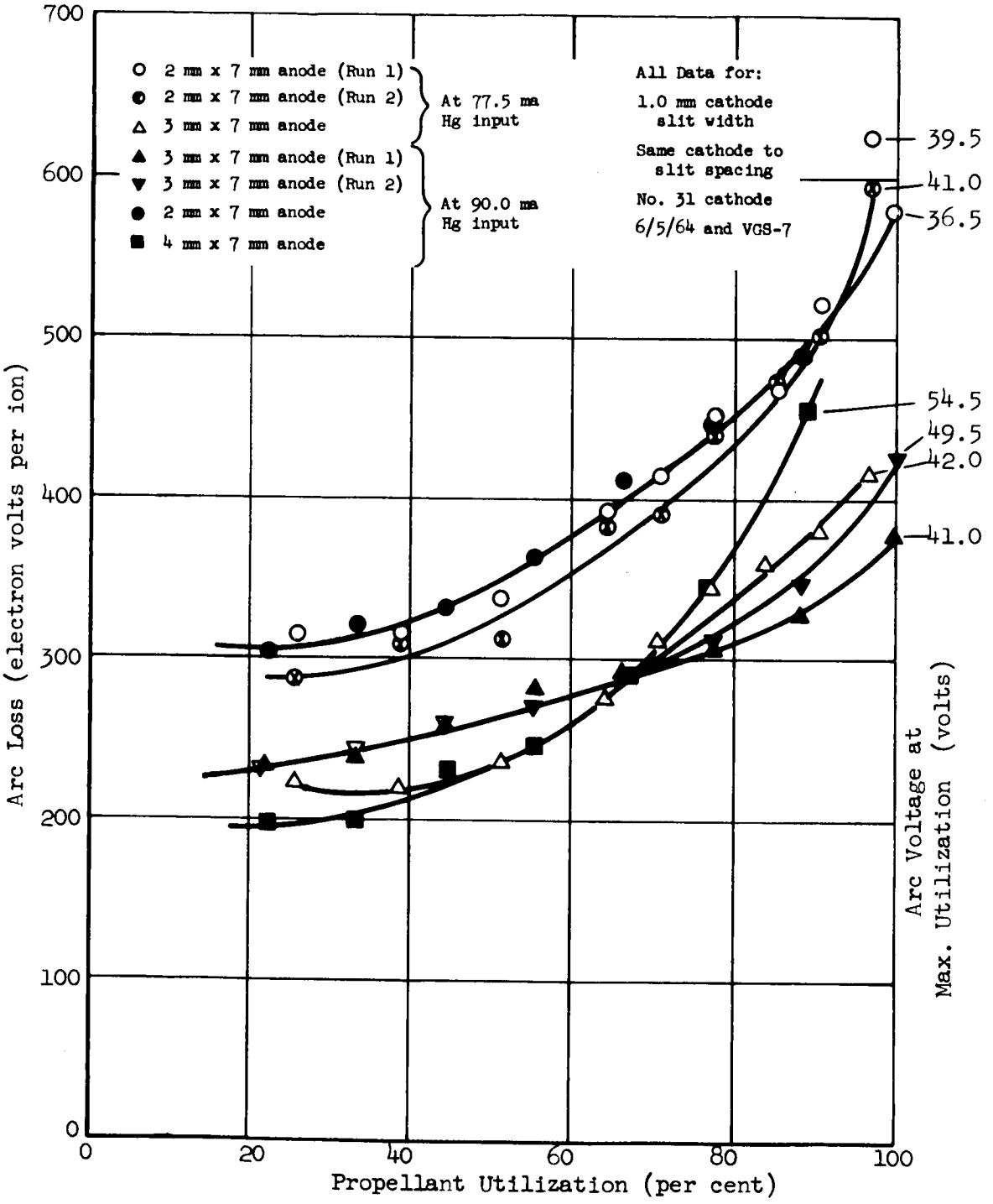

Figure 2.4-3

Ion Generation Characteristics of Variable Geometry Source (VGS-7)

the presence of a thermal loss in the cathode mounting arrangement. This loss, presumably correctable, had been of secondary concern, the primary interest being the determination of ionization chamber dimensions resulting in minimum arc power per generated ion. Nevertheless, the total engine performance was sufficiently encouraging to warrant some preliminary measurements of ion beam generation based on the arc and cathode losses combined.

Such data was obtained in VGS-8, -9, -10. Despite the fact that the same cathode was employed in these tests as was used in VGS-7, the resulting data, summarized in Tables 2.4-1 and 2.4-2, showed highly satisfactory performance. Of significance is the fact that, considering the arc and cathode efficiencies in combination, a decrease in cathode temperature resulted in more efficient operation, but not without an increase in arc voltage. High arc voltages appeared to constitute an essential requirement for simultaneously achieving high propellant utilization and low power losses. The measured decel interception currents are not included in Tables 2.4-1 and 2.4-2 because of the high interception experienced due to the absence of beam neutralization and the nonoptimum mounting design of the extraction system.

The possibility of operating the source at somewhat less than optimum conditions (in terms of arc power efficiency) to take advantage of the reduced arc voltage upon cathode lifetime was suggested. (In general this could be done by operating with an increased cathode slit width). The arc power efficiency penalty might be small, say an extra 100-150 ev/ion over high arc voltage operation, but the cathode lifetime gains would make this trade-off well worthwhile. This power penalty, furthermore, was shown to be small relative to the power efficiency of the entire thrustor (including accel and decel drains) and could perhaps be compensated by improvements in other areas, particularly thermal insulation of the cathodes. The above approach was used subsequently in the program to optimize the performance of the thrustor. Unfortunately its success was limited.

The apparent necessity for arc operation at voltage levels in excess of the sputtering threshold prompted the experimental investigation of alternate approaches to the problem. As described in detail in Section 3.2, these efforts included attempts to develop a "cavity" cathode and the fabrication of conventional nickel matrix cathodes with surfaces designed to minimize the adverse effects

Table 2.4-1, Performance of Variable Geometry Source (VGS-8)

Source Current (ma)	75	75	75	75	85	85	85	85	85	85	85	85	85	85
Accel Current (ma)	.78	.83	.75	NR	1.0	.90	NR	NR	NR	NR	NR	NR	NR	NR
Accel Interception (%)	1.04	1.1	1.0	NR	1.17	1.06	NR	NR	NR	NR	NR	NR	NR	NR
Accel Voltage (kv)	17.5	17.5	17.5	17.5	17.5	17.5	17.5	17.5	17.5	17.5	17.5	17.5	17.5	17.5
Decel Voltage (kv)	5.7	5.7	5.7	5.7	5.7	5.7	5.7	5.7	5.7	5.7	5.7	5.7	5.7	5.7
Specific Impulse (sec)	7550	7550	7550	7550	7550	7550	7550	7550	7550	7550	7550	7550	7550	7550
Arc Current (amps)	.94	.92	.75	.90	.85	.82	.98	.825	.87	.95	1.3	.93	.92	.95
Arc Voltage (volts)	41.5	39	42.5	42	39	38	34.5	37	37.5	37	30	37.5	39	36
Arc Power (watts)	39.0	35.9	31.9	37.8	33.1	31.2	33.8	30.5	32.6	35.2	39.0	34.9	35.9	34.2
Arc ev/ion	520	479	425	503	390	367	388	359	384	414	460	411	422	402
Heater Current (amps)	6.2	5.8	5.4	5.4	5.4	5.4	5.4	5.4	5.4	5.4	5.4	5.4	5.45	5.45
Heater Voltage (volts)	10.25	9.2	8.2	8.2	8.2	8.2	8.2	8.2	8.2	8.2	8.2	8.2	8.2	8.2
Heater Power (watts)	6.35	53.3	44.2	44.2	44.2	44.2	44.2	44.2	44.2	44.2	44.2	44.2	45.3	45.3
Cathode Temp. (°F)	1860	1800	1730	1730	1740	1740	1740	1740	1740	1740	1740	1740	1720	1725
Cathode ev/ion	848	712	590	590	520	520	520	520	520	520	520	520	534	534
Hg Input (equiv. ma)	78.5	78.5	78.5	78.5	88.5	88.5	88.5	88.5	88.5	88.5	88.5	88.5	88.5	88.5
Propellant Utilization (%)	95.5	95.5	95.5	95.5	96.0	96.0	96.0	96.0	96.0	96.0	96.0	96.0	96.0	96.0
Arc + Cathode ev/ion	1368	1191	1015	1093	910	887	908	879	904	934	980	931	956	929
Cathode Slit Width (mm)	1.5	1.5	1.5	2.0	1.5	1.5	2.0	1.5	1.5	2.0	3.0	1.5	1.5	1.5
Anode Width (mm)	3	3	3	3	3	3	3	3	3	3	3	3	3	3
Anode Length (mm)	6	6	6	6	6	6	6	6	5	5	5	5	6	6
Other							*	*	*	*	*	*	*	*

Notes: All data obtained 6/12/64.

Tank pressure $\simeq 10^{-5}$ torr.

"NR" ≡ not recorded.

No. 31 cathode (flat) used.

* ≡ Input propellant flow distribution changed.

Cathode initially positioned within 0.2 mm of shorting to cathode slit.

Table 2.4-2, Performance of Variable Geometry Source (VGS-9, -10)

Source Current (ma)	85	85	85	85	85	85	85	85	85	85	85	85	85	85
Accel Current (ma)	1.5	1.1	.8	.8	NR	.7	.8	NR	NR	NR	.66	NR	.68	.80
Accel Interception (%)	1.77	1.3	.94	.94	NR	.83	.94	NR	NR	NR	.78	NR	.80	.84
Accel Voltage (kv)	19.5	19.0	16.0	16.0	16.0	16.2	16.6	16.6	16.6	16.6	16.5	16.5	16.2	16.5
Decel Voltage (kv)	5.6	5.7	5.8	5.8	5.8	5.7	5.7	5.7	5.7	5.7	5.6	5.6	5.6	5.6
Specific Impulse (sec)	7480	7550	7620	7620	7620	7550	7550	7550	7550	7550	7480	7480	7480	7480
Arc Current (amps)	.75	1.12	.62	.80	.96	.85	.83	.70	.59	1.2	.90	.84	.83	.87
Arc Voltage (volts)	46	44.5	41.5	40	38	40	41	47	52	40	41	48	40	40
Arc Power (watts)	3.45	49.7	26.7	32.0	36.5	34.0	34.0	32.9	30.7	48.0	36.9	40.3	33.2	34.8
Arc ev/ion	407	585	303	377	430	400	400	387	362	565	435	475	391	367
Heater Current (amps)	5.7	5.7	5.2	5.2	5.2	4.8	4.8	4.8	4.8	4.5	4.5	4.5	5.2	5.6
Heater Voltage (volts)	9.45	9.45	8.3	8.3	8.3	7.45	7.45	7.45	7.45	6.6	6.6	6.6	8.2	9.2
Heater Power (watts)	53.9	53.9	43.2	43.2	43.2	35.8	35.8	35.8	35.8	29.7	29.7	29.7	42.6	51.5
Cathode Temp. (°F)	1800	1800	1720	1720	1720	1650	1650	1650	1650	1610	1600	1600	1705	1715
Cathode ev/ion	635	635	508	508	508	422	422	422	422	350	350	350	502	543
Hg Input (equiv. ma)	88.3	88.3	88.3	88.3	88.3	88.3	88.3	88.3	88.3	88.3	88.3	88.3	88.5	97
Propellant Utilization (%)	96	96	96	96	96	96	96	96	96	96	96	96	96	98
Arc + Cathode ev/ion	1042	1220	811	855	938	822	822	809	784	915	785	825	893	910
Cathode Slit Width (mm)	1.0	1.5	1.0	1.25	1.5	1.5	1.5	1.25	1.0	3.0	2.0	1.5	1.1	2.5
Anode Width (mm)	3.0	3.0	3.0	3.0	3.0	3.0	3.0	3.0	3.0	3.0	3.0	3.0	3.0	3.0
Anode Length (mm)	5.5	5.5	6.0	6.0	6.0	6.0	6.5	6.5	6.5	6.5	6.5	6.5	6.5	6.5
Date	6/19/64 - - -	- - -	- - -	- - -	- - -	- - -	- - -	- - -	- - -	- - -	- - -	- - -	6/23/64 -	

Notes: Tank pressure $\leq 6 \times 10^{-6}$ torr, in all cases.

"NR" ≡ not recorded.

No. 31 cathode (flat) used.

Cathode positioned as close as possible to cathode slit without shorting.

of sputtering (in effect, to increase the sputtering threshold). One of these latter types, a so-called "saw-tooth" cathode was used in VGS-11 through VGS-14. In these and several subsequent tests, the variable geometry source served the role of a cathode test facility, wherein cathodes of various designs were studied under conditions of engine operation.

The performance of a saw-tooth cathode (overlapping teeth separated by about 0.010 inch) in the variable geometry source is summarized in Table 2.4-3. No data is given for VGS-11 since a high-voltage power supply failure prevented the obtaining of any reliable results. The symbols and abbreviations used are defined in the List of Symbols. The primary purpose of tests VGS-12 through VGS-14 was to evaluate the stability of the saw-tooth cathode under conditions of high-voltage engine operation. Previous experience with conventional (flat) cathodes indicated a trend with time toward increasing arc voltages (decreasing arc current) plus a gradual beam degradation. As is shown in Table 2.4-3, a similar situation was experienced during VGS-13. Unfortunately a broken cathode lead prevented further experimentation with this cathode with the result that it was impossible to determine whether the degradation observed was the result of cathode sputtering, insufficient cathode activation, propellant starvation, or some other cause. For example, during periods of source operation, the beam target was heated by some 400 watts and considerable target sputtering occurred as evidenced by the plating of the inside of the glass bell jar. A gradual rise in tank pressure indicated target heating and outgassing. The cathode deterioration observed, therefore, could not be inherent in the cathode, but rather perhaps could be attributable to gradual cathode poisoning by material released from the beam target (aluminum) or its supports (stainless steel).

A conventional (flat) cathode was next employed. Four VGS tests were run with the objective of achieving good mass utilization at reduced arc voltages. The results of these tests are summarized in Table 2.4-4. It is apparent by observing V_A values for test VGS-17 engine performance improved as more operating time was accrued. The last data set of VGS-18 was obtained by optimization of the cathode slit width. Unfortunately extraction system shorting forced premature shutdown of the test making impossible and extended stability check of source operation at the conditions listed. Test VGS-18 was run for approximately three hours with each data point representing a minimum of 10 minutes duration at that point.

Table 2.4-3

Summary of Experimentation with Saw-Tooth Cathode in Variable Geometry Source

(No. 34 Cathode Stock)

Test No.	Purpose	Remarks
VGS-12	Preliminary cathode evaluation.	3 x 7 anode, data for $\eta_M = 92.5\%$: $28 < V_A < 40$, for $480 > \eta_A > 400$ and CS = 3.0 $37 < V_A < 40$, for $450 > \eta_A > 420$ and CS = 2.0 $530 < \eta_C < 840$
VGS-13	Cathode stability.	3 x 7 anode, data for I_F = 81 ma. For CS = 3.0 and P_C = 40.8 watts, V_A rose from 39 v. to 47 v. I_B dropped from 76 ma to 58 ma } in 35 min. Initially, $\eta_A + \eta_C = 355 + 535 = 890$ ev/ion For CS = 3.0 and P_C = 45 watts, V_A rose from 40 v. to 46 v. I_B dropped from 74 ma to 65 ma } in 45 min. For CS = 2.5 and P_C = 51.5 watts, V_A rose from 35 v. to 48 v. I_B dropped from 79 ma to 71 ma } in 2 hours (Initial performance was V_A = 35 v at $\eta_M = 97.5\%$ and η_A = 408 ev/ion, η_C = 650 ev/ion).
CGS-14	Continuation of VGS-13.	Anode to ground short stopped test prematurely. Cathode lead broke during anode repair. Replaced cathode with flat type. (See Table 2.4-4).

Table 2.4-4

Summary of Experimentation with Flat (Conventional) Cathode in Variable Geometry Source

(No. 34 Cathode Stock)

Test No.	Purpose	Remarks
VGS-15	Cathode activation.	After activation, I_A = 2.5 a, V_A = 20 v. (for cathode temperature = 1770°F). Also, I_A = 1.3 a, V_A = 30 v (For cathode temperature = 1660°F).
VGS-16	Preliminary cathode evaluation.	Ran η_M = 97.5% at V_A = 37 v (3 x 6.5 anode, CS = 2.0) but η_A = 600 ev/ion. (I_F = 81 ma) Attempted 3 x 5.5, 2 x 5.5, 3 x 6.5 anodes at various CS; $\eta_M \rightarrow$ 95% required V_A = 38 to 40 v.
VGS-17	Operation at reduced V_A.	Increased I_F to 88.5 ma. Results:

η_M(%)	η_A(ev/ion)	η_C(ev/ion)	V_A(v)	Anode	CS
95	840	407	32	3 x 5	3.0
88	710	407	29	3 x 5.5	3.0
98	587	324	34	3 x 7	3.0
95	625	382	35	3 x 8	3.0

VGS-18 Continuation of VGS-17

η_M(%)	η_A(ev/ion)	η_C(ev/ion)	V_A(v)	Anode	CS
93	685	358	28	3 x 7.5	3.0
90	462	356	25	3 x 7.5	3.0
99	587	396	30	3 x 7.5	2.7

The variable geometry source was next run with a "cavity" cathode (VGS-19 through VGS-21). The results of these tests are summarized in Table 2.4-5. The engine power efficiency was considerably reduced by the high cathode powers required for accaptable arc performance. All indications were, however, that the cavity cathode was physically too large for the cathode chamber of the variable geometry source; the cathode was found to be electrically shorted to the cathode chamber and, presumably, thermally shorted also to some extent. This situation was correctable by a redesign of the cathode chamber, a time-consuming procedure of doubtful merit. Of more immediate interest, on the other hand, was the preliminary indication of improved cathode stability, at least relative to the sawtooth cathode (Table 2.4-3). The actual performance comparison must be qualified since the two cathode types were fabricated from different lots of cathode stock and the increased cathode heater power in the case of the cavity cathode may have helped its stability.

A rise in tank pressure (ultimately traced to a vacuum leak) forced the premature termination of test VGS-21. The situation was subsequently corrected, but further experimentation (VGS-22) showed poor performance for the cavity cathode presumably because of the pressure rise during VGS-21. It was consequently replaced with a conventional cathode (No. 33 stock), which remained in use for tests VGS-23 through VGS-28.

The purpose of these tests was to determine if any further performance gains were possible. Most of the work consisted in the operation of the engine in modes so as simultaneously to achieve both good power efficiency and mass utilization while maintaining a minimum level of arc voltage. Some of the data obtained is presented in Table 2.4-6. In general it was observed (as previously) that mass utilization of about 90 per cent required arc voltages of at least 30 volts, and 95 per cent utilizations required about 35 to 40 volts. The power efficiencies of Table 2.4-6 are downgraded considerably by the decel drains listed. These are not true decel electrode drains, since it was observed visually that the (unneutralized) beam blow-up resulted in beam impingement upon structural supports and insulator shields which were maintained at the decel potential but were not really part of the decel focusing electrode.

The variable geometry ion source used through test VGS-25 was constructed such that both the anode length and width could be varied without removing the engine

Table 2.4-5

Summary of Experimentation with Cavity Cathode in Variable Geometry Source

(No. 33 Cathode Stock)

Test No.	Purpose	Remarks
VGS-19	Initial operation in engine	For 2 x 6.5 anode, CS = 2.0 measured η_M = 98.5%, V_A = 42 v, η_P = 410 ev/ion (But η_C = 885 ev/ion). After one hour of running, measured η_M = 95%, V_A = 39 v, η_P = 450 ev/ion.
VGS-20	Cathode stability.	For 2 x 6.5 anode, CS = 2.1, measured V_A drop from 34 to 29.5 v in 1/2 hour. For 2 x 6.5 anode CS = 1.25, observed decreasing V_A (39 to 34.5 v), decreasing η_M, over one hour. No apparent cathode degradation. For 2 x 6.5 anode, CS = 0.8, observed degradation in 3 hour test: η_M from 94% to 69%, V_A from 44 v to 50 v. (P_C = 76 watts; cavity cathode was somewhat oversized for cathode chamber, had possible thermal shorts).
VGS-21	Continuation of VGS-20.	Observed some difficulty "reactivating" cathode, presumably because of high V_A near end of VGS-20. Ran 2 hour test with 2 x 6.5 anode, CS = 1.25 (P_C = 80.5 watts)

	Initial	After 2 hours
V_A (volts)	33	31
η_M (%)	91.5	90.5
η_A (ev/ion)	405	407

Table 2.4-6

Performance of Variable Geometry Source (Unmodified)

Test No.	VGS-23	VGS-23	VGS-24
Tank Pressure, Beam On (torr)	10^{-5}	10^{-5}	NR
Anode Length x Width (mm)	6.5 x 3	6.5 x 3	6.5 x 2.9
Cathode Slit Width (mm)	3.0	3.0	1.8
Cathode Voltage (volts), Current (amps)	6.45, 4.6	6.45, 4.6	7.3, 4.9
Cathode Power, P_C (watts)	29.7	29.7	35.8
Cathode Temperature (°F)	1730	1730	1840
Cathode Current Density (amp/cm^2)	1.7	1.7	2.9
Hg Feed Rate (eq. Hg^+ ma), I_F	88.5	88.5	88.5
Source Current, I_S (ma)	80	85	80
Mass Utilization, $\eta_M = I_S/I_F$ (%)	90.5	96	90.5
Arc Voltage (volts), Current (amps)	32, 1.28	37.5, 1.32	30, 1.3
Arc Power, P_A (watts)	41	49.5	39
Arc ev/ion, η_A	513	782	488
Cathode ev/ion, η_C	372	350	447
$\eta_A + \eta_C$ (ev/ion)	885	832	935
Magnet Current (amps)	5.5	5.5	5.5
Accel Voltage (kv), Current (ma)	17.2, 1.0	17.2, 1.0	18.4, 1.0
Accel Power, P_{Acc}, (watts)	17.2	17.2	18.4
Decel Voltage (kv), Current (ma)	5.0, 5.6	5.0, 5.4	5.0, 5.3
Decel Power, P_{Dec}, (watts)	28.0	27.0	26.5
I_{SP} (sec)	7070	7070	7070
Beam Power, $P_B = V_{Dec}\ I_S$ (watts)	400	425	400
Power Efficiency, η_P, (%) $\left[\eta_P = P_B/(P_B + P_A + P_C + P_{Acc} + P_{Dec})\right]$	77.5	77.5	77.0
Rocket Efficiency, $\eta_R = \eta_M\ \eta_P$ (%)	70.0	74.5	69.6

from the test facility; that is, changes in anode geometry were made under engine operating conditions and the resulting effect upon performance immediately determined. As it turned out, however, the feature of a variable-length anode required a tapered anode construction, with the anode wider at the entry (cathode) end than at the exit (extraction) aperture. Prior to the construction of the variable geometry source, all other bombardment ion sources tested at TRW had parallel-wall anodes. Since the experimentation with the variable geometry source had, by this point, shown the performance to have a fairly broad optimum for (tapered) anode lengths of about 5 to 7 mm, it was decided to modify the variable-geometry-source anode so that its walls would be parallel, of fixed length (6 mm), but variable in width (separation) between about 1 and 6 mm in order to determine the effect, if any, of tapered anodes.

Initial tests of the modified source (VGS-26, -27, -28) quickly established that anode widths of 2.5 to 3.0 mm have good performance; anode spacings less than 2.0 mm or greater than 3.5 mm resulted in poor operation. The performance difference between parallel and tapered anode walls was slight, with no clear-cut advantage for either configuration, except that the parallel-wall anode invariably required higher magnet currents, more current being required for narrower anode channels. This was not unexpected, since the useful portion of the magnetic field was basically a fringing field, more of which was available in tapered anodes of wider separation. (It should be noted the permanent-magnet engine designed for extended testing had a tapered anode of 3 mm (exit) width so as to achieve maximum utilization of the permanent magnets with minimum weight). Some of the results obtained with the modified variable geometry source (parallel anode walls) are listed in Table 2.4-7. All the data of Tables 2.4-6 and 2.4-7 was obtained using the same cathode; that is, the anode modifications were made without requiring a change of cathode.

The final tests made under the program with the variable geometry source (VGS-29, -30, -31) tested a new cathode composition under conditions of engine operation. The cathode stock (No. 40) was 30 per cent emission carbonate (by weight). Limited operation of this cathode in the variable geometry source established that the cathode performance was considerably less satisfactory than was obtained with the 20 per cent carbonate cathodes used previously. The cathodes were about average on a thermal basis (cathode surface temperature for input heater power) but displayed some nonuniformity characteristics and evidenced

Table 2.4-7

Performance of Modified Variable Geometry Source (Parallel Anode)

Test No.	VGS-27	VGS-27	VGS-28
Tank Pressure, Beam On (torr)	8×10^{-6}	5×10^{-6}	4.2×10^{-6}
Anode Length x Width (mm)	6 x 2.5	6 x 2.5	6 x 2.9
Cathode Slit Width (mm)	2.0	2.1	2.1
Cathode Voltage (volts), Current (amps)	7.85, 5.0	8.2, 5.3	7.6, 5.0
Cathode Power, P_C (watts)	39.3	43.5	38.0
Cathode Temperature (°F)	1800	1860	1800
Cathode Current Density (amp/cm^2)	2.6	2.2	2.2
Hg Feed Rate (eq. Hg^+ ma), I_F	88.5	88.5	88.5
Source Current, I_S (ma)	84	80	80
Mass Utilization, $\eta_M = I_S/I_F$ (%)	95	90.5	90.5
Arc Voltage (volts), Current (amps)	32.5, 1.32	32, 1.15	32, 1.17
Arc Power, P_A (watts)	42.9	36.8	37.4
Arc ev/ion, η_A	510	460	468
Cathode ev/ion, η_C	468	544	475
$\eta_A + \eta_C$ (ev/ion)	978	1004	943
Magnet Current (amps)	15	15	13
Accel Voltage (kv), Current (ma)	17, 1.0	17.4, 0.57	18.0, 0.55
Accel Power, P_{Acc}, (watts)	17	9.9	9.9
Decel Voltage (kv), Current (ma)	4.6, 3.0	4.9, 0.53	4.8, 0.28
Decel Power, P_{Dec}, (watts)	13.8	2.7	1.35
I_{SP} (sec)	6780	7000	6930
Beam Power, $P_B = V_{Dec}\ I_S$ (watts)	386	392	384
Power Efficiency, η_P (%) $\left[\eta_P = P_B/(P_B + P_A + P_C + P_{Acc} + P_{Dec})\right]$	77.5	80.8	81.7
Rocket Efficiency, $\eta_R = \eta_M\ \eta_P$ (%)	73.7	64.7	65.4

less emission current than the more conventional cathodes operating at the same temperature. Cathode temperatures from 2050 to 2200°F were necessary for satisfactory arc operation.

2.5 Conclusions

The experimental source studies carried out under the program with the variable geometry ion source have established the influence upon ionization efficiency of the geometric parameters of the ionization chamber. As a result of these efforts, modes and conditions of engine operation have been established which, although not necessarily "optimum" from an efficiency standpoint, represent a reasonable compromise between engine power efficiency, propellant utilization, and cathode life. Based on these determinations a permanent magnet engine was designed, constructed, and tested.

During the course of the program, a wealth of data was obtained with the variable geometry source. Apart from a few points of doubtful accuracy the data obtained showed excellent consistency relative to the variation of the geometric parameters of the source. The day-to-day reproducibility of data for the same "geometry" was remarkably good, considering the virtual impossibility of exactly duplicating all the parameters and conditions involved.

Early in the program it had become evident that the achievement of propellant utilizations of 95 per cent together with good arc power efficiency almost invariably required arc voltages of 35 to 40 volts, a range in which sputtering damage could be expected severely to limit cathode life. Propellant utilizations of 90 per cent, on the other hand, could be obtained at somewhat lower voltages. For either level of mass utilization it had been observed that ionization efficiency could be traded for arc voltage, that is, that lower voltage arcs could be obtained, but at the expense of more power per generated ion. Efficient engine operation at an arc voltage of 30 volts or less was highly desirable. (The 30 volt figure is somewhat in excess of the commonly accepted sputtering threshold for mercury arcs, but represents the approximate voltage level at which an oxide cathode was operated for over 100 hours in an extended engine test under Contract NAS3-2522 and for over 300 hours in the present work.) It was felt, furthermore, that the simultaneous attainment of lower arc voltage and acceptable efficiency should be possible by reducing the cathode losses. In

many instances, the cathode heating power was found to constitute half (if not more) of the total power required to generate an ion. Cathodes of increased efficiency (that is, high emission current densities for a given temperature plus reduced cathode thermal losses) were fabricated and led to substantially improved engine power efficiency.

The engine design optimization process, therefore, resulted in a trade-off between arc ionization efficiency and arc voltage, at an approximately fixed level of propellant utilization. The lower arc voltage had two beneficial effects, namely the promise of increased cathode life and a probably lower percentage of doubly ionized propellant. Based upon the limited data available in the latter area (Reference 3), it may be shown a 40 volt arc at 96 per cent utilization and a 25 volt arc at 92.5 per cent utilization yield the same singly-ionized beam, other factors being equivalent.

The fact that arc voltages in excess of the sputtering threshold were consistently required remains a problem. The results of the cathode testing using the variable geometry source are somewhat inconclusive. For both the flat and a sawtooth cathode the trend toward increasing arc voltages with time has been observed. For arc voltages above 35 volts the trend was evident in times less than 35 minutes but was a function of the cathode input power. Increasing the cathode power from 40.8 watts to 51.5 watts increased the time (from 35 minutes to two hours) for the arc voltage to change from the initial value to approximately 46 volts. The cavity cathode indicated improved stability relative to the sawtooth cathode; however, this result must be qualified since the two cathode types were fabricated from different cathode lots and increased heater power was required for the cavity cathode as described on page 33. In general it was impossible to determine whether the observed degradation was the result of cathode sputtering, insufficient activation, propellant starvation, poisoning, or some other cause.

Finally it should be mentioned that during the course of the VGS tests, only one extraction system was used. The system employed was basically that developed under Contract NAS3-2522 and previously reported (Reference 2). No components of this accel-decel structure ever required repair or replacement, apart

from periodically brushing out metallic flakes which caused shorting. When considered in the light of the continual and sometimes severe testing to which the system was subjected, the extraction system performance was excellent. For example, in some instances source geometry changes were made which led to badly defocused beams causing direct beam impingement upon the extraction electrodes. Despite these adverse conditions, the extraction system performance left little to be desired

3.0 CATHODE STUDIES

3.1 Introduction

The cathodes used throughout the program were dispenser cathodes consisting of nickel matrices impregnated with alkaline earth oxides. The cathode studies were undertaken to:

1. insure the availability of cathodes having adequate performance for the ion-engine parameter studies,
2. determine what might be done to improve their performance in the ion-engine environment.

The first goal was essentially accomplished when it was discovered that the batch of alkaline-earth carbonates used in fabricating the cathodes was contaminated. A new batch was obtained, and a high percentage of the cathodes produced since then have been good emitters. A set of fabrication and activation procedures which have resulted in good cathodes has been developed. The second objective resulted in suggested geometries to increase cathode lifetime and decrease cathode-heater power.

3.2 Cathode Fabrication and Activation

3.2.1 Ingredients, Mixing and Pressing

The cathodes were of the dispenser type having a nickel matrix base impregnated with BaO, SrO, CaO, and an activator, ZrH_2 (Reference 4). Inco Grade A carbonyl nickel powder (4-7 micron particle size), G.E. triple carbonate powder (No. 118-5-2; 57% $BaCO_3$, 39% $SrCO_3$, 4% $CaCO_3$), and Metal Hydrides Inc. zirconium hydride powder were blended in a twin-cone blender for thirty minutes, ball-milled in a porcelain ball mill for twenty hours, and passed through a 40-mesh screen. The usual composition was 79% Ni, 20% (Ba, Sr, Ca) CO_3, and 1% ZrH_2, although a few were made with 69% Ni, 30% (Ba, Sr, Ca) CO_3, and 1% ZrH_2. The mixture of powders was then hydrostatically pressed to 40,000 pounds per square inch into slugs approximately 3/4 inch x 3/4 inch x 4-1/2 inches.

Limited use was made of cathodes fabricated by Ion Physics Corp. and furnished by NASA-Lewis. The composition of these was 79% Ni, 20% (Ba, Sr, Ca) CO_3 and 1% ZrH_2. They were compressed into slugs of approximately 1/2 inch in diameter and 2-1/4 inches in length.

3.2.2 Sintering

The TRW-fabricated cathodes were usually sintered in hydrogen and nitrogen atmospheres. An H_2 atmosphere was used while heating the slug to 815°C, and an N_2 atmosphere was used while heating the slug to 980°C and subsequently cooling it to room temperature. A Marshall tube furnace containing an "inconel" tube 1-1/2 inches in inside diameter and 36 inch in length was used for gaseous-atmosphere sintering. The temperature varied from room temperature at the ends of the tube to 980°C over a two-inch zone at the center of the tube. The slugs were cut to approximately 2-1/8 inches in length and were placed on a piece of (CaO-stabilized) ZrO_2 in an Inconel boat which was pushed through the furnace in steps with a stainless-steel rod fed through an O-ring seal. The gas flow rates were 310 standard cubic inches per minute for the hydrogen and 83 standard cubic inches per minute for the nitrogen. After leaving the furnace, the gas was passed through a bubbler containing a low-vapor-pressure liquid to prevent back-diffusion of air.

Some of the TRW-fabricated cathodes were sintered in vacuum. Various slug sizes were cut from the pressed slugs (of dimensions 3/4 inch x 3/4 inch x 4-1/2 inches), fitted with a nickel foil radiation shield, and suspended inside the radio-frequency coil of a 30 kilowatt induction heater.

The sintering procedure used by Ion Physics Corporation is not known in detail by us and, therefore, will not be reported here.

3.2.3 Machining

It was considered necessary to take precautions to prevent surface contamination during machining and subsequent handling. Therefore, all cathode machining and handling equipment was washed with acetone and rinsed with alcohol before each use. Disposable nylon gloves were used when handling tools could not easily be used.

Various sizes and shapes of cathodes were machined. Most of these were approximately 1-15/16 inches long. The geometries used are shown in Figure 3.2-1 with typical dimensions shown in inches.

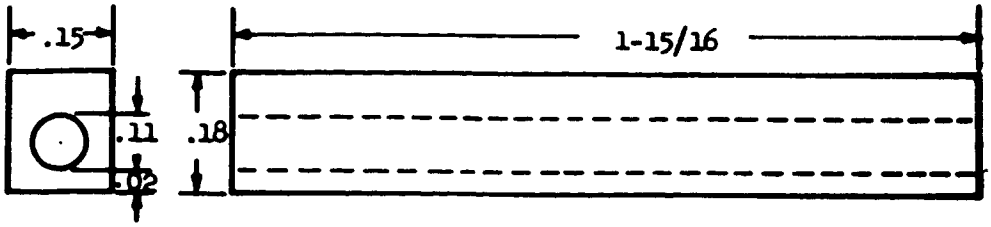

Flat Cathode

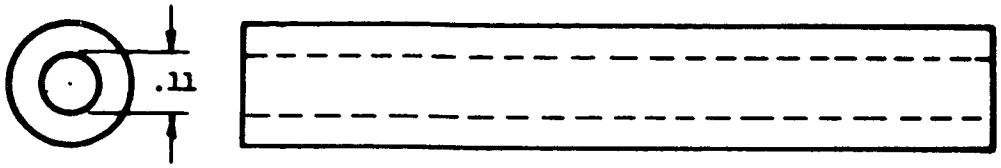

Cylindrical Cathode

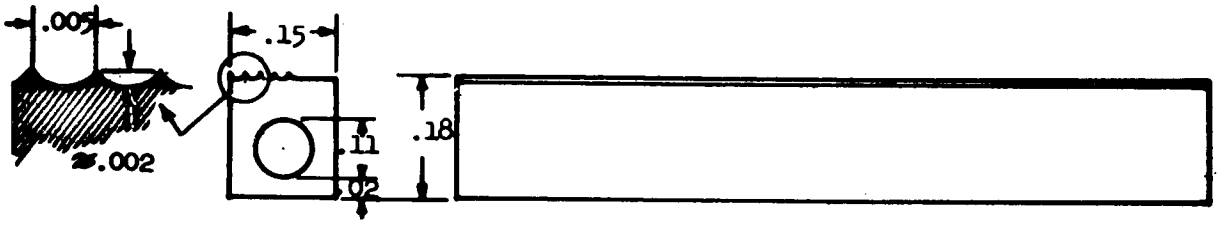

1/2-Grooved, 1/2-Flat Cathode

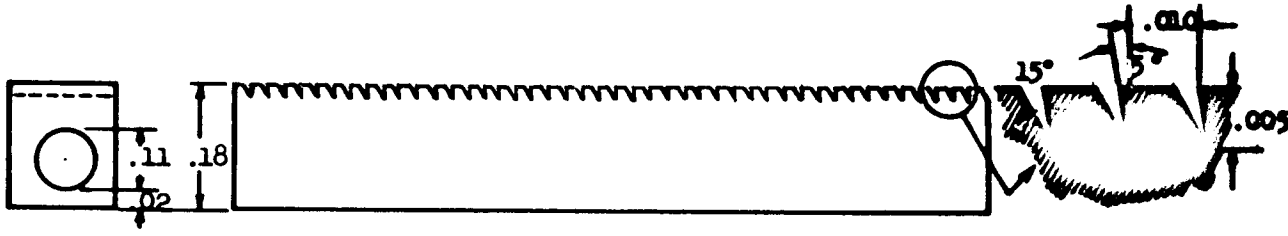

Sawtooth Cathode

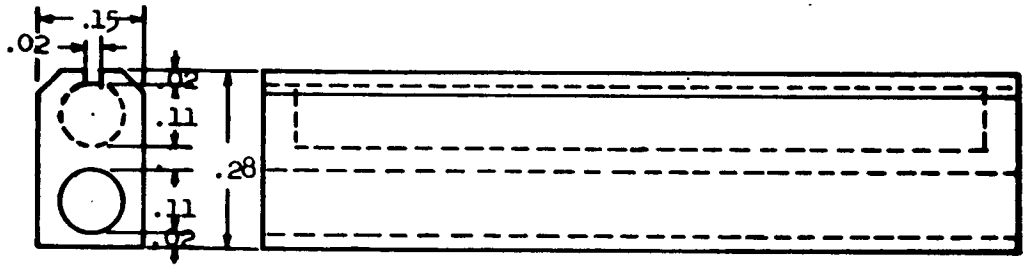

Cavity Cathode

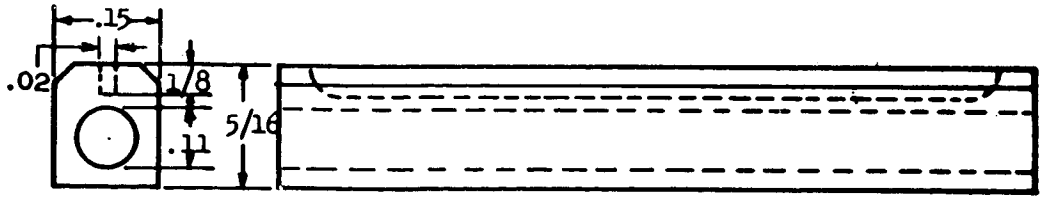

Slotted Cathode

Figure 3.2-1

Cathode Geometries

3.2.4 Mounting

After machining, the cathodes were fitted with heaters, heat shielding, and sometimes alumel-chromel thermocouple junctions. The heaters were manufactured by Pemco Inc. by placing Al_2O_3 beads on two 0.010-inch tungsten-rhenium wires, then slipping a nickel tube over the beads, and swaging the assembly down to an outside diameter of 0.110 inch. The heaters also served as the cathode-supporting members.

Two basic types of heat shielding were used. One type consisted of several layers of 0.005-inch nickel foil which was dented in spots to separate the layers. The other type of shielding consisted of alternate layers of 0.001-inch nickel foil and quartz fiber (Linde SI-4) with a piece of 0.005-inch molybdenum foil on the outside to hold the shielding on the cathode.

3.2.5 Activation

Activation consists of evolving CO_2 from the carbonates remaining after sintering, transporting the oxides to the surface, and probably forming some free barium at the surface. Only after activation is the cathode a suitable electron emitter. Activation was accomplished by heating the cathodes to between 1000°C and 1050°C and pumping the evolved gas away. Three different activation environments were used:

1. the mercury-vapor diode environment in which the pumping speed was fairly small but an arc voltage was easily applied for determining the extent of activation,
2. a high-vacuum environment in which the pressure could easily be maintained below 10^{-5} torr during activation but no current could be drawn from the cathode, and
3. the environment of the ion-engine test facilities in which the pressure could be held low and a continuous current could be drawn from the cathode, indicating the degree of activation.

3.3 Cathode Testing Methods

3.3.1 Mercury-Vapor Diode

The mercury-vapor diode test chamber is shown schematically in Figure 3.3-1. This chamber was placed inside a bell jar evacuated by a mercury

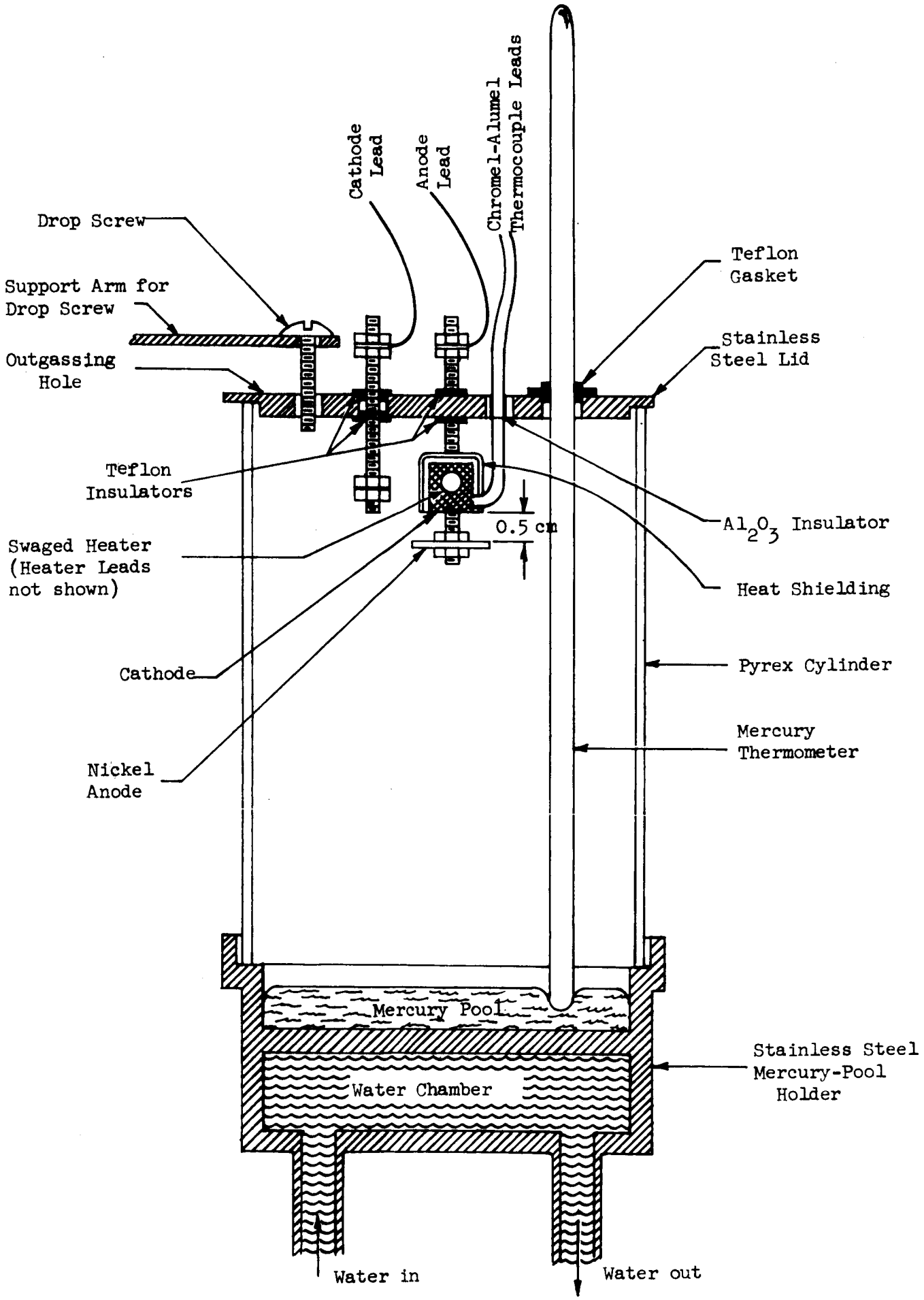

Figure 3.3-1

Schematic, Cross-section View of Mercury-vapor Diode Test Chamber

diffusion pump. During activation, outgassing of the cathode was accomplished through the outgassing hole shown in the figure. After activation was complete, the hole could be closed by rotating the drop-screw support arm, allowing the drop screw to fall and close the hole. With the hole closed, mercury was not continually pumped away and the mercury pressure was approximately known, viz., the vapor pressure of mercury at the measured pool temperature. This temperature was a function of the temperature and mass flow of the water and, to some extent, of the thermal conditions at the diode at the top of the chamber. The water temperature could be varied from tap water temperature to 100°C, and the mass flow was controlled by the laboratory water-main pressure and a needle valve.

The cathode was heated by means of the tungsten-rhenium filaments imbedded in the swaged heater. The heater leads are not shown in Figure 3.3-1, but they were connected to the low-voltage side of an 11 volt, 10 ampere filament transformer which was driven by a variable autotransformer and a constant-voltage transformer. The temperature of the cathode was sensed by the thermocouple shown in the figure. The thermocouple voltage was placed across an Assembly Products Inc. pyrometer in series with a total resistance of approximately 10 ohms (when the junction temperature was 1000°C). In addition, measurements of the sight temperatures of the cathode were made by means of an optical pyrometer.

The diode was driven by the circuit shown in Figure 3.3-2. The usual excitation voltage E was alternating at 60 cycles per second, but occasionally a DC voltage was applied. The 100 milliampere DC milliammeter was used to observe the cathode emission during the activation process. When the rectified-average-current exceeded 100 milliamperes, the milliammeter was switched out, and the 3 ampere DC ammeter indicated the rectified-average current. The current-limiting resistor R was normally a 25 ohm resistor, but on one occasion a 2 ohm resistor was used to obtain higher currents. It is usually desirable to make R of the order of the diode resistance to obtain stable operation. When E was an alternating voltage the current-voltage characteristic of the diode was traced on the oscilloscope screen since a voltage proportional to the instantaneous diode voltage was impressed on the vertical deflection plates and the instantaneous diode voltage was impressed on the horizontal deflection plates. When E was a DC voltage the diode current was indicated by the ammeter

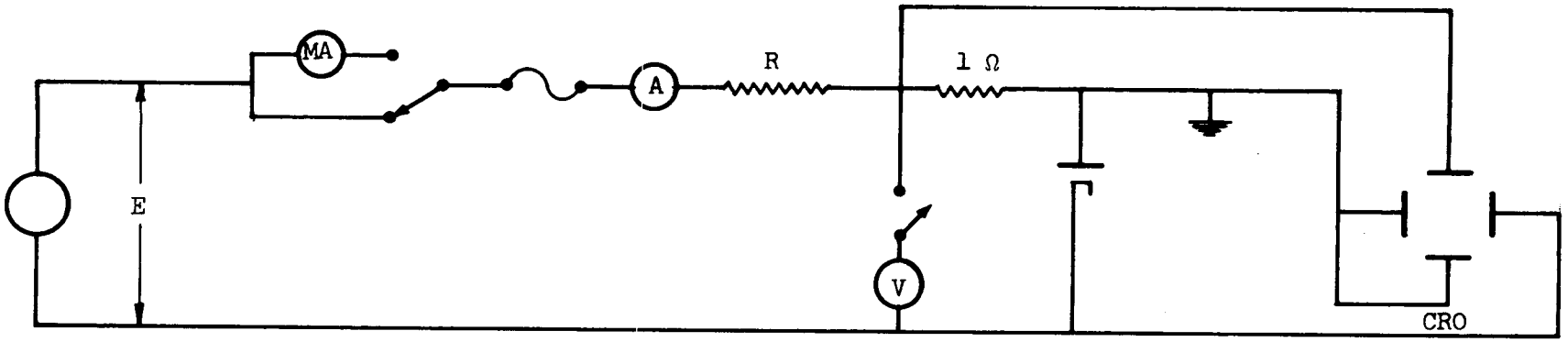

Figure 3.3-2

Circuit for Driving Mercury-Vapor Diode

and although the DC voltmeter was inadvertently connected across both the diode and the 1 ohm resistor, the diode voltage could be obtained by correcting its readings for the extra voltage drop.

A Bausch and Lomb spectrophotometer was used in conjunction with the mercury-vapor diode to observe the light-emission spectrum of the discharge. While an image of the discharge was focused on the entrance slit of the spectrophotometer, it recorded the spectrum between the wavelengths of 3500 angstroms and 6500 angstroms.

3.3.2 Variable-Geometry Ion Source

Cathode data were obtained for cathodes installed in the variable-geometry ion source, described in Section 2.3. A DC discharge was usually drawn. The measurable parameters included discharge voltage and current, cathode heater voltage and current, cathode temperature, cathode sight temperature, mercury mass flow, and magnet currents. The variable-geometry-source cathode studies were usually of much shorter extent than the mercury-vapor diode studies, but they provided data for the cathodes in the ion-engine environment.

3.3.3 Extended-Test Ion Engines

Cathode data were also obtained from cathodes mounted in the extended-test ion engines (cf. Section 4.2 for a description of the extended-test facility). The measurable parameters were the same as for the variable-geometry ion source except for the cathode temperature (the temperature was measured optically instead of by utilizing thermocouples as in the variable-geometry source) and the use of permanent magnets instead of the electromagnets of the variable-geometry source.

3.3.4 Heat-Transfer Study

The high-vacuum system, mentioned in Section 3.2.5 as a cathode-activation system, was also used for a heat-transfer study. This system which is pumped by an oil diffusion pump consists of a bell jar and base plate. The cathode was heated in the usual manner except that no constant-voltage transformer was used. Chromel-alumel thermocouple junctions were attached to the cathode and the outer radiation shield. The thermocouple voltages were

each applied to the series combination of an Assembly Products Inc. pyrometer and approximately 10 ohms. Optical pyrometer readings were taken at various locations on the cathode, heater, and leads to estimate thermal losses from the cathode assembly.

3.4 Test Results and Conclusions

The cathode studies have demonstrated that good cathode performance can be obtained from porous nickel dispenser cathodes when the fabrication and operation procedures described here are used. Four typical AC operating points for a sawtooth cathode in the mercury-vapor diode are:

0.34 amperes/cm^2 at 36 volts, 940°C, 0.042 torr Hg pressure,
0.37 " " " 34 " , 910°C, 0.031 " " " ,
0.53 " " " 34 " , 950°C, 0.052 " " " ,
2.1 " " " 13 " , 915°C, 0.048 " " " ,

and a typical DC operating point for a flat cathode in an extended-test engine (ET-1) is:

0.43 amperes/cm^2 at 34 volts, 925°C, 78.5 milliamperes Hg feed

after 35 hours of operation. We cannot draw any conclusions at this time about cathode lifetimes. The flat cathode just mentioned was operated at:

0.43 amperes/cm^2 at 30 volts, 1080°C, 75.8 milliamperes Hg feed

after 326 hours of operation. Thus the increased temperature necessary to obtain the same emission indicates the possibility of cathode degradation. However, the sawtooth cathode mentioned above showed no apparent degradation; the second data point given above for that cathode was obtained 460 hours after the first data point.

3.4.1 Composition

The importance of using uncontaminated emission mix has been amply demonstrated. In a previous ion-engine program a series of very poor cathodes was fabricated before finally buying a new quantity of emission mixture. The cathode performance quickly improved, and it was concluded that the original batch of carbonates had become contaminated. However, the conclusion was not remembered by the personnel mixing and pressing the cathode material, and when

the new jar became empty, the original emitter mix batch was reverted to. Again bad cathodes resulted, but the performance quickly improved when a new batch of emission carbonates was used.

No conclusions can be drawn about the effect of varying the cathode components; what can be stated is that the usual composition, viz.,

79% carbonyl nickel power (4-7 microns),
20% G.E. triple carbonate powder No. 118-5-2,
1% zirconium hydride,

is satisfactory but not necessarily optimal. Some cathodes containing 30% (Ba, Sr, Ca) CO_3 were made late in the program, but they were not used. Longer lifetimes might be expected of such cathodes because of increased oxide inventory and larger pore sizes.

3.4.2 Sintering Method

Some of our cathode material has been noticeably non-uniform in appearance, hardness, and initial emission. (The emission can usually be made more uniform by the application of a discharge voltage approximately 30 volts). It is suspected that these non-uniformities are due to the non-uniform environment seen by the slug during sintering. A furnace tube of larger diameter would reduce the temperature difference across the slug by allowing the slug to be pushed sideways, rather than lengthwise, through the tube. Another possibility is the use of the induction furnace, in which the temperature of the slug is varied by varying the heater power rather than by moving the slug through thermal gradients. The induction furnace was occasionally used for vacuum sintering during this program, and although sintering in vacuum facilitated, the observation of CO_2 evolution, it required a much slower sintering schedule to prevent cracking the slug than was required by the gaseous-atmosphere method. Therefore, it is suggested that a cover gas at approximately one atmosphere be used with future induction-furnace sintering. It is not obvious that it is necessary to use hydrogen as used in Reference 4; possibly the use of nitrogen throughout the sintering schedule is as effective as the presently used combination of hydrogen followed by nitrogen at the upper temperatures.

3.4.3 Machining Method

The flat cathode geometry, shown in Figure 3.2-1, was the most commonly used cathode shape. The outer surface, including the emitting face, was shaped by a milling machine. This type of cathode usually required a few hours of activation before full emission could be obtained. When two cylindrical cathodes required very short activation times, however, it suggested that the lathe tool used to form the cylindrical cathodes might have some special advantage over the mill used to form the flat cathodes. It presented the possibility that the use of the lathe tool was resulting in open pores while the mill tended to close them and that the longer activation times for the flat cathodes were because of the reduced open pore area. Therefore, the 1/2-grooved, 1/2-flat cathode was fabricated (cf. Figure 3.2-1). Half of its emitting surface was milled in the usual way and half consisted of longitudinal grooves cut by a lathe tool in a shaper operation. The cathode was tested in the mercury-vapor diode, and no difference in arc intensity associated with the two surfaces was observed (although there were differences in arc intensity along the length of the cathode). Later several sawtooth cathodes were made by a shaper operation. These did not show particularly rapid activation either. Thus, there was no explanation for the extremely short activation times of the two cylindrical cathodes.

3.4.4 Activation Method

It was observed that activation times for cathodes in the mercury-vapor diode were much longer than those for cathodes in the environment of the ion engines. Probably this was because of the much greater pumping capacity of the ion engine systems (recall that the mercury-vapor chamber had only a small hole for outgassing) which allowed the CO_2 to be evolved at a greater rate. Therefore, the high-vacuum system described in Section 3.2.5 was set up to activate cathodes before they were placed in the mercury-vapor diode. A cathode was heated to 1010°C in the high-vacuum system while the pressure was held below 2×10^{-5} torr. It was then transferred to the mercury-vapor diode and required considerably less emission time than previously for full activation.

Another reason for setting up the high-vacuum system was to activate the Ion Physics Corporation cathodes according to their recommendations. These cathodes

were originally obtained as substitutes for ours which were not performing well (because of contaminated carbonates, cf. Section 3.4.1). However, they required such long activation times that little use was made of them, and our cathode problem was solved before the high-vacuum system was set up. Thus the Ion Physics Corporation cathodes were never fairly tested. It might be of interest to note here the procedure used by Ion Physics Corporation for their cathode activation (Reference 5). They first outgas them at about 10^{-6} torr for 24 to 72 hours at room temperature. Then the temperature is increased to about 1050°C while the pressure is held to less than 10^{-5} torr. After the cathode has been held at the upper temperature for an hour, it is allowed to cool. Finally, the chamber is purged with dry nitrogen at a pressure greater than 10^{-4} torr before exposure to air. One more comment should be made about the Ion Physics Corp. cathodes. In our attempts to activate them, a black material was given off by them and deposited on the walls of the surrounding chamber. Spectrographic analysis of the material deposited on a nickel anode showed the presence of nickel and carbon. Thus the carbon was throught to be arc-dissociated CO_2 from the incompletely-activated cathode. The nickel might not have been part of the deposited material since the base material from which the sample was taken was nickel. However, nickel deposits can be expected from a cathode operated for several days at a temperature of say 1050°C where the vapor pressure of nickel is about 0.7×10^{-6} torr. Nickel was probably the major component of a black material deposited inside the high-vacuum activation system when a cathode was held at 1010°C for several days; this deposit was ferromagnetic, and since there was no discharge it is doubtful that carbon was formed in that instance.

3.4.5 Cathode Shape

Since high propellant utilization seems to require the use of a discharge voltage well over the sputtering threshold for oxide-film cathodes (22 volts), it has been feared that the cathode lifetime would be severely shortened by the sputtering loss of Ba and BaO. Therefore, the cavity, slotted, and sawtooth geometries were suggested; these geometries might conceivably be less damaged by operation at high discharge voltages. As noted in the introduction to Section 3.4, no obvious degradation of a sawtooth cathode occurred in 460 hours in the mercury-vapor diode. However, the operating conditions varied rather widely during this time, and so one should not expect to observe

sputtering damage until the BaO supply was gone. A gradual degradation because of sputtering damage could only have been observed if the cathode voltage, mercury pressure, and cathode temperature had been kept reasonably constant. Otherwise, the emissive film would be quickly restored by the uncontrolled increases in cathode temperature. The basic difficulty with this experiment was that, in attempting to operate at high voltages, the arc power was the primary cathode heating source. This was an unstable operating condition since any change in cathode temperature produced a change in emission which changed the temperature still further in the perturbed direction. An attempt was made with the same cathode to observe barium emission lines in the discharge spectrum using the Bausch and Lomb spectrophotometer and a DC discharge. The principal lines could not be positively identified in the spectrum even at 70 volts, 0.53 amperes/cm^2, 1030°C, and 0.666 torr mercury pressure.

It is interesting to note that the sawtooth cathode in the mercury-vapor diode did not exhibit the marked degradation shown by the flat cathode in the extended test engine ET-1 (cf. introduction to Section 3.4). There were, however, several differences between these two tests. Perhaps the most important difference was the deposition on the cathode of tantalum from the extraction electrodes. A spectrographic analysis of the cathode surface after 334 hours of operation is given in Table 3.4-1. Possibly the tantalum deposit was the emission inhibiting means and the cathode lifetime could be lengthened by using a different extraction electrode material. Other differences between the two cathodes were that: (1) the ET-1 flat cathode was operated in a DC discharge while the sawtooth cathode was operated with an alternating voltage and spent only about a fourth of its time above 22 volts, (2) the mercury pressure was probably higher for the sawtooth cathode, and (3) the difference in shape. We have not yet run flat cathodes at high voltages in the mercury-vapor diode system. Therefore, at present, we cannot say what caused the degradation of the extended-test cathode or whether such degradation can be avoided in the future.

Table 3.4-1

Spectrographic Chemical Analysis of Cathode Surface After 334 Hours of Operation in Extended Test ET-1

Range	Element
Major > 10%	Ni
Near Major 5-25%	Ba, Ta
Minor 1-10%	Zr
Near Minor .5-5%	Sr
Low .1-1%	Al, Ca
Low-Very Low .05-.5%	Si
Trace .01-.1%	Cu, Mn, Mg, Mo
Strong Trace .005-.05%	Fe, Na
Weak Trace < .01%	Cr, Co

Not Detected: Ti, V, Bi, Pb, Sn, Ag, Sb, As, B, Zn, K, Li, Ce, Cb, W.

The cavity cathode and the slot cathode depicted in Figure 3.2-1 were tested both in the variable geometry engine and in the mercury vapor diode of Figure 3.3-1. In both cases poor performance characteristics were observed. It is believed the poor characteristics were due not to the presence of the cavity but rather to the poor emission capability of the cathode material used at that time (Ion Physics stock). Important information nevertheless was obtained from this testing; due to the physical nature of impregnated porous nickel cathode material, considerable warpage of the cavity shape is encountered upon thermally cycling the cathode. In all cavity cathodes tested some portion of the slit associated with the cavity closed up. It is not known if the slit closure occurred during heat up, during the period at elevated temperature, or during cool down. Simple thermal analysis has led to the suspicion, however, that the closure probably occurs during cool down. From this limited information no evaluation of the cavity cathode can be made except that even if acceptable emission parameters were displayed by virtue of its cavity the slit closure for this approach to the cavity design would make it unsuitable.

Photomicrographs of the ET-1 cathode are shown in Figures 3.4-1, 3.4-2, 3.4-3, and 3.4-4. These are magnifications of 35x, 100x, 250x, and 250x respectively of the cathode cross-section. Figure 3.4-1 shows the swaged heater and the edge of emitting surface. Apparently the size of the pores just below the surface is much less than that of the pores farther inside the cathode. Thus another possible explanation for the degradation in performance of this cathode is that the BaO concentration near the surface was reduced by evaporation and sputtering, allowing further sintering of the nickel, reducing the pore size, requiring higher temperatures for a constant BaO flow. However, this is the first cathode from which photomicrographs have been made, and it is possible that all flat cathodes have an apparent reduction of pore size near the surface because of stresses exerted during machining and/or preparing the surface for the photomicrograph.

3.4.6 Heat-Transfer Study

Heat-transfer measurements were made for two sawtooth cathodes in the high-vacuum system. One cathode had three 0.005 inch nickel shields; the other had alternate layers of quartz fiber and 0.001 inch nickel foil. One basic difference between the thermal environment of these cathodes and that in the ion engines was that these cathodes were supported by tantalum wires spot-welded to the heater sheaths instead of the lava pieces used in the ion engine. Another difference was that there was no arc heating of these cathodes. By measuring temperatures at various points on the cathodes, heaters, and connecting leads and by estimating the thermal conductivities and emissivities of the materials involved, it was possible to estimate the thermal loss contributions of the various paths. For each cathode almost half the thermal loss was radiation from the front surface. The next largest loss was through the shielding with the two types of shielding about equally effective. Thus it appears that the next step in reducing cathode-heating power would be to reduce the frontal area of the cathode, e.g., by using a slotted or cavity cathode and shielding all the frontal area except the emitting slot.

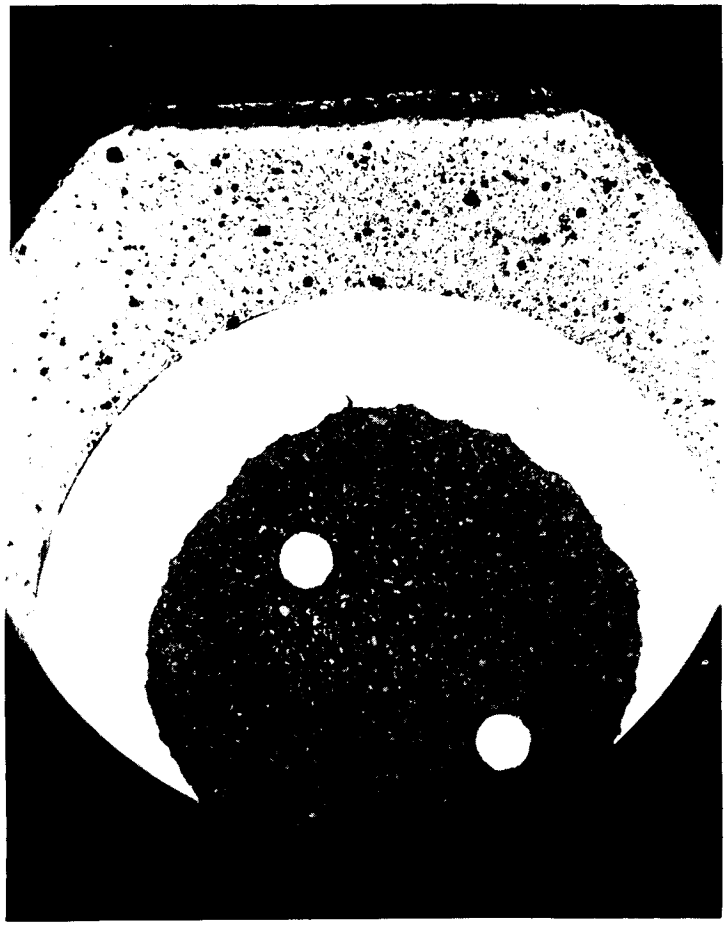

Figure 3.4-1
ET-1 Cathode Cross-Section, 35x

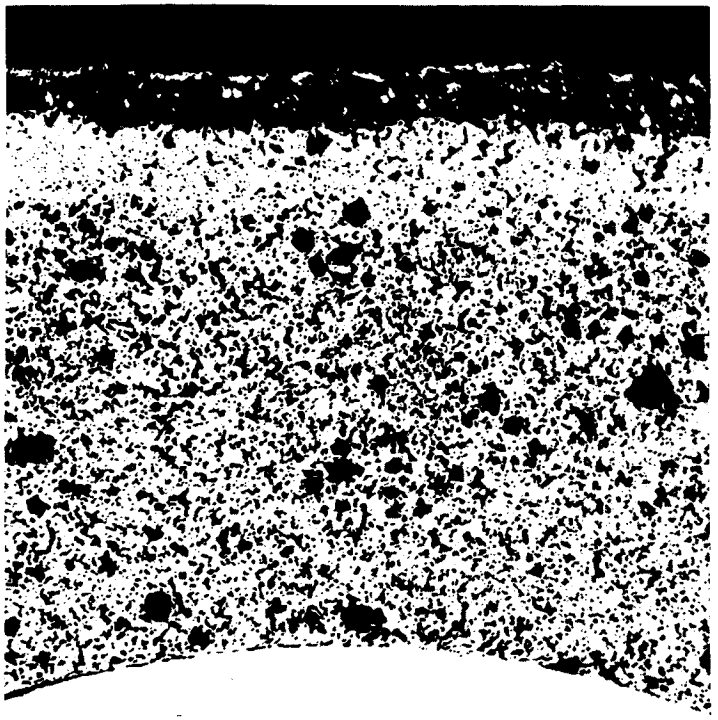

Figure 3.4-2
ET-1 Cathode Cross-Section, 100x

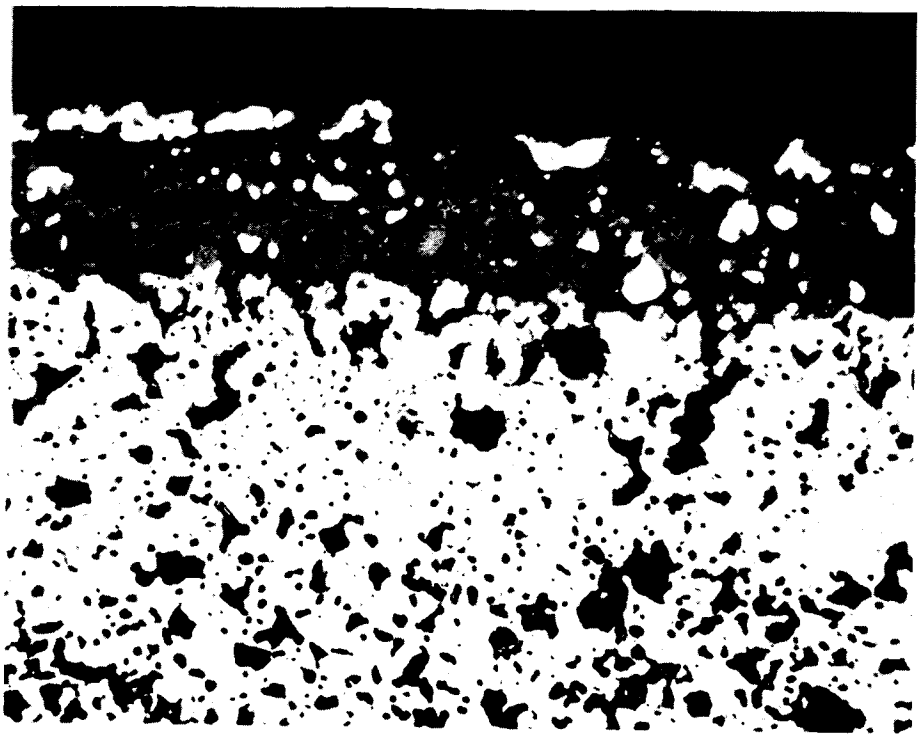

Figure 3.4-3

ET-1 Cathode Cross-Section, 250x

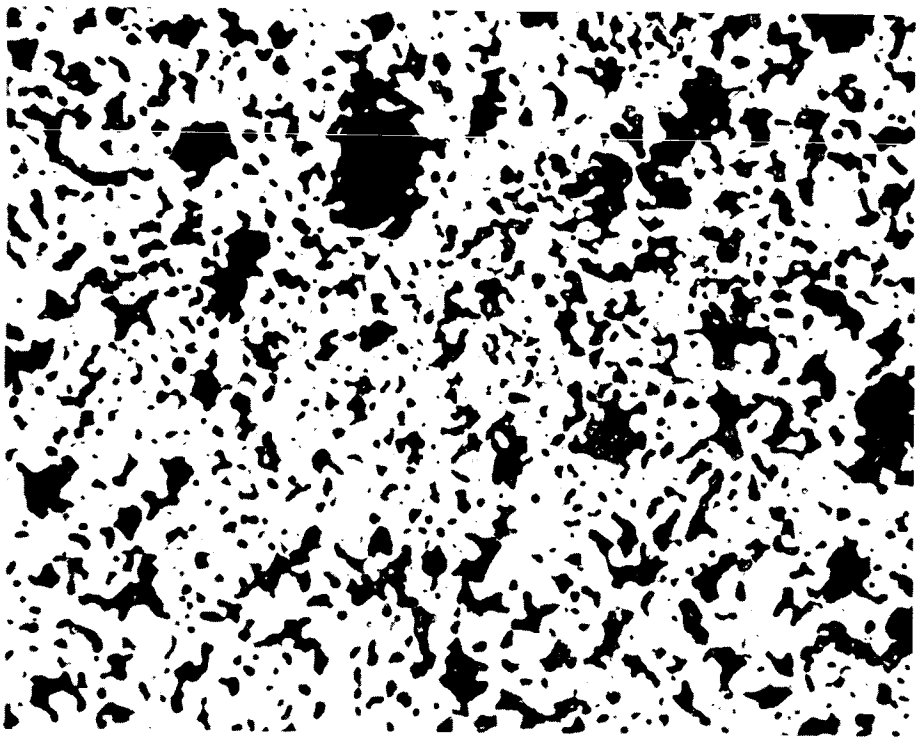

Figure 3.4-4

ET-1 Cathode Cross-Section, 250x

3.5 Summary

The cathode studies indicated that good initial cathode performance can be obtained from porous nickel, alkaline-earth oxide dispenser cathodes. Attention is called to the following points:

1. The (Ba, Sr, Ca) CO_3 mixture is apparently easily contaminated, resulting in poorly emitting cathodes.
2. Gaseous-atmosphere sintering can be accomplished much more quickly than vacuum sintering.
3. A larger tube furnace than was used in this program or an induction heater would probably provide more uniform sintering and hence more uniform hardness and initial emission.
4. Activation is best accomplished at low pressures. An acceptable procedure is to heat the cathode to approximately 1000°C holding the pressure below 10^{-5} torr. Then a voltage can be applied and activation should be complete within several hours.
5. The present configurations have a significant radiation loss from the emitting face. Perhaps this loss can be reduced by decreasing the frontal area.

The lifetime or the lifetime-determining mechanism of these cathodes in the ion-engine environment is not yet known. One flat cathode was run in an ion engine for 334 hours and showed considerable degradation in performance. On the other hand, another cathode having a sawtooth surface was run in the mercury vapor diode for 460 hours and displayed no degradation in performance. It is suspected that the deposition of tantalum onto the cathode in the engine environment was responsible for the performance degradation.

4.0 EXTENDED TESTING

4.1 Introduction

The program requirement for extensive testing of improved ion sources necessitated the preparation of a special test facility. This extended testing phase had originally been scheduled to include two 250 hour tests with the same source and extractor assembly. The extractor electrodes were to be weighed initially and then assembled into the ion source. After establishing proper high performance operation with the source, and (when possible) beam neutralization, a period of 250 hours of run time would be accumulated. At this point, the test was to be stopped, the electrodes weighed again, and photographed. The source was then to be reassembled and the second 250 hour run carried out. Later in the program a revision of the test objectives brought about a slight change in this test approach and this revised approach was in turn tempered by the actual test experience. The details of the overall extended testing activity are covered in Section 4.6.

In consideration of the relatively long term tests which were contemplated and the past experiences with similar extended tests, it was decided to completely rework the existing test vacuum chamber and support equipment, and to build a completely new instrument and control console to support the test program. The rework of the vacuum chamber included the design of high efficiency cold traps, the addition of a 300 gallon liquid nitrogen storage tank and dispenser controls, and the design of a deep well target or beam catcher. The instrumentation and control console was designed to serve several purposes. It incorporated precision (one per cent) meters for direct indication of source performance, and also a battery of low-speed strip-chart recorders to produce a continuous record of all test occurances. Finally the console metering was also coupled with a complete parametric type control and protection system which maintained all key operational set points and at the same time provided for automatic shutdown and recycle start-up in the event of a temporary malfunction of the system or source. The new test facility provided for precise data measurement, data recording, protection of the system and ion source in the event of malfunction, and relieved the project of the substantial expense of maintaining a round-the-clock work crew to monitor and adjust source performance. This automated approach allowed project personnel to continue other studies and tests directed

towards obtaining further refinements in source and extractor geometry and improved cathode configurations.

After the fabrication of the extended test facilities, the instrumentation and all control functions were checked out and the apparatus was used for testing a variety of extraction system geometries and in some neutralization tests; additional tests were conducted with the facility to establish the performance capabilities of the prototype permanent magnet ion source fashioned to incorporate all the design features and geometries established in the variable geometry source tests. This period of testing resulted in a few minor modifications and additions to the facility, and provided a thorough check-out of the equipment.

4.2 Test Facilities

The test facility which was built around a 2-1/2 foot diameter by 5 foot long vacuum chamber is shown in Figure 4.2-1. The high voltage power supplies which provide the extraction voltages and the liquid nitrogen storage tank are not shown. The ion engine was mounted directly in the vacuum chamber door and was fitted with extra long cables and water cooling lines to permit swinging the door open for examination and servicing of the source without removal from the door. The chamber was equipped with a 12-inch diameter view port on one side and an assortment of high voltage feed-through insulators to carry power to the structures and extraction electrodes within the vacuum chamber. The mechanical and diffusion pump system are to be seen below the main chamber along with the precision mercury propellant feed system mounted to the frame by means of a perforated channel.

The two consoles to the right of the chamber housed the complete automatic control and instrumentation system. The high voltage meters and control components were mounted on acrylic panels in the upper section of the left hand console. The lower section of this console housed the main relay logic circuitry and provided for the attachment of the high voltage power supply controls to the console. The high voltage power supplies and the arc voltage power supply (located in the lower right hand console) were motorized and controlled by means of the control boxes attached to lead cables and plugged directly into the left hand console. For manual operation these boxes could be removed and the power supplies activated by the appropriate toggle switches. By plugging

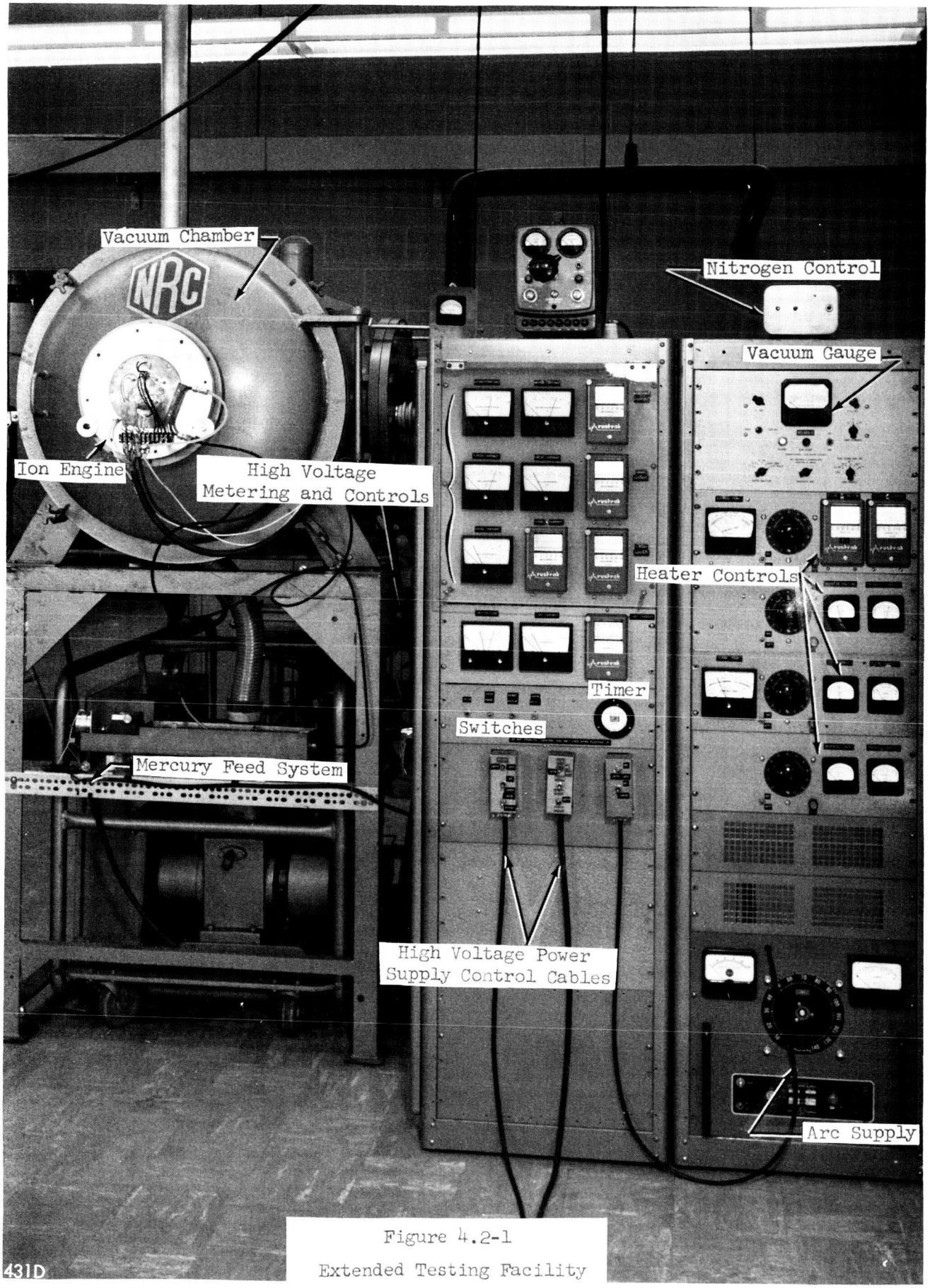

Figure 4.2-1

Extended Testing Facility

the control boxes into the console, operation became automatic and was controlled by relays acting within the console. The right hand console contained the low voltage heater supplies which serviced the arc cathode, vaporizer, transfer tube, and neutralizer cathodes. The top section also contained the vacuum gage controller. Located on top of the left hand console was a small bias power supply used only during beam neutralization tests. The small controller atop the right hand section is the liquid nitrogen feed regulator used to maintain the cold traps within the vacuum chamber at proper temperature.

Shown in Figure 4.2-2 are the deep-well beam catcher and chamber cold trap structure as they appeared at the conclusion of the 400 hour test run. The basic facility was also equipped with magnetically controlled shutters on the window to insure a clear view of the source throughout the test duration despite the sputtering which normally took place when the ion beam struck the catcher or other structures within the chamber. An optical pyrometer was used to measure the temperature of the cathode which could be viewed through the side port and a retractable motorized door on the beam catcher.

The design of the target or beam catcher was based upon previous experience with tests of long duration and the desire to make most efficient use of the vacuum system pumping capacity. Several problems had plagued earlier long term test activities because of the designs used in calorimeter type beam catchers employed in these tests. It had been found that the use of smaller targets in close proximity to the ion engine created problems due to the back-plating of sputtered target materials on insulators and electrode surfaces. Also it was suspected that the confinement of the beam (which ultimately reverted to neutral mercury atoms) in the vicinity of the extraction system might have caused an increase of the extraction system interceptions.

To best utilize the volume available in the vacuum system and to minimize the problems previously encountered, the target was made in the form of a deep well. This deep-well target was constructed of heavy aluminum tubing and machined to include several large pumping passages along the side region and a large annular pump-out region at the far end of the well. These openings were covered with an open aluminum screen to maintain the continuity of the potential field associated with the target. The side openings were also covered by motorized doors which were spaced away from the walls to facilitate pumping.

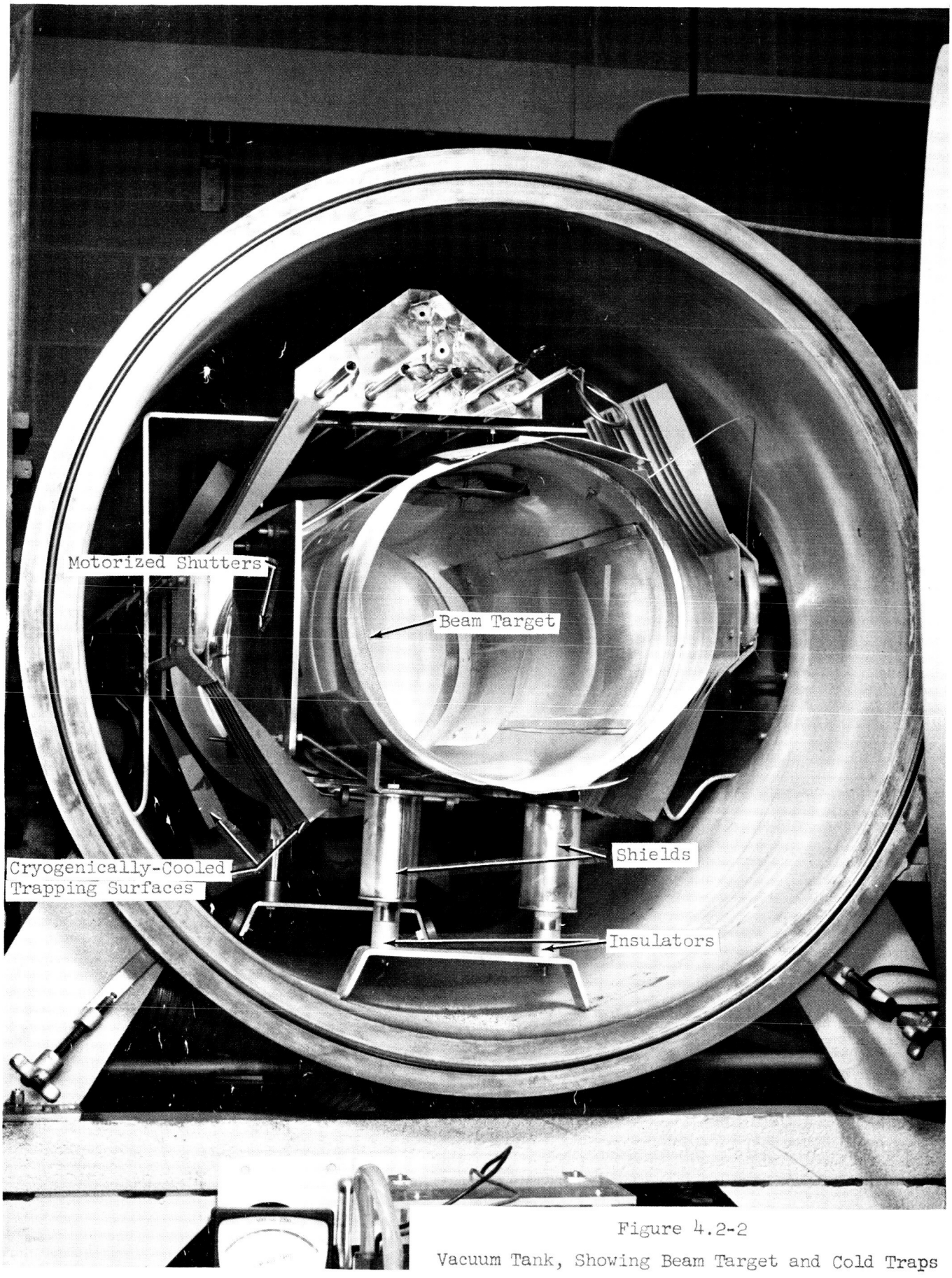

Figure 4.2-2

Vacuum Tank, Showing Beam Target and Cold Traps

The extended test target assembly is shown in the layout of Figure 4.2-3. Aluminum, which appeared to be the best choice was used for this assembly. Other materials were considered but were found to have objectionable features. Carbon, for example, has a lower sputtering rate than does aluminum but tends to act as a sponge for mercury and other gases thus requiring long periods of target outgassing. Carbon and most other metals also tend to coat the cathode emitting surface and thereby plug the pores or otherwise rapidly destroy the emission capability of the active materials. Aluminum, on the other hand, is easily evaporated from the cathode at normal operating temperatures and, therefore, does not readily affect operation. Iron based materials have a disadvantage in that these metals are magnetic and tend to build "needles" in the region of the source magnet structure which quickly short out the anodes and extractor electrodes.

The liquid nitrogen trapping provisions in the extended test facility were of great importance in obtaining a proper test environment and in protecting the pumping system. With mercury propellant it was necessary to trap-out spent neutral atoms to prevent erosion of the aluminum towers, the valve housings, and the brass bellows used in the diffusion pumping system. It was of equal importance to quickly and permanently remove the spent propellant for the sake of obtaining reliable test results and minimum extractor interception levels. Because of these factors and the considerable expense involved in maintaining a liquid nitrogen supply over long periods, careful consideration was given to making the trapping system as efficient as possible.

The chamber traps which collected the major portion of the spent mercury were made of a series of slotted copper plates clamped to a continuous stainless steel formed tube which served as a low inventory liquid nitrogen reservoir. The copper plates were positioned so as to enclose optically the openings in the target assembly. This provided for efficient trapping without adding substantial heat loading due to a needless enclosure of the hot target tube over the solid portions. Small quantities of mercury or other condensibles which might have escaped the main traps were removed at the pump inlet by a second optical cryogenic baffle.

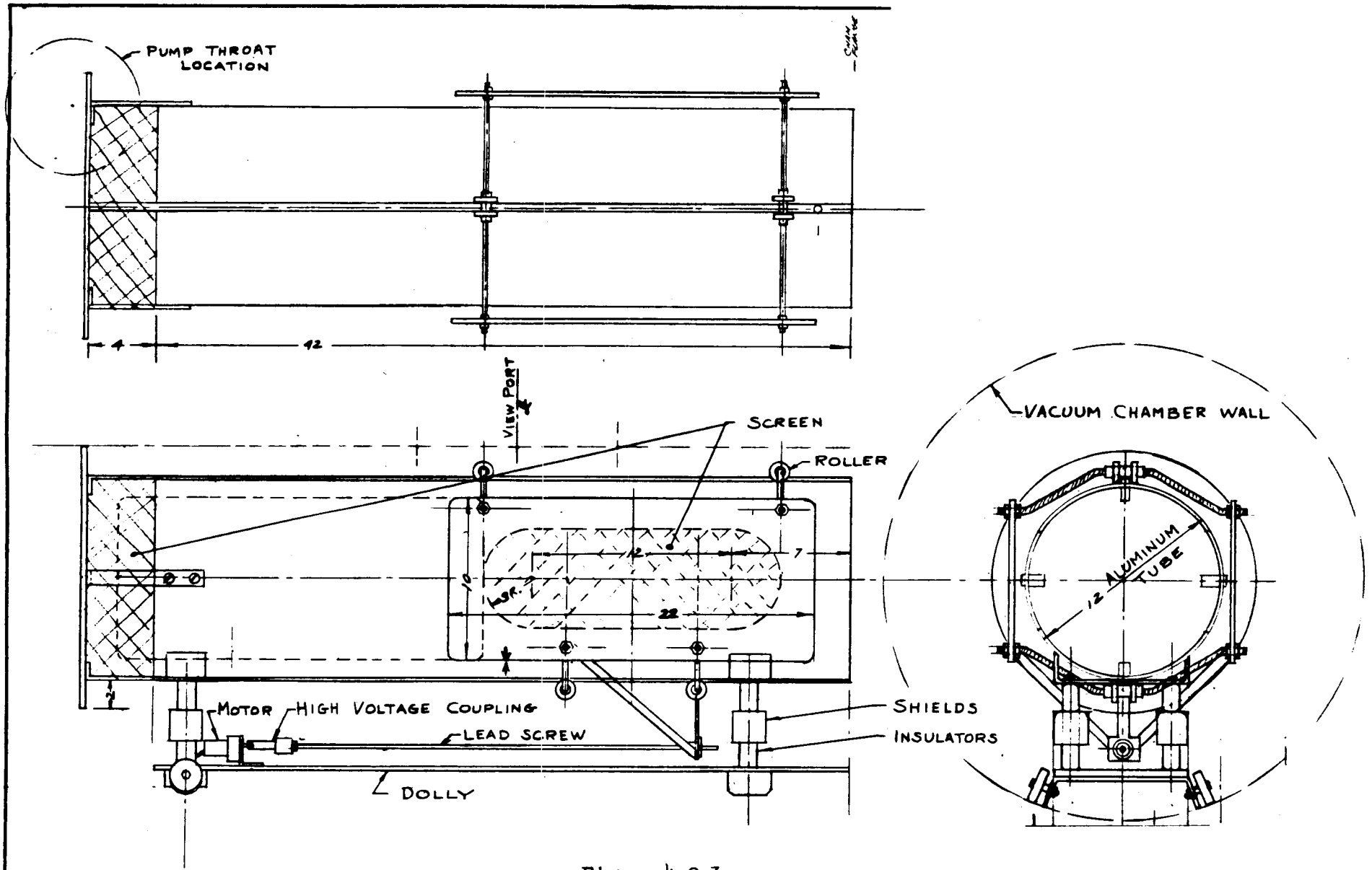

Figure 4.2-3

Extended Test Target Assembly

Both nitrogen traps were supplied from a 300 gallon dewer located as close as convenient to the test area. The delivery of liquid nitrogen was controlled by a temperature sensing controller which opened a solenoid in the feed line whenever the nitrogen vapor temperature in the trap lines rose above a pre-set point. Both traps were series connected to simplify the plumbing and to minimize losses in the transfer line. With the reservoir capacity available the test system was able to operate unattended for periods of about three days. In this way, week-end servicing and the need for a special nitrogen delivery schedule by the vendors was reduced.

The test facility was also equipped with an improved mercury feed system. Past experiences had been very favorable using small plunger-type positive displacement systems. The systems, designated FS-1, used before, however, were limited to a 12 hour propellant inventory and were subject to small feed-rate variations due to room temperature changes and imperfections in the drive gears and pump bore (References 1 and 2).

The new feed system configuration as shown in Figure 4.2-4 and designated FS-2 was designed to eliminate all the shortcomings previously encountered. The entire feed mechanism was submerged in a water bath which was fed by a continuous flow of tap water through a jacket tube which enclosed the delivery line leading to the vaporizer. The excess water spilled over a weir plate trap located between the pump and synchronous drive motor and was drained off. This circulating water bath arrangement had proven itself capable of holding temperatures to within a few tenths of a degree while room air temperatures varied as much as 25 to 30°F. Variations in feed rate were minimized by using a clock-type synchronous motor and a Graham miniature transmission to permit feed rate changes to be made manually. This arrangement and the use of a precision ground piston as the displacement member in a closed mercury-filled reservoir was expected to maintain flow to within $\pm$ 1/2 per cent at the 60 ma level.

Early check-outs of the FS-2 feed system indicated the performance would be quite satisfactory. After a number of days of preliminary operation, however, it was found that the feed rate was subject to periodic excursions amounting to several percent. A careful check indicated that a film build-up on the ground piston was causing a dimensional change and an increase in drag. As the drag

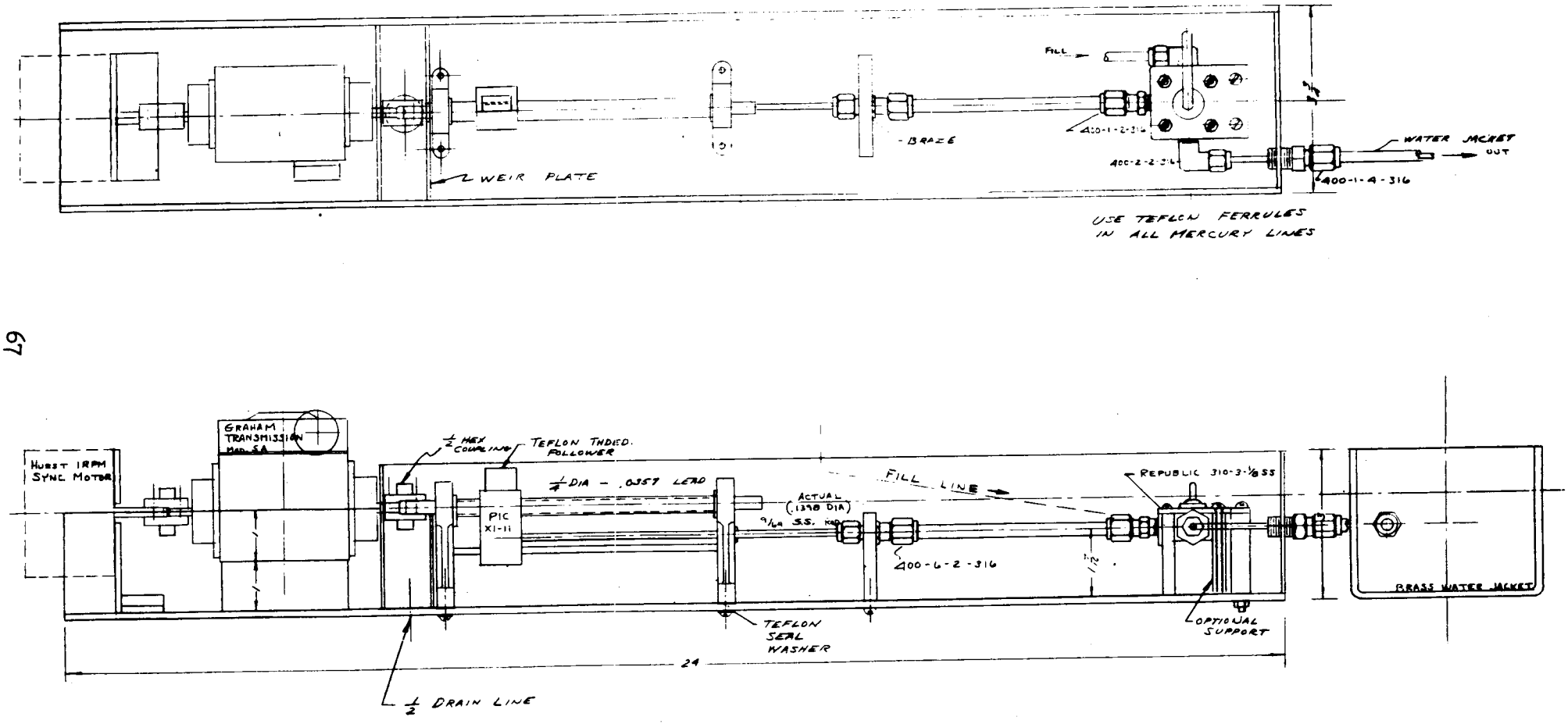

Figure 4.2-4

Precision Feed System Layout

increased the piston would stick, and then would be sprung forward as the ball-bearing assemblies in the feed screw assembly would load. Attempts to clean the plunger and to preload the bearings were only partially successful. The film build-up, which was presumed to be a form of carbonate deposit from the water bath, continued and the feed rate remained unsteady.

A second feed system designated FS-3 was designed based on the original configurations used in earlier programs. This system was found to be much more satisfactory and is shown in the photograph of Figure 4.2-5. An attempt was made in this revised design to eliminate all previous problem areas. The drive screw was made of a 3/8-32 precision rod instead of 8-32 as used previously. A gear reducer assembly of the worm and wheel type was used in place of the spiroid type used in previous designs. The plunger was made of a close-fitting tungsten rod with a fitted teflon cap or piston. The drive motor was a 72 rpm Slo-Syn synchronous motor loosely coupled to the Graham variable speed transmission. The feed system inventory was made sufficient to provide over 24 hours of operation at a 100 ma feed rate. A water jacket was employed on the transfer line to the vaporizer. Enclosing the feed system in a simple plexiglass housing was all that was necessary for reasonable temperature control and stabilization of the feed rate.

Testing of the FS-3 feed system revealed the presence of short term variations in the rate of advancement of the rider up the threaded shaft. For example, it was found that the time required for the rider to advance 0.005 inch varied by as much as $\pm$ 5 seconds out of 30 seconds. However, the time required to advance one thread width (1/32") was found to be 240 seconds with an error of $\pm$ 5 seconds. Thus, the long term error was on the order of two per cent while the short term error was as much as 15 per cent.

It was decided that the short term instabilities of the feed system could be effectively damped out by increasing the response time of the vaporizer. Because of the simple structure of the capillary vaporizer (a 1/16" O.D. stainless steel tube inserted into a 1/8" O.D. stainless steel tube) it was a simple matter to increase the cross-sectional area of the vaporizer by removing the 1/16" insert. The cross section was, therefore, increased from about 0.020 inch in diameter to about 0.060 inch in diameter, thus increasing the response time by a factor

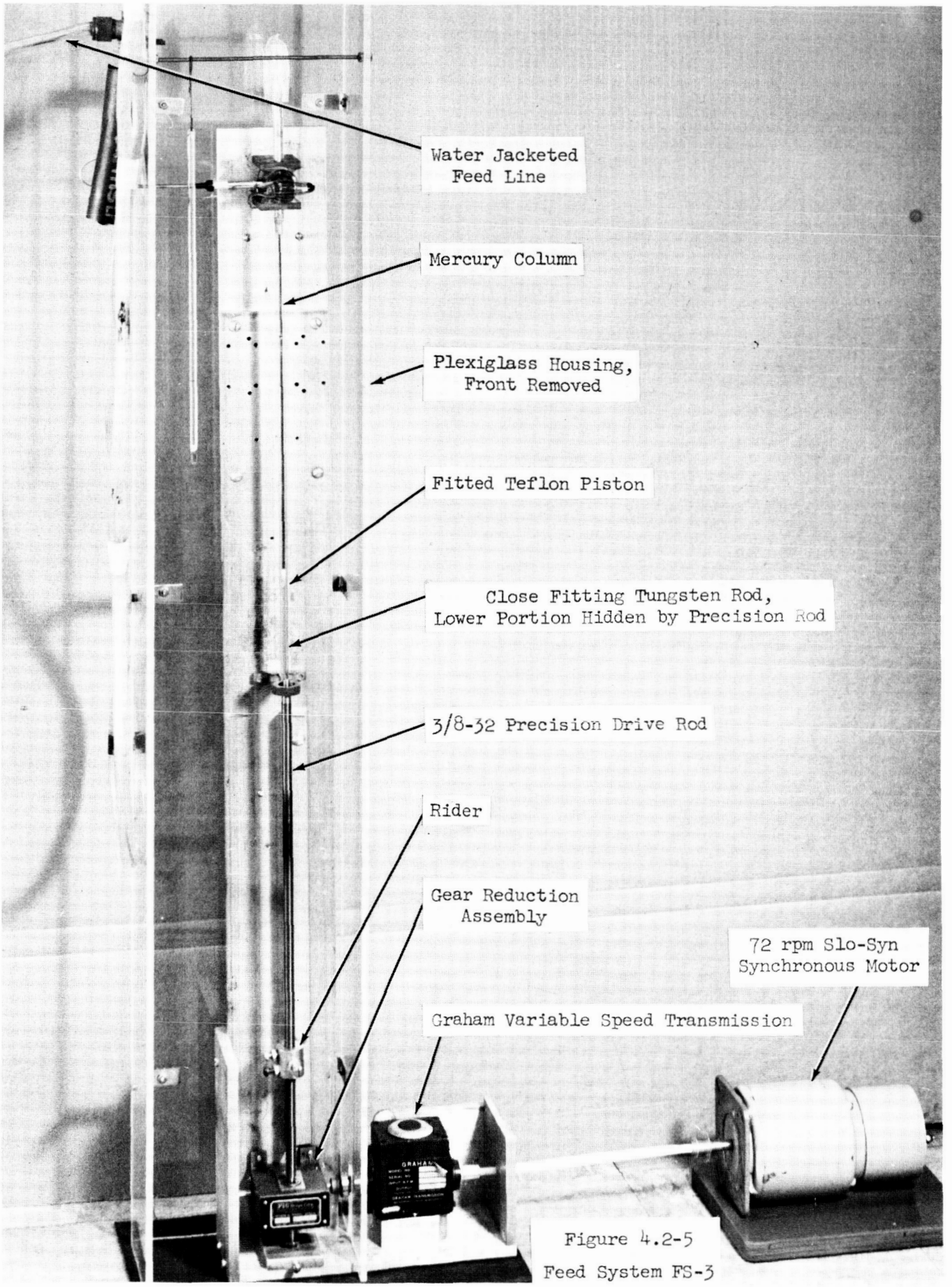

Figure 4.2-5
Feed System FS-3

of 9. (Reference 2). Later measurements have revealed to response time to be about 10 minutes.

The requirements for long periods of engine operation and more precise control over test conditions together with economic considerations prompted the development of the completely automatic instrumentation and control system shown in Figure 4.2-6. A number of major areas or considerations were taken into account in the development of this system. These considerations are listed briefly as follows:

1. The need for accurate instruments to measure system performance.
2. The need for continuous recording.
3. Requirements for manual as well as fully automatic operation.
4. The need for regulation and/or control of several parameters.
5. High voltage isolation requirements in the extractor electrode control and metering circuitry.
6. Safety requirements for operating personnel.
7. Sufficient logic circuitry to insure source operation only under favorable and pre-set conditions.
8. Test stoppage in the event of failure or improper operation.
9. Programmed automatic restart of the test after the cause of failure or improper operation had been corrected or eliminated.
10. Reversion to "standby" if attempts to correct for cause of (8) were unsuccessful.
11. Sufficient recorded data to permit an analysis of the failure or operational fault when the system was next serviced.
12. Protection against in-plant failures (loss of cooling water, nitrogen, electrical power, etc.)

Since it was possible to regulate many of the voltages throughout the source and extraction system by means of the control function, the recording requirements could be reduced to monitoring currents. An exception was the arc voltage which was both controlled and recorded. The principal controller device was the optical relay meter used in conjunction with drive motors or power relays. With the use of optical relay meters incorporating one per cent taut band suspensions and controlled relays, precise control, as well as precise measurement

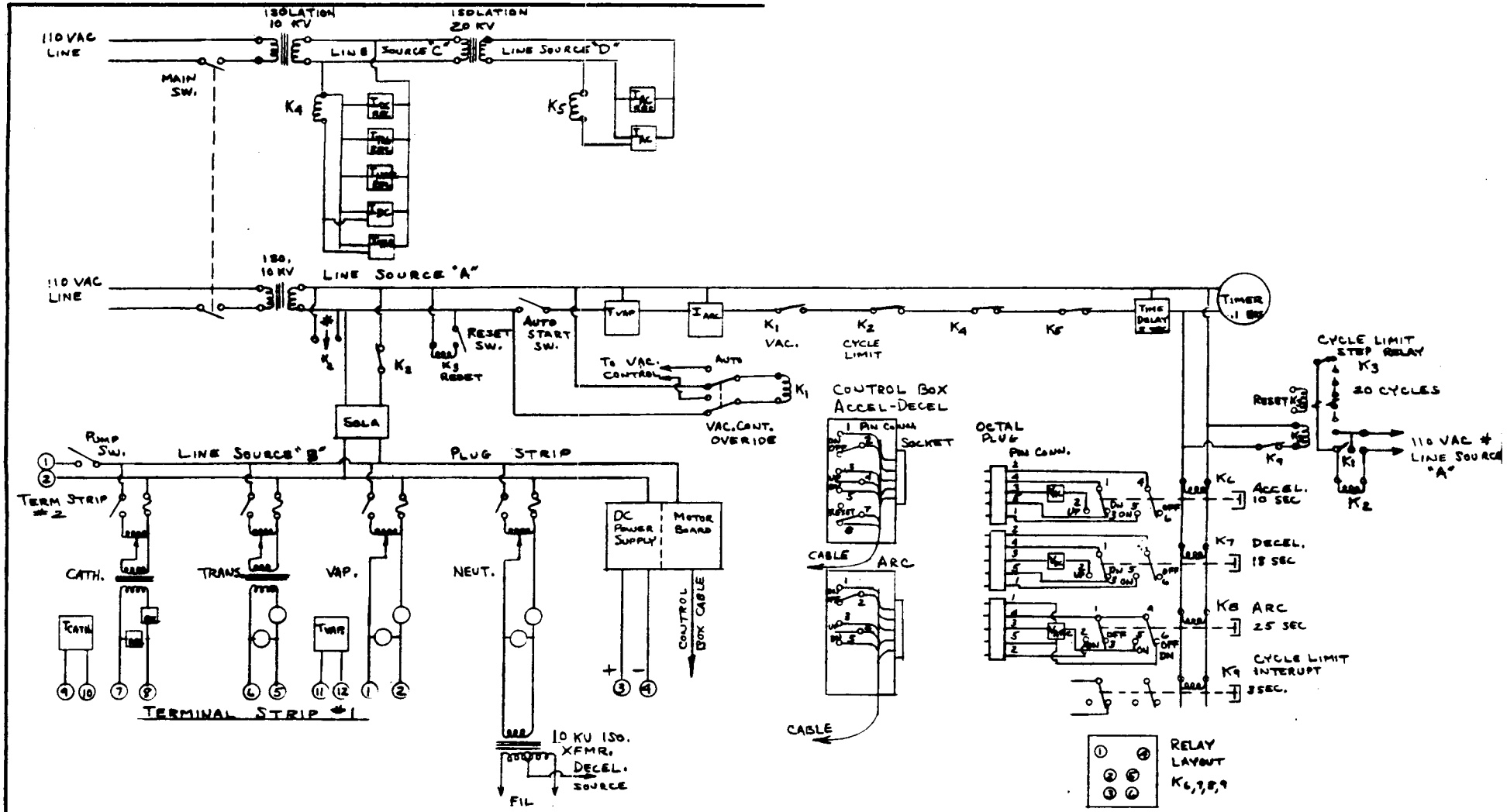

CONTROL	FUNCTION	RELAY CONN.	LINE VOLTAGE SOURCE	RECORDER
T_{VAP}	LO LIMIT 90%	C - NO	A	No
I_{ARC}	HI LIMIT 90%	C - NO	A	Yes
V_{AC}	HI LIMIT 90%	C - NO	B	No
V_{DC}	HI LIMIT 90%	C - NO	B	No
V_{ARC}	HI - LO LIM 90%	Hi C-NC Lo C-NO	B	No
I_{TARG}	HI. LIMIT 90%	C - NC	C	Yes
I_{AC}	HI. LIMIT 90%	C - NC	D	Yes
I_{DC}	HI. LIMIT 90%	C - NC	C	Yes
T_{CATH}				No
VAC	LO PRESS.	NO	B	No
NITROGEN	HI. TEMP.	NO	B	No
I_{FIL}			B	Yes
V_{FIL}			B	Yes
I_{NEUT}			C	Yes

Figure 4.2-6

Extended Test Stand Scehmatic

of key parameters, was possible. Also by using upper limit set points on parameters such as extractor interception current, an overload short or progressive deterioration in system performance could be used to signal immediate test stoppage when pre-set limits were reached.

The operation of the control circuitry can best be explained by a desription of the sequence of events that was normally encountered. To start operation the main switch in Figure 4.2-6 was turned on. This energized three isolation transformers which in turn supplied power to a Sola regulated transformer and a series of optical meter relay control circuits. The high voltage power supplies, nitrogen supply and vacuum pump system were turned on and sufficient time allowed for warm up and stabilization. The reset switch in the control diagram was tripped to ready the console. All manually operated variable transformers which power the cathode, vaporizer, and propellant transfer line were brought to proper settings and sufficient time allowed for the ion engine to warm up. After warm-up the console could be started by throwing the feed-pump switch and the auto-start switch. If all conditions were acceptable (including sufficient vaporizer temperature), the start sequence would begin.

The starting sequence operation would begin on the condition that all series elements from the start switch (T_{vap}, I_{arc}, and relays K_1, K_2, K_4, K_5) were closed. This series arrangement assured that the proper start conditions had been reached and that no shorts or improper circuit connections existed. After a 3 to 5 second time delay, the time lapse timer and relays K_6, K_7, K_8 and K_9 were adjustable time delay relays that scheduled the turning on and motoring up of the accel electrode power supply, decel electrode power supply, and arc voltage power supply. At pre-set intervals each in turn was motor-driven up to the voltage limit controlled by the optical meter relay controllers. The extractor voltages were applied prior to the initiation of the arc to avoid the very high interceptions that would be experienced if the extractor voltages were elevated with the arc on. The relay K_9 was activated last to put a single step in the counting or ratcheting relay K_3. K_3 was designed to step at the time of line voltage application to the power supply control relays but the relay coil voltage had to be removed after each step to avoid overheating and burn out. At this point the ion engine system should have been operating at the proper pre-set conditions. Any change in a controlled voltage would be corrected

automatically by the meter relay circuits. All key voltages and currents, including engine heater power inputs and electrode interception currents, were recorded on slow-speed strip-chart recorders during this "on" condition.

In the event of a malfunction such as excessive arc current, electrode shorting, or loss of vacuum, a stoppage of the test would be signaled immediately. For example, any of the three optical meter relays used to monitor decel current, target current, or neutralizer current (if used), would activate and open relay K_4 causing the timer to stop and relays K_6 through K_9 to open. All power supplies would shutdown and the control motors would run back to zero and reset. The time delay would allow several seconds to insure full reset. After the time delay had been completed, the line voltage would again be applied to relays K_6 through K_9 assuming all other initial conditions (such as good vacuum and proper vaporizer temperature) were present. If the cause of shutdown had been a simple arc in the electrode structure which had cleared itself in the shutdown process, the high voltage power supplies would again be activated and brought to their proper levels and the test resumed. The relay K_3 would register another step. If the fault had not cleared itself since the initial shutdown, as would be the case in which a permanent interelectrode short had developed, the system would again sense this fault as excessive current drain when the associated power supply was turned on or motored up. This would cause another shutdown. A total of 20 such cycles would permanently open relay K_2 by the action of K_3. At this point no further attempts at start up would be made and the heater circuits and arc supply connected to the constant voltage transformer would be shutdown. The system would revert to a "standby" mode in which tank pumping and cold trapping were continued but the engine itself was unpowered and no propellant delivered to it.

The recordings could be examined at a later time by personnel and the exact fault determined. If it could be easily corrected the cycle limit relay could be reset and the start-up sequence repeated as previously described.

The basic electrical circuit is shown in Figure 4.2-7. The principal engine structures and associated heater, arc, and high-voltage power supplies are shown schematically. The metering and recorder instrumentation are also indicated in their appropriate locations in the circuit.

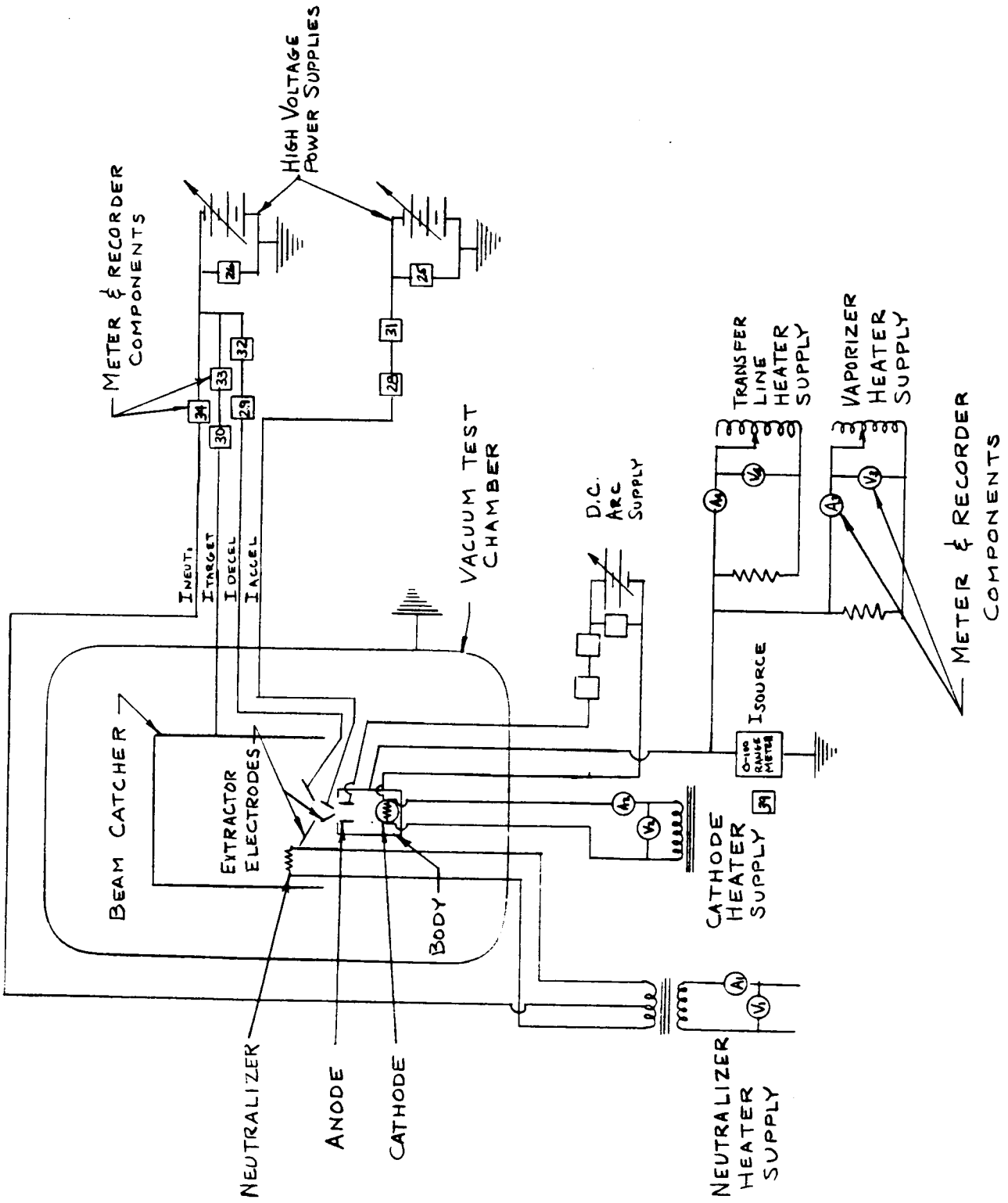

Figure 4.2-7

Basic Test Circuit Schematic

A more detailed presentation of the high voltage panel arrangement is shown in Figure 4.2-8. The dropping resistors used and recorder and meter capacities are shown for each high-voltage circuit. The components designated there by the encircled numbers are to be found in the circuit shown in Figure 4.2-7 under the same numbers. Components such as the 1.6 millihenry chokes and the OA3 regulator tubes were included in the test circuits as protective devices for ion engine components and meters. The chokes serve as high-speed current limiters in the event of interelectrode arcing. The regulator tubes (which are shunted across a dropping resistor) and the meter and recorder in each circuit branch fire and thus control the voltage-drop when the current in that branch exceeds full-scale for the meter or recorders. In this way, arcing in the test engine is prevented from causing severe overloads in these instruments which would otherwise frequently cause burn-out.

An additional feature concerned with arc ignition had to be incorporated into the automatic control sequence before suitable operation could be obtained. It had been determined that the most satisfactory way of initiating engine operation was to first apply the extractor potentials and then to ignite the ion-source arc. Experience had shown that it is very difficult to effect such an arc ignition because of the penetration of the extractor fields into the anode region in the absence of a plasma. Three ways have been found to overcome this negative field penetration. These are: 1) the temporary connecting of the anode to the source body; 2) the application of substantially higher anode potentials; 3) the application of an AC excitation voltage between the cathode and the source body.

Because the first two approaches held some risk of damage in the event of shorts developing within the source, the third approach was selected. Figure 4.2-9 shows that an isolation transformer was placed across the motor windings used to raise the arc supply voltage. In this way a 60 cycle, 110 volt, AC voltage was impressed between the cathode and engine body when the arc supply was motor-driven to its pre-set voltage level. A small current-limited arc was initiated in the cathode chamber and then transferred to the anode as the anode voltage rose to about 20 volts. When the arc-supply motor action stopped, the arc in the cathode chamber extinguished, but the cathode-to-anode arc was sustained in the normal manner.

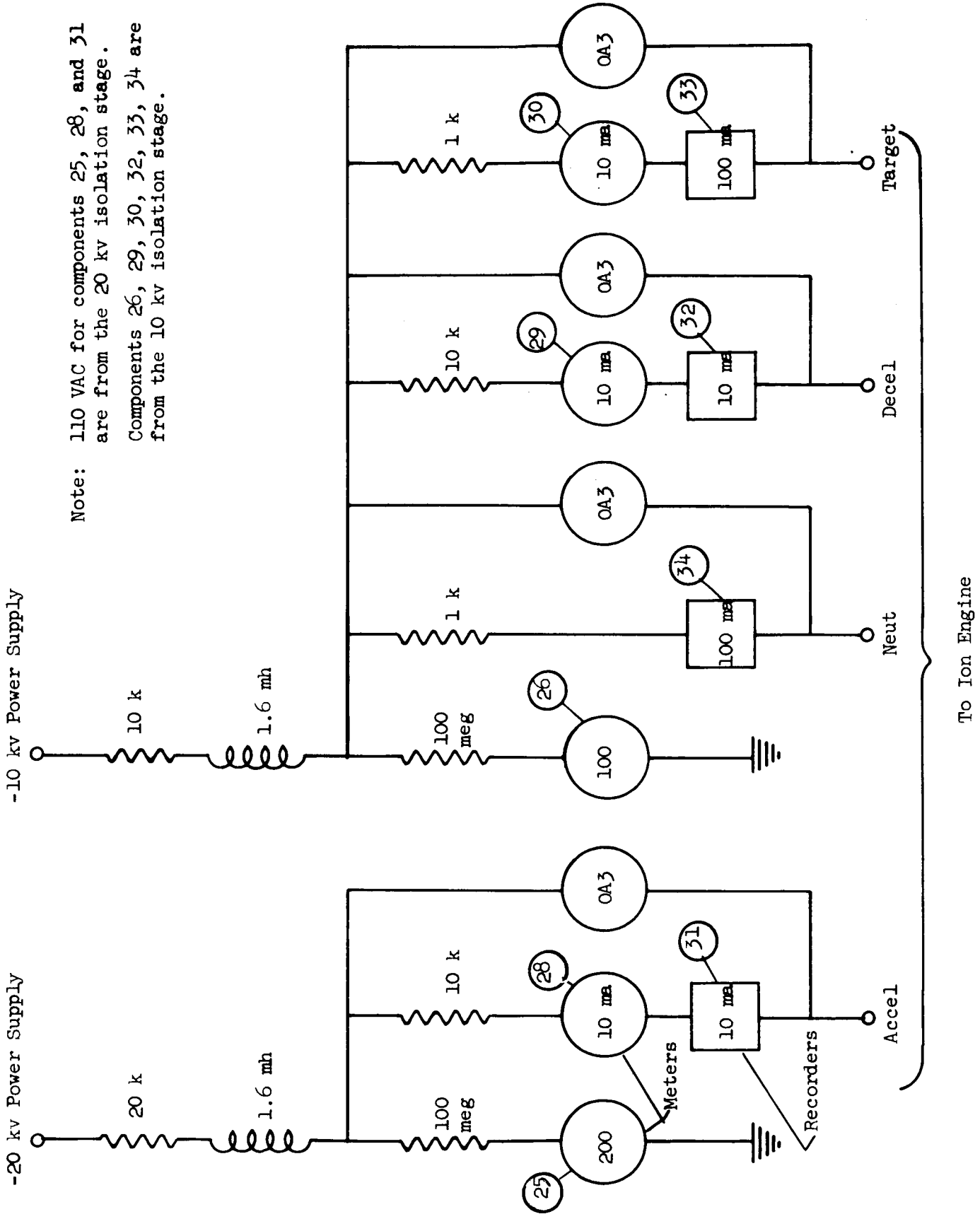

Figure 4.2-8

High Voltage Panel Schematic

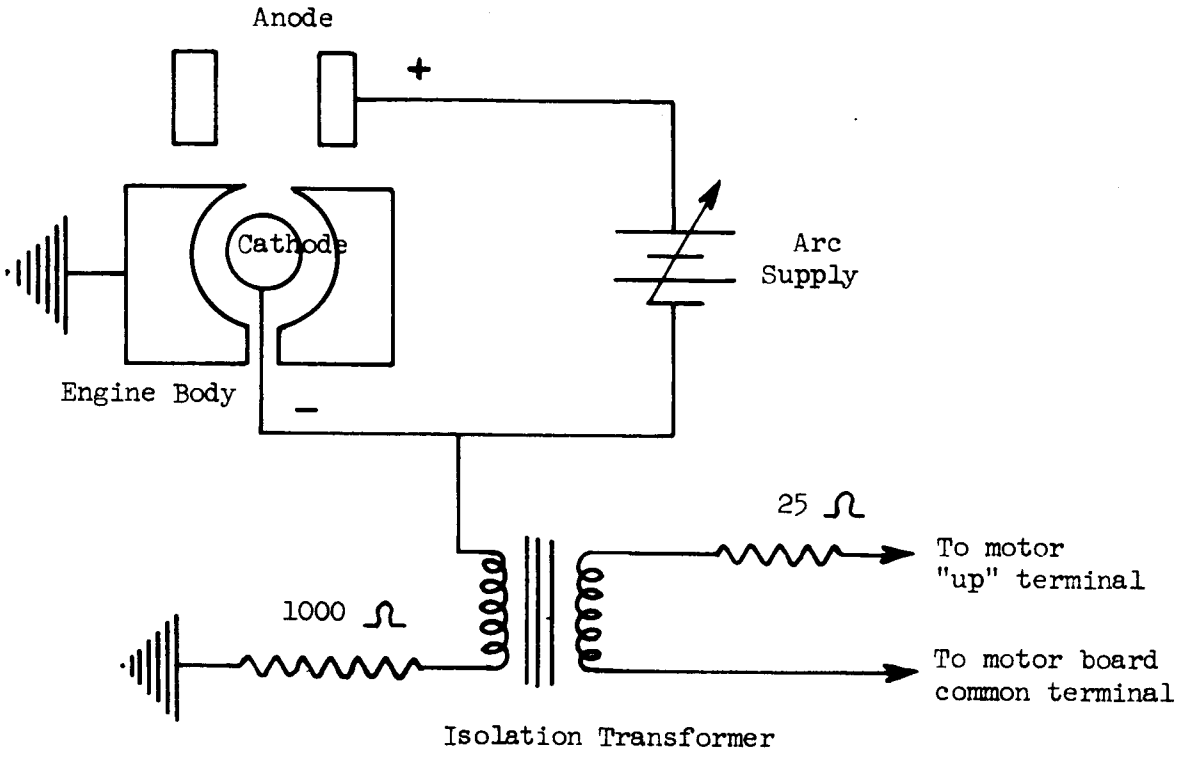

Figure 4.2-9

Arc Exciter Circuit for

Automatic Starting with High Voltage On

4.3 Preliminary System Tests

All major test facility components were individually tested to determine their complete qualification prior to any ion source testing. These facility component tests included a check-out of the vacuum system, liquid nitrogen trapping system, mercury feed systems, power supplies and motor drives, and the control console and instruments.

The entire vacuum system had been cleaned including the complete disassembly and flushing of all diffusion pump and manifold valve parts in acetone and alcohol. The mechanical pump and associated control panels had also been checked for proper operation and, in the case of the mechanical pump, for satisfactory condition of the pump oil. The system was reassembled and a fresh charge of diffusion pump oil added. Also a 12 inch side view port was mounted on the chamber and the nitrogen trap reservoir lines inserted into the feedthrough in the flange opposite the view port. The chamber was closed and pumped down for 14 hours overnight to test the system. A complete helium leak-check was conducted to make certain no leaks existed. Following the leak-check the system was allowed to run an additional 24 hours to permit the total removal of water vapor and other surface contaminents. After approximately 40 hours of pumping, the system was found to register very nearly 8×10^{-7} torr. This vacuum was considered very satisfactory and very near the system ultimate capacity without the use of liquid nitrogen trapping.

The system was opened and the target assembly and the copper trapping plates were mounted in the chamber. The system was again pumped down and allowed to run overnight. The following morning nitrogen was introduced and the vacuum progress monitored for a period of several hours. An ultimate vacuum of slightly better than 2×10^{-7} torr was recorded using liquid nitrogen trapping. Several short-term runs were made with the nitrogen supply close coupled to the traps to determine trap efficiency. The trap consumption was found to be approximately 12 liters per hour with no thermal load except the chamber. This consumption rate plus estimates of the line losses and ion engine thermal loads indicated that the 300 gallon dewer supply would be sufficient for about three days of continuous engine testing.

Following the installation of cable-controlled motor drives on each of the accel, decel, and arc voltage power supplies, these units were checked out. The motor drives were carefully adjusted to insure a zero output in the "full down" or lower limit position, and to insure proper setting of the upper limit switches. The high voltage lead lines and terminal installations were subjected to 50 per cent overvoltages to make certain no arc-over or leakage would be experienced during normal ion source operation.

The entire control console instrumentation was checked to insure proper meter indication and control operation. All meters were checked at their full scale and half scale points against a Keithley 600 A electrometer. A simple battery-potentiometer voltage divider source was used in these tests. At the time of installation all current meters were found to register correctly to within ± 1 per cent of full scale. The recorders used were not calibrated in this way but were observed to agree with their series connected meters within ± 2 per cent during subsequent ion engine tests. The high voltage meters which indicated accel and decel potentials utilized 100 meg-ohm dropping resistors in series to provide the proper relation between meter current scales and the applied voltages. In this case, the 200 microamp accel meter read 20 kv at full scale deflection, and the 100 microamp decel meter read 10 kv at full scale. The resistors used, however, were 30 per cent components and, therefore, errors in the indicated voltage of this same order could be expected. Ohmic checks using a simple VTVM indicated that the dropping resistors were actually better than 3 per cent components but their performance under actual test operation was not considered reliable to any greater accuracy.

The control portion of the console was checked out in stages to determine the proper operation of each circuit. Finally the high voltage power supplies were connected to the console and lines run to the terminals which would normally service the ion source in the test chamber. The system was started and a simulated operational sequence carried through to demonstrate the full automatic operation of the control console. Each limiting and overload circuit was checked in turn to insure its proper operation and the correct sequence of responses in the automatic restart controls. All check tests were found to give fully satisfactory results.

4.4 Early Engine Tests

At this point in the program the test activities with the variable geometry source were not sufficiently complete to allow a precise determination of an optimum geometry for the permanent-magnet extended-test engine. Considerable data had been obtained, however, and the required geometry was known well enough to permit the design of a preliminary test engine to facilitate additional extractor studies and neutralization studies in the extended test chamber.

The permanent magnet ion engine design used in these preliminary tests is shown in Figure 4.4-1. The source is shown with the conventional extraction system in place. Most tests, however, were conducted using extraction assemblies containing one or more additional electrodes and/or a neutralizer cathode. Following the checkout of the ion engine, there were several attempts to neutralize the ion beam. The difficulties that were encountered led to the experiments with alternate neutralizer cathode arrangements and several trial runs using multiple electrode extraction assemblies.

The first neutralization attempts were only a partial success. The neutralizer cathodes were made of a coil of closely spaced turns of 0.010 inch diameter tungsten wire mounted at the face of the decel electrode as shown in Figure 4.4-2(A). The neutralization was found to be only about 50 per cent effective in that electrons escaped from the region of the beam and migrated to the (ground potential) engine body or test chamber walls. Additional shielding, in the form of screening and sheet metal baffles, was added to the ends of the extractor assemblies and extended from the target assembly to improve the retention of electrons in the region of the ion beam. These shields helped but there was still considerable neutralizer-to-ground leakage. Subsequent attempts to move the neutralizer cathodes closer to the beam improved the efficiency of the neutralization process but greatly limited neutralizer cathode life due to beam interception.

An additional approach to improve the electron trapping was tried. The method consisted of suspending a single strand of 0.010 inch diameter tungsten wire at a point from one to two inches downstream of the extraction system on the center line of the beam. This arrangement, shown in Figure 4.4-2(B), was found to be more efficient in neutralizing the beam but, as before, some emission to the

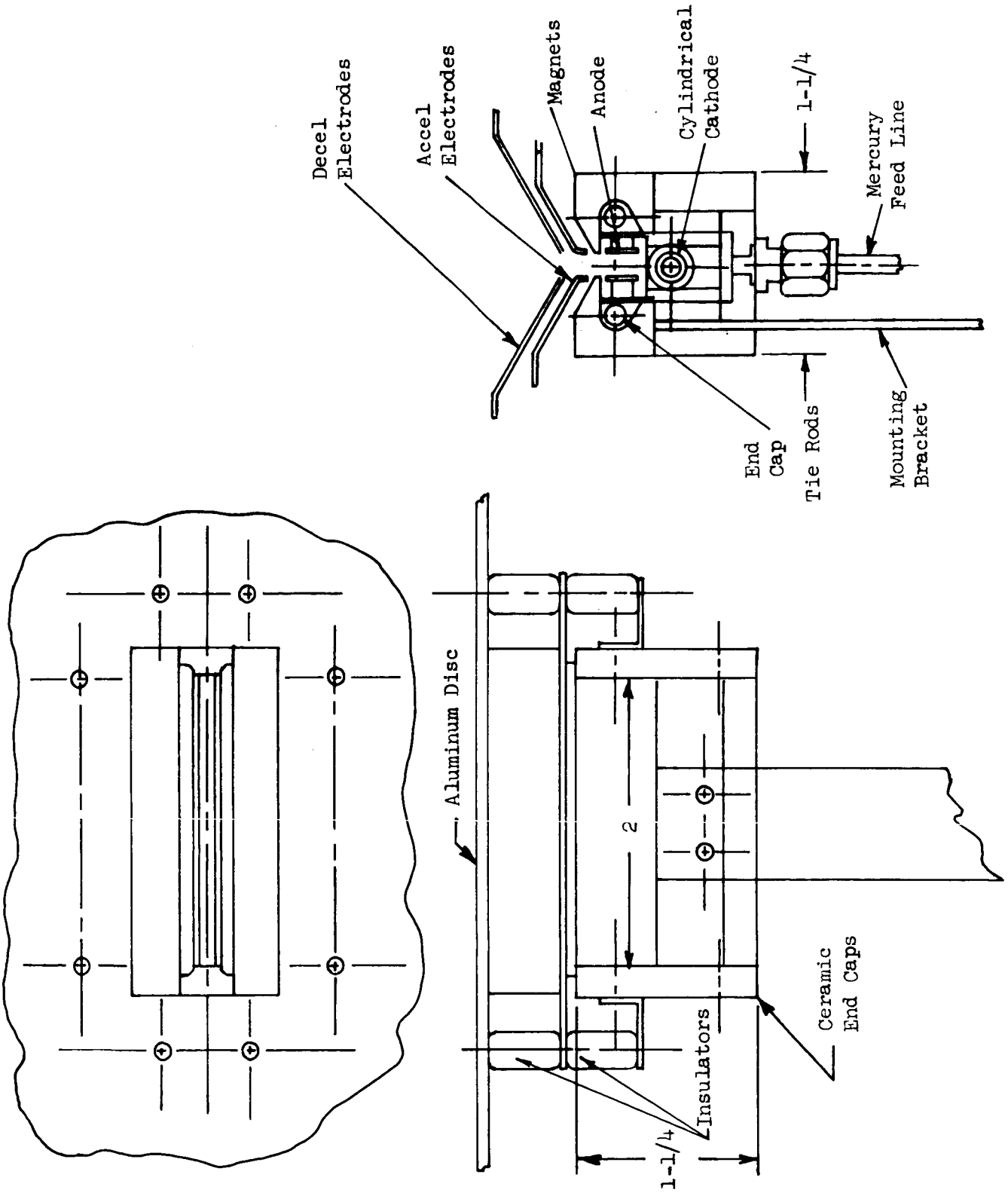

Figure 4.4-1

Preliminary Permanent Magnet Ion Engine Assembly

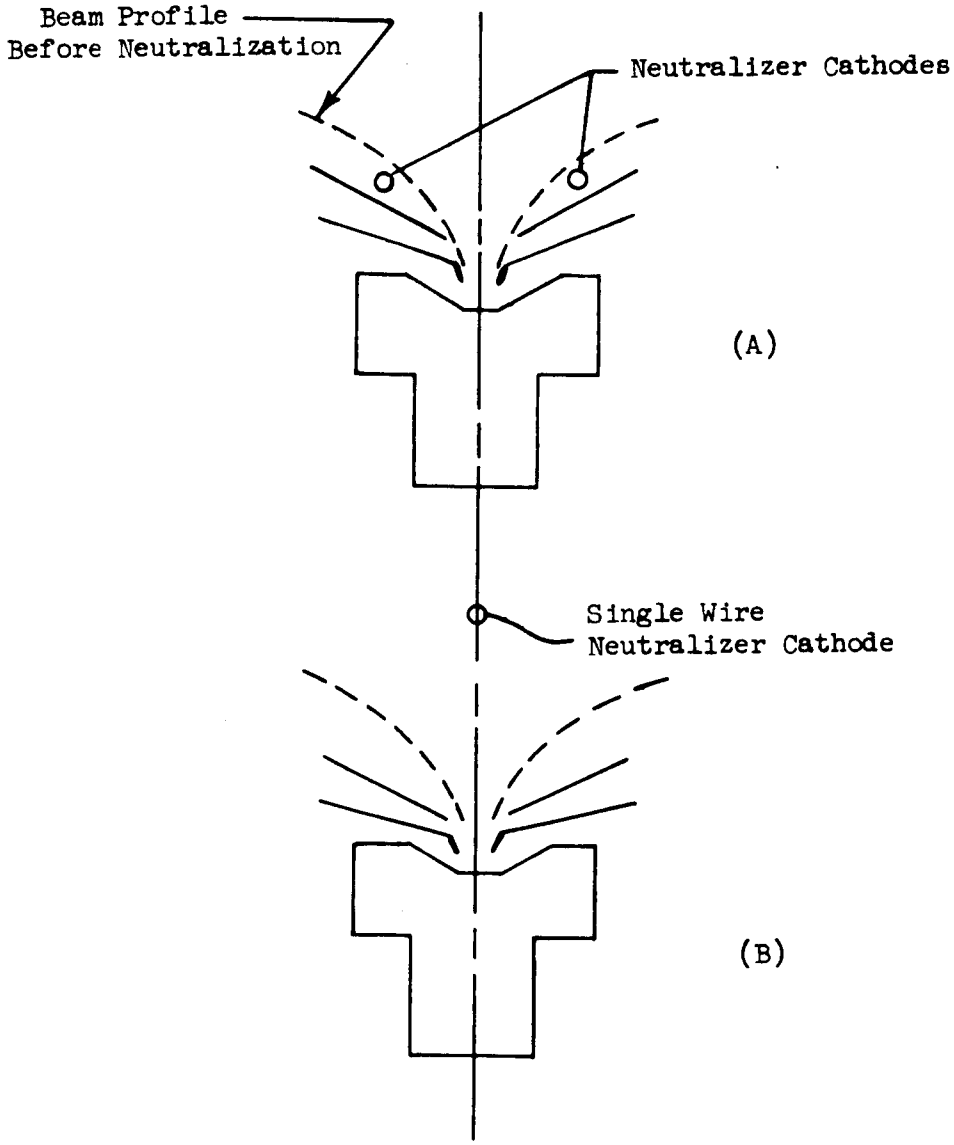

Figure 4.4-2
Experimental Neutralization Geometries

chamber or other ground potential structures was experienced. Under a test using a 70 ma beam current approximately 100 ma of neutralization current was emitted from the filament cathode to yield complete current neutralization. In this case approximately 30 per cent of the neutralizer current was lost. The same approximate percentage loss was noted for beam currents ranging from 30 to 80 ma. Attempts to shield or prevent neutralizer current from escaping from the ion beam region were only partially successful and in every case an excess of neutralizer emission was required.

The limited data obtained during the neutralization tests gave indications that reasonable neutralizer filament lifetimes could be realized for extended testing if the filament could be located in a region of sufficiently low beam density. Short runs of four hours duration had produced an unmeasurable reduction in the 0.010 inch filament diameter when used at a point 1-3/4 inch forward of the extraction system.

Since it had been planned to conduct extended tests with the ion beam neutralized, some experiments were conducted using multi-electrode lens systems to evaluate the possibility of collimating and neutralizing the beam after the density had dropped to approximately 3 to 5 milliamperes per square centimeter. It was reasoned that if the beam could be collimated, the neutralizer filament could be located farther forward of the source and hence would have a lifetime sufficient to last the 250 hours anticipated for the extended tests. The rate of beam blow-up after collimation, furthermore, would be much more gradual at the now reduced beam density. This latter fact would make the neutralizer more effective and offer an increased likelihood that the ions would be proceeding directly away from the source, rather than at an angle, to provide for a maximum forward thrust component at the time of neutralization. At the same time an additional diverter electrode was introduced between the accel and decel electrodes to reduce the accel interception.

An arrangement of the multi-electrode structure that was tested is shown in Figure 4.4-3. Other runs were made using only the diverter electrode between the accel-decel system also to evaluate the effectiveness of this method of reducing accel interception. The beam profiles shown in Figure 4.4-3 are interpreted from the sputtered patterns seen on the edges of the various electrodes after a run.

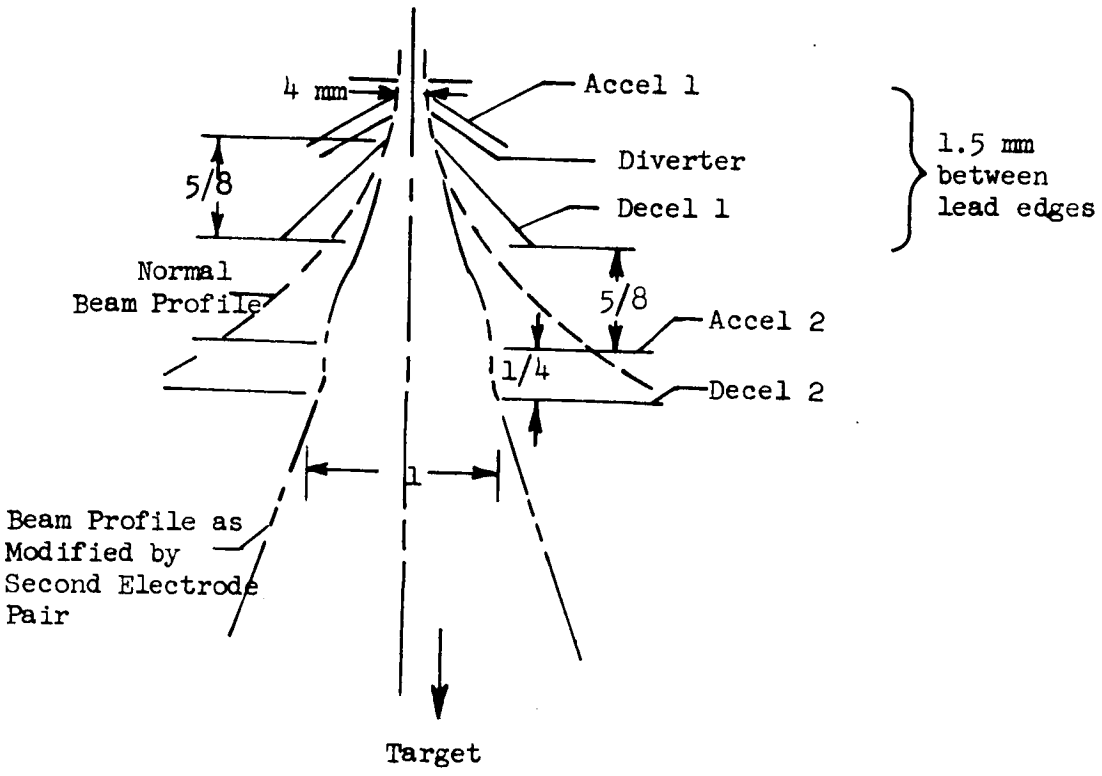

All units in inches except where indicated

Figure 4.4-3

Experimental Electrode Arrangement

Only very limited tests were conducted using the diverter and/or second electrode lens system combination before the extended tests were scheduled to begin. These tests were moderately successful as is shown in the follwwing typical interception data obtained with the extractor system of Figure 4.4-3:

Typical Extraction System Interception Data

V_A	Arc Voltage (volts)	35
I_A	Arc Current (amps)	0.4
V_{Acc_1}	No. 1 Accel Voltage (kv)	12.7
I_{Acc_1}	No. 1 Accel Current (ma)	0
V_{Dec_1}	No. 1 Decel Voltage (kv)	7.7
I_{Dec_1}	No. 1 Decel Current (ma)	2
V_{DV}	Diverter Voltage (kv)	14.9
I_{DV}	Diverter Current (ma)	1.5
V_{Acc_2}	No. 2 Accel Voltage (kv)	12.7
I_{Acc_2}	No. 2 Accel Current (ma)	4.5
V_{Dec_2}	No. 2 Decel Voltage (kv)	7.7
I_{Dec_2}	No. 2 Decel Current (ma)	2
I_T	Target Current (ma)	25
I_S	Source Current (ma)	35

The first accel electrode was made to intercept zero current by the interposition of a more negative diverter electrode between the accel-decel members. Also the second electrode lens set was shown to be capable of focusing 80 per cent of the beam leaving the first extractor set through the second accel-decel aperture. This test series concluded very shortly after obtaining the above numbers and, therefore, can only be considered a feasibility demonstration of the use of electrostatic lens systems for beam control. No neutralization runs were made using the multi-electrode system nor were any variations in the location or shaping of the electrode structures attempted. It is conjected,

however, that longer lifetimes may be realized for neutralizer filaments placed directly in the expanded and collimated ion beams and it is concluded that accel interception due to charge-exchange ions may be eliminated by the use of a diverter electrode.

A redirection of the extended test objectives which eliminated the requirement for beam neutralization simplified the extended testing and deemphasized the importance of the above studies. Also an examination of the more conventional two-electrode structures showed that the charge-exchange ions which normally strike the accel electrode do not damage the lead or focusing edge of this electrode. Since this lead edge is untouched for the most part there is little to be gained by protecting the flat or structural portion of this electrode with a substitute electrode like the diverter. Problems associated with the depositing of sputtered electrode metal still exist; engine efficiency is reduced slightly since the diverter voltage is somewhat more negative than the accel with approximately the same interception currents, and the entire structure is complicated by the addition of another electrode. For these reasons and because of the somewhat inconclusive and very limited results with the more complicated extraction systems, they were abandoned in favor of the usual two-electrode extractor system for the extended testing.

4.5 Extended Test Engine

The extended test (ET) engine was designed during the conclusion of the variable geometry source tests. The ET engine made use of the most efficient interior and extraction system geometries as determined by the several months of variable geometry source experiments and at the same time incorporated permanent magnets and an efficient and reliable cathode heater and support arrangement. A cross-section of the extended test engine is shown in Figure 4.5-1. Two such engines were fabricated and mounted on feedthrough plates as shown in Figure 4.5-2. The first engine (ET-1) was tested in two steps to accumulate over 400 hours of run time. The second engine (ET-2) was then installed in the test facility and run at a significantly higher performance level for a period of over 100 hours. The details of these test runs are described in more detail in Sections 4.6 and 4.7.

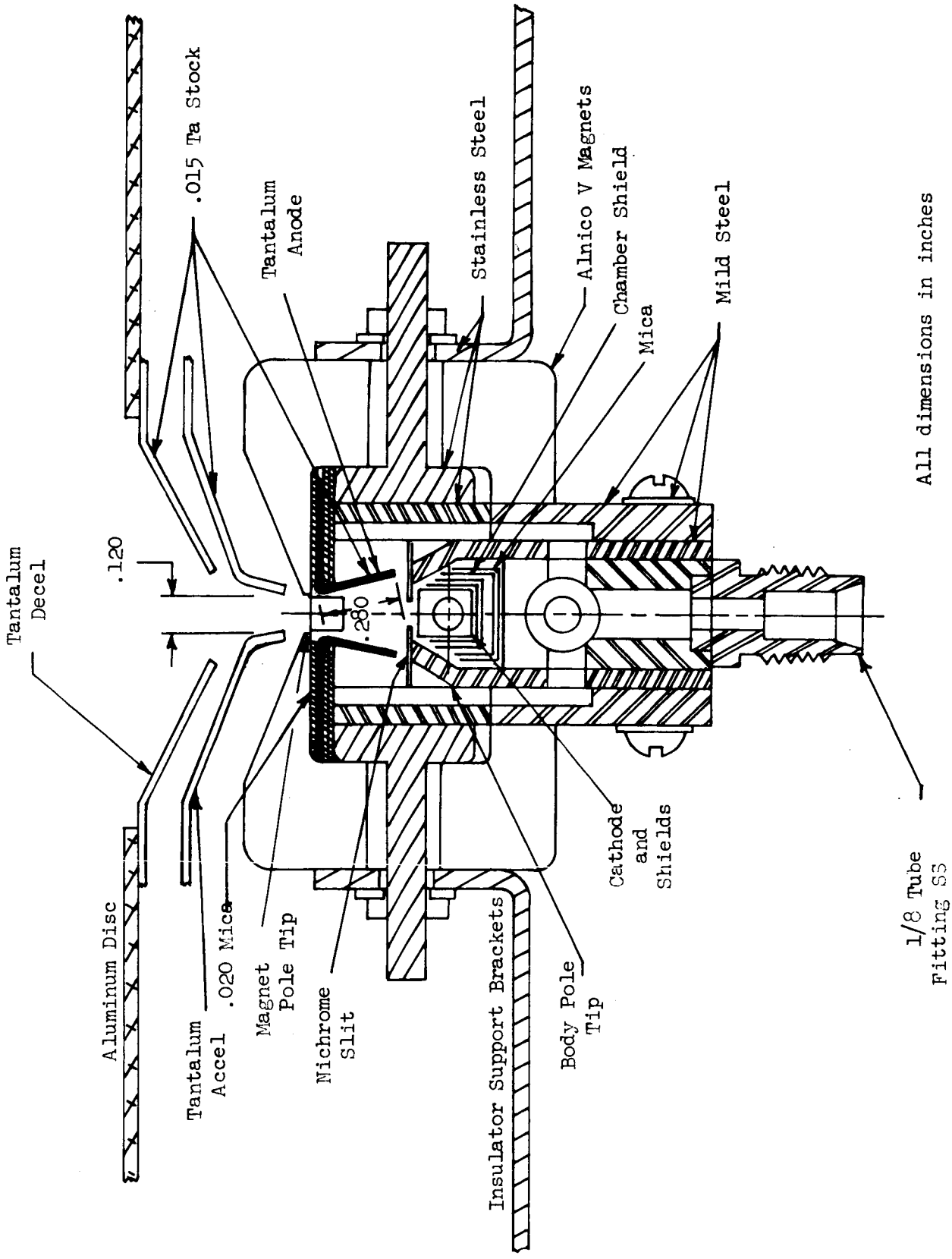

Figure 4.5-1

Extended Test Engine Assembly

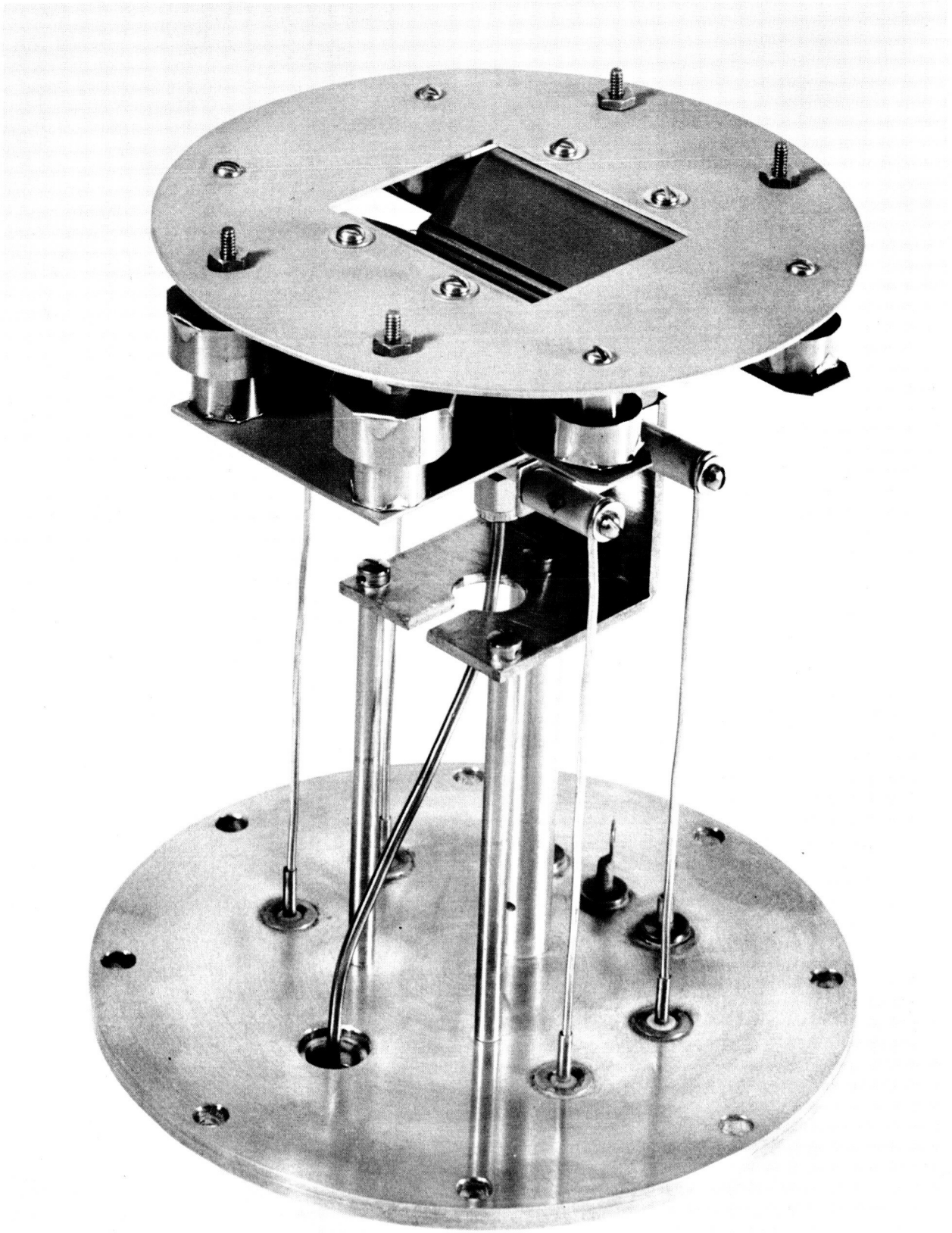

Figure 4.5-2
Extended Test Engine (ET-2)

The ions were extracted from the opening formed by the magnet poles shown in Figure 4.5-1. This opening was 3 mm wide by 2 inches long at the exit aperture and provided a beam current density of 53 ma per square cm assuming extraction of the full 80 ma design output beam. The accel electrode width was also set at 3 mm to coincide with the source opening. The accel was shaped to conform to the normal profile of the expanding beam and the lead or focusing edges were placed 1.3 mm from the magnet pole tips. The decel electrodes were provided with an initial opening of 5.5 to 6 mm and a separation of 1 mm from the accel electrode surface.

The actual volume occupied by the test engine and extractors can be defined as 2-1/4 inches wide x 1-3/4 inches thick x 2 inches high. The frontal area was 3.93 square inches. Other brackets, shield discs, and insulator support straps extended beyond these dimensions but could be eliminated in a more nearly prototype design. The thickness could also be easily reduced to 1-3/16 and the the height to 1-1/2 inches by incorporating magnets which are especially designed and cast for the engine. The magnets used were made from modified stock channel magnets which were considerably oversized.

In the assembly shown in Figure 4.5-1, the body of the engine can be seen to be made of a combination of stainless and mild steel parts. The choice of materials was such as to provide the proper flux path between the magnet pole tip and the body pole tip. The strong magnetic field in the region outside the cathode slit was carefully shaped to enclose the anode pieces. The slight taper in the anode pieces resulted in an improvement in the ion to electron current ratios by a factor of two or more over that obtained for parallel anode surfaces. Tapering the anode surfaces in this manner permitted the use of a considerably wider cathode slit width which made available more of the cathode surface for emission thus reducing the heater power requirements. In this design, a cathode slit width of 2 to 2.2 mm was used as compared with slits of 1 to 1.5 mm widths used in previous extended tests (Reference 2).

The cathode size and general location with respect to the cathode slit was nearly identical to that used in the variable geometry source. The ET engines did, however, utilize a substantially more reliable support and heater connection arrangement along with a slightly improved shielding technique. Figure 4.5-3 shows the basic cathode assembly exclusive of the multi-layer radiation

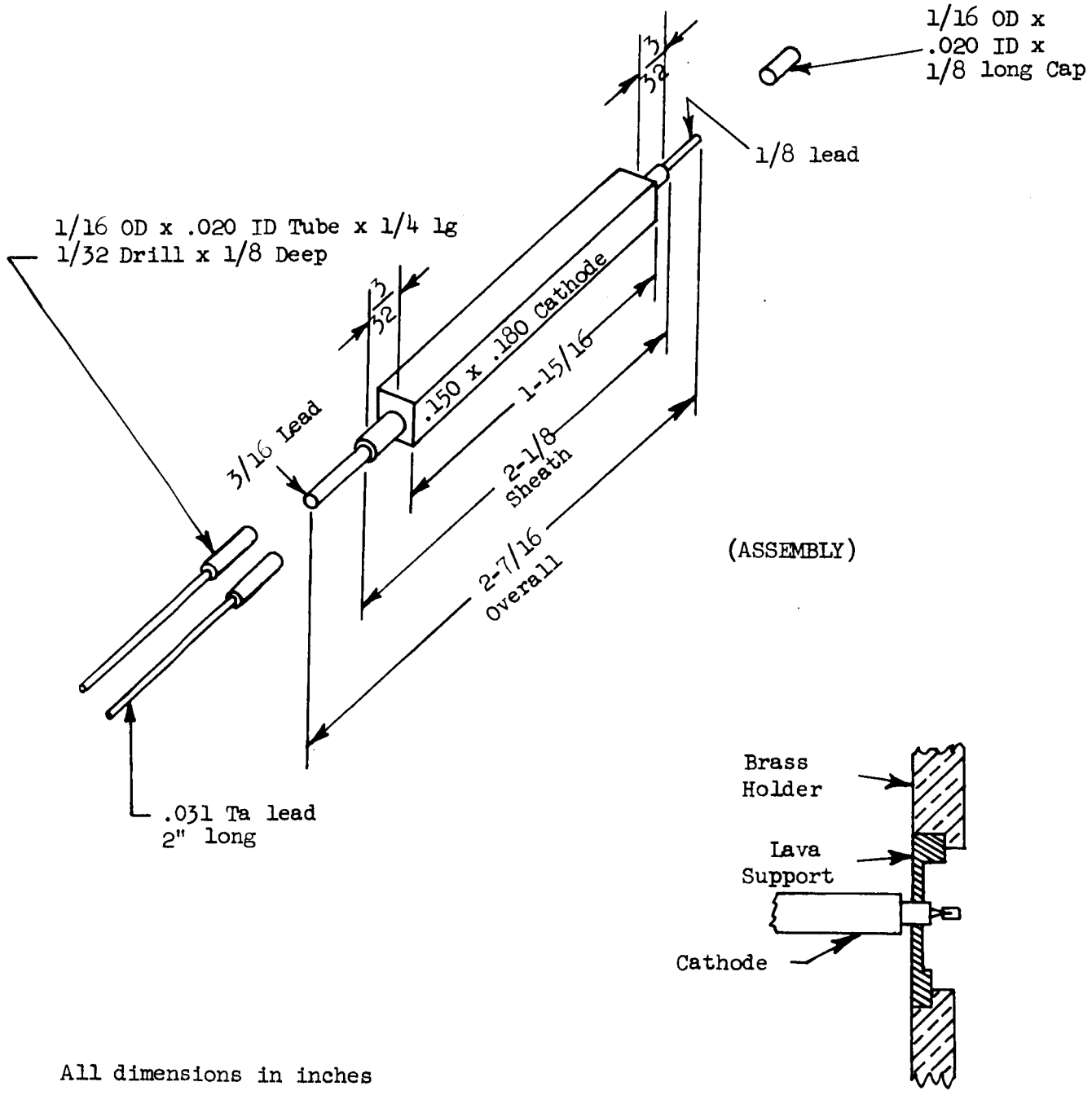

Figure 4.5-3
Cathode Detail

shields which were added upon assembly into the engine. In the engine the cathode was supported on each end by a thin lava ceramic support mounted in each brass end-plate used on the engine body. The lava provided excellent thermal and electrical insulation and at the same time insured the precise location of the cathode with respect to the ionization chamber and cathode slit. Initially a good cathode using this support arrangement would operate with less than 20 watts of heater power input.

The electrical connections to the heater lines were made by crimping a small stainless steel sleeve to each lead wire in the heater and to an extension lead of tantalum. The opposite end of the heater was connected by putting both heater leads through a single small sleeve and crimping the sleeve. The use of the sleeve connection method has proven very reliable and efficient. The radiant losses from the short heater leads were reduced almost to zero and by selecting the proper lead lengths it was possible to minimize both the electrical and thermal conduction losses in these leads.

The entire cathode assembly with its shielding of alternate layers of nickel foil and micro quartz was electrically isolated from the engine body. The cathode was fitted with a 0.025 inch diameter nickel lead which passed through the lava support at one end and was connected to the negative side of the arc power supply. The engine body and the cathode could be connected electrically during operation without ill effects, but this arrangement was not convenient for an engine requiring automatic start up (Section 4.2). To insure the absence of an electrical short between the cathode and the engine body, a second set of shields was inserted in the body cavity. These shields, formed by a single molybdenum channel and three strips of mica, were maintained in place in the body by the spring action of the channel. The molybdenum surface was of high reflectivity and thus helped to limit radiant heat transfer from the cathode, and the mica strips provided an electrical insulation and a modest thermal barrier in the event the cathode or some of the cathode shielding sagged or dropped into the body cavity after long periods of operation.

The extraction system electrodes and the source anodes were fabricated of tantalum. The use of tantalum permitted the vaporizing off of materials (such as aluminum sputtered from the beam target) without removing the engine from the

vacuum chamber or interrupting the test for more than a few moments. Also momentary arcs between extraction electrode structures did not result in melting or vaporization of the electrode materials. Furthermore, tantalum is not affected by mercury, is not overly sensitive to sputtering, nor does it absorb mercury or other products during engine start-up or operation.

The mica used to position the anodes was a high quality electronic grade which has proven very satisfactory in most instances. The mica was carefully pressed against the heavy body parts to prevent local overheating and possible decomposition. On occasion the mica has been found to break down, however, and this factor made the material less than optimum. The extended test failure with the ET-1 engine at 400 hours was in fact precipitated by such a breakdown which produced a short between anode and ground. The use of mica, however, has been successful enough, and its convenience and workability have been such as to allow its use in the test engines.

The method of introducing the mercury vapor is seen in Figure 4.5-1. The main source of mercury was through the tube fitting in the bottom of the body. This fitting was connected to a 1/8 inch diameter transfer line leading to the vaporizer located at the feed-through plate. Mercury vapor introduced into the body was carried through the large-bore passage in the center of the body and directed upward to the anode chamber through a multiplicity of feed passages which were connected to this bore. The vapor was introduced behind the anode pieces and had to flow under the lower edge of these electrodes to enter the ionization region.

4.6 Extended Tests

In attempting to initiate the extended testing phase of the program several difficulties were encountered. They were instabilities of the newly designed and fabricated feed system, FS-2 (Section 4.2), mechanical instabilities of feed system FS-3, the occurrenceof air bubbles in the mercury feed line, and the occurrence of high decel electrode interception currents. Not until these difficulties were analyzed and solutions obtained was it possible for extended testing to be initiated.

Because of the instabilities encountered when initially testing the ET-1 engine in the extended testing facility, it was decided to test the engine in the facility used for testing the variable geometry source, the VGS test facility described in Section 2.3. Since at that time, it was not known but it was suspected that the feed system FS-2 was responsible for the instabilities, it was decided to use the feed system, FS-1 (Reference 1), which existed at the test facility location depicted in Figure 2.3-1. That feed system, which had been used during testing of the variable geometry source, was known to be stable and was known to display a predictable periodic variation of feed rate of magnitude approximately $\pm$ 2 ma equivalent. The period of the variation was that of the rotating threaded drive shaft and thus the variation was mechanical in nature probably due to a slight bend in the threaded drive shaft.

The data obtained while operating the ET-1 engine in the VGS test facility is presented in Table 4.6-1. The stability and good performance demonstrated by the ET-1 engine operating in conjunction with the FS-1 feed system led to the conclusion that the FS-2 feed system must have been the cause of the instabilities observed in the extended testing facility. It was at this point that the FS-2 feed system was abandoned in favor of FS-1.

The ET-1 engine together with the FS-1 feed system were then removed from the VGS test facility and mounted in the extended testing facility. Initial testing revealed the decel interception current to be in the range of 2 to 5 ma compared to less than one ma obtained in the VGS test facility. Examination of the geometry involved revealed that the engine was placed too far away from the deep well target thus allowing regions of low potential to exist between the engine and the target. Excessive beam blow-up, therefore, resulted. The problem was remedied by attaching an extension of aluminum screening onto the end of the target. The anticipated reduction of the decel interception current resulted.

After affecting the reduction of the decel interception current, testing of the ET-1 engine was resumed. However, initial tests indicated the feed system to be unacceptable for extended testing for two reasons. First, it was desirable to have to refill the feed system as infrequently as possible. The FS-1 feed system had sufficient inventory for about 15 hours at an 80 ma delivery rate. A minimum time of at least 24 hours appeared to be desirable. Second, the $\pm$ 2

Table 4.6-1

Performance of the ET-1 Engine in the VGS Test Facility

	Spec. 1	Spec. 2	Spec. 3	Spec. 4
Chamber Pressure (10^{-6} torr)	8	8	4.5	5.1
Cathode Voltage (volts)	4.9	5.5	5.4	4.5
Cathode Current (amperes)	4.0	4.5	4.3	3.7
Cathode Power (watts)	19.6	24.8	23.2	16.6
Hg Feed Rate (Equivalent ma)	71.0	71.0	71.0	88.5
Source Current (ma)	56	56	59	80
Propellant Utilization (%)	79	79	83	90.5
Arc Voltage (volts)	31	32	31	31
Arc Current (amperes)	0.65	0.65	0.72	1.35
Arc Power (watts)	20.2	20.8	22.3	41.9
η_A (ev/ion)	361	371	378	524
η_C (ev/ion)	350	443	394	208
$\eta_A + \eta_C$ (ev/ion)	711	814	772	732
Magnet Power	0	0	0	0
Accel Voltage (kv)	12.7	13.4	13.0	16.2
Accel Current (ma)	0.7	0.8	0.76	1.0
Accel Power (watts)	8.9	10.7	9.9	16.2
Decel Voltage (kv)	5.0	5.0	5.3	5.1
Decel Current (ma)	0.1	0.19	0.07	0.22
Decel Power (watts)	0.5	0.95	0.37	1.1
Specific Impulse (sec.)	7070	7070	7280	7150
Beam Power (watts)	276	272	308.5	402.0
Total Power (watts)	325.2	329.2	364.3	477.8
Power Efficiency (%)	84.9	82.6	84.6	84.1
Rocket Efficiency (%)	67	65.2	70.3	76.0

ma periodic feed rate variation was unacceptably large. Thus, the FS-3 feed system was designed, fabricated, and tested as indicated in Section 4.2.

With the above described modifications of the testing facility and the feed system, the extended test was initiated on September 17, 1964 and on that date was run unattended overnight for the first time. Unfortunately due to a poorly calibrated liquid level gauge on the newly installed liquid nitrogen storage tank, there was inadequate liquid nitrogen inventory to last through the night and the system shut off automatically after approximately 14 hours of operation. Upon replenishing the liquid nitrogen the next day the test was restarted and ran uninterrupted for the next 54 hours when again the test had to be interrupted, this time manually, when it became apparent that the liquid nitrogen inventory would not be sufficient to last through the following night. During restart efforts the next day it was found that excessive arcing occurred when attempting to turn on the high voltages and additionally, the cathode performance was very poor. It was, therefore, decided to open up the vacuum system in order to clean up the excessive mercury which had accumulated on the target and target stand off insulators and to replace the cathode. This mercury accumulation was due to the release of the entrapped mercury from the cryogenic surfaces subsequent to allowing them to warm up. In addition, it is believed that the release of other materials along with the mercury resulted in cathode poisoning. During later extended testing great care was taken to be sure that sufficient liquid nitrogen would always be available so that warm up of the cryogenic surfaces would not be necessary until termination of the extended test was dictated by other factors. Even for temporary test interruptions lasting as long as eight hours (because of malfunctions exterior to the vacuum system) the cryogenic surfaces were not allowed to warm.

After cleaning the vacuum system and replacing the cathode, extended testing was resumed. A new problem developed at this time. There was evidence that air bubbles were occurring in the feed system. This was indicated by observing that the beam current would increase in time, gradually at first with the rate of increase increasing in time (almost exponentially) until the extraction electrode interception levels were high enough to exceed the set limits, thus, automatically turning off the test. Bubbles were observed to occur at 69 hours,

81, hours, and 130 hours of test time. At this point, it was decided that positive steps must be taken to ensure that the mercury introduced into the feed system was free of entrapped air. A method, therefore, was developed to vacuum outgas the mercury just prior to and during the transfer of the mercury to the feed system reservoir. After utilization of this technique the engine was run without the occurrence of feed system bubbles for the next 272.6 hours and a total of 402.6 hours was accumulated before the test was terminated because of a persistent short between the accel electrode and the source.

The engine performance parameters at four times during the extended test ET-1 are given in Table 4.6-2. The indicated parametric values are typical and indicate the trend of change in performance with time. Throughout the test an attempt was made to maintain the source current at a constant value of approximately 61 ma thus maintaining a propellant utilization of approximately 81 per cent. In addition the arc voltage was maintained at approximately 30 volts and the specific impulse was held at approximately 7500 seconds. In order to hold the desired values of utilization and arc voltage it was necessary periodically to adjust the cathode power.

The first cathode was changed at 68.8 hours because of poisoning when the cold traps were allowed to warm up. The second cathode, fabricated from the same stock as the first, was used for the next 334 hours.

After termination of the test the engine was removed from the test facility, photographed and examined. The cathode surface was analyzed spectrographically and the cathode cross section was examined by means of photomicrophotography. The extraction electrodes were weighed to determine the amount of erosion.

The engine was examined to determine the nature of the materials deposited onto the various regions. The principal deposits were found to be aluminum, tantalum, and nickel; the aluminum coming from the target, the tantalum from the extraction electrode, and the nickel from the cathode. Figure 4.6-1 shows a sketch of the ET-1 engine cross section showing the principal deposits at the various positions. The arrows show the possible sources of the deposits.

The results of the spectrographic chemical analysis of the cathode surface are given in Table 3.4-1. Of interest is the presence of a large amount of tantalum which may result in plugging the pores of the nickel matrix thus reducing the oxide migration rate to the surface.

Photomicrographs of the cathode cross section are shown in Figures 3.4-1, 3.4-2, 3.4-3 and 3.4-4, and a discussion of them appears in Section 3.4.

Table 4.6-2

Typical Performance Parameters During Extended Test ET-1

Date	9/17/64	9/24/64	10/2/64	10/6/64	10/9/64
Time of Day	3:15	10:55	11:10	11:15	13:10
Run Time, hrs.	0.1	81.3	222	317.2	391.2
Chamber Pressure (10^{-6} torr)	4.6	1.0	1.0	1.0	0.6
Cathode Voltage (volts)	7.0	6.8	8.4	10.15	11.9
Cathode Current (amperes)	4.6	4.95	5.6	6.2	6.8
Cathode Power (watts)	32.2	33.7	47.0	62.9	81.0
Cathode Temperature (°C)	-	925	~965	1040	1090
Hg Feed Rate (Equivalent ma)	77.4	75.3	75.8	75.8	75.8
Source Current (ma)	62	61	61	62	61
Propellant Utilization (%)	80.2	81	80.5	81.7	80.5
Arc Voltage (volts)	37.5	30.5	31.0	29.2	30.0
Arc Current (amperes)	0.76	0.79	0.76	0.85	0.74
Arc Power (watts)	28.5	24.1	23.6	24.8	21.2
η_A (ev/ion)	460	395	387	400	347
η_C (ev/ion)	520	552	770	1012	1328
$\eta_A + \eta_C$ (ev/ion)	980	947	1157	1412	1675
Magnet Power	0	0	0	0	0
Accel Voltage (kv)	15.1	14.0	14.7	13.8	14.3
Accel Current (ma)	0.75	0.45	0.7	1.0	0.8
Accel Power (watts)	11.3	6.3	10.3	13.8	11.4
Decel Voltage (kv)	5.75	5.45	5.45	5.62	5.80
Decel Current (ma)	0.30	0.05	0.05	0	0
Decel Power (watts)	1.7	0.2	0.2	0	0
Specific Impulse (sec.)	7590	7390	7390	7500	7610
Beam Power (watts)	350.5	330	328	343	349
Total Power (watts)	424.2	394.3	409.1	444.5	462.6
Power Efficiency (%)	82.7	83.6	80.2	77.2	75.6
Rocket Efficiency (%)	64.0	67.6	64.6	63.0	60.9

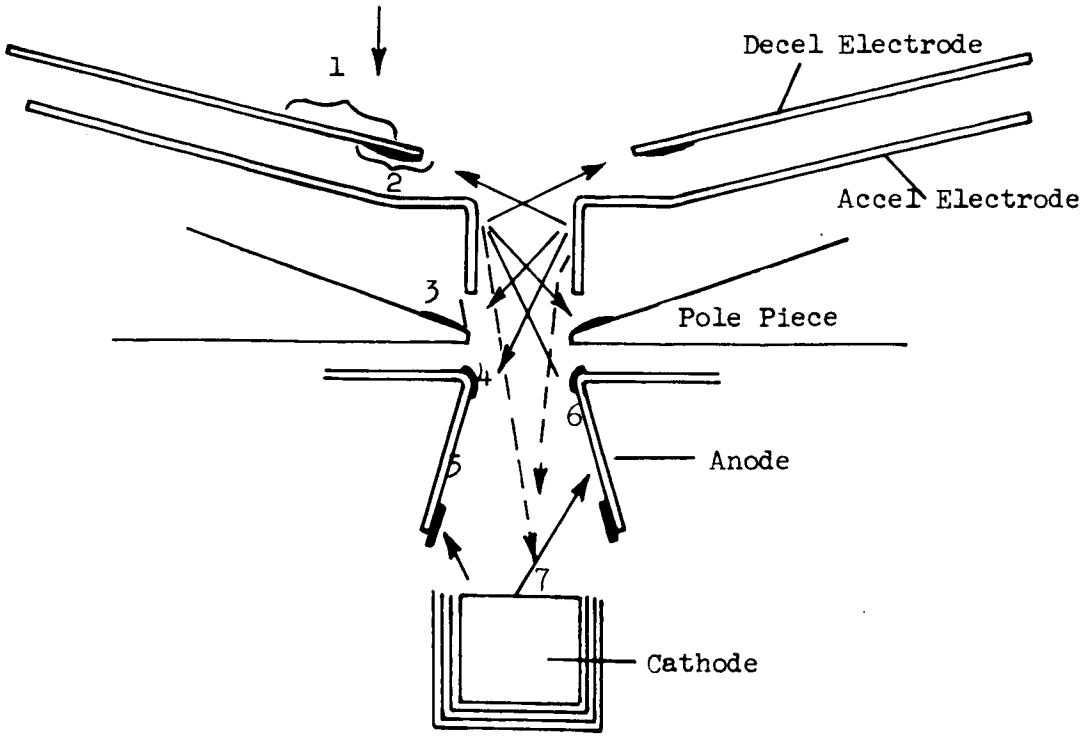

(Arrows show apparent path of material transfer)

Principal Deposit at Each Location:

1. Aluminum
2. Tantalum
3. Aluminum + Tantalum + Nickel
4. Tantalum
5. Nickel
6. Dark Deposit (Cathode is source)
7. Tantalum (Not certain)

Figure 4.6-1

Sketch of the ET-1 Engine Cross Section Showing the Principal Deposits at the Various Positions

Figures 4.6-2 through 4.6-7 are photographs of the ET-1 engine after 402.6 hours of operation. Figure 4.6-2 shows the ET-1 engine mounted in the door of the vacuum chamber. The build up of aluminum on the decel electrode is evident. Note the aluminum deposit on the chamber walls as displayed by the shadow pattern. Figure 4.6-3 shows the engine profile. It is apparent that the accel electrode had been eroded completely through with just its outer edges remaining. However, the extraction system was functioning well before shut-down. Thus, it is evident that the leading edge of the extraction electrode was primarily responsible for extracting a focused beam and the remaining surface area had little influence. The build up of material on the magnetic pole piece is evident. It was this build up which terminated the test. Figure 4.6-4 shows the underside of the extraction system showing again how the accel electrode was eroded through. After eroding through the electrode surface the charge exchange ions began sputtering the underside of the electrode. This is discernible in the figure. Figure 4.6-5 is the top side of the extraction system showing the aluminum build up on the decel electrode surface and also showing the decel electrode erosion. It is suspected that the erosion pattern of the decel electrode is related to be beam profile. Figure 4.6-6 is a view of the source looking down into the ionization chamber. The material build up on the magnetic pole piece is shown, a crack in the pole piece is evident (this was present at the start of the test), and at the bottom of the ionization chamber is the cathode having a marbled appearance.

Weighing of the acceleration electrode before and after the ET-1 extended test yielded a measured weight loss of 2.732 grams. Combining this value with the time integrated accel electrode current of 0.337 ampere hours yields a measured erosion rate of 8.11 grams per amp-hour. The lifetime of an extraction system is determined by the number of ampere hours required to erode away a critical amount of electrode material. This amount will be assumed to be that contained in two parallelapipeds of dimension 0.2 x 0.2 x 5 cubic centimeters, one parallelpiped located in each accel electrode. For tantalum electrodes this corresponds to a total weight loss of 6.62 grams. For this allowed weight loss the predicted accel electrode lifetime as a function accel interception current becomes

$$T = 815/I_{Acc} \qquad (4.6\text{-}1)$$

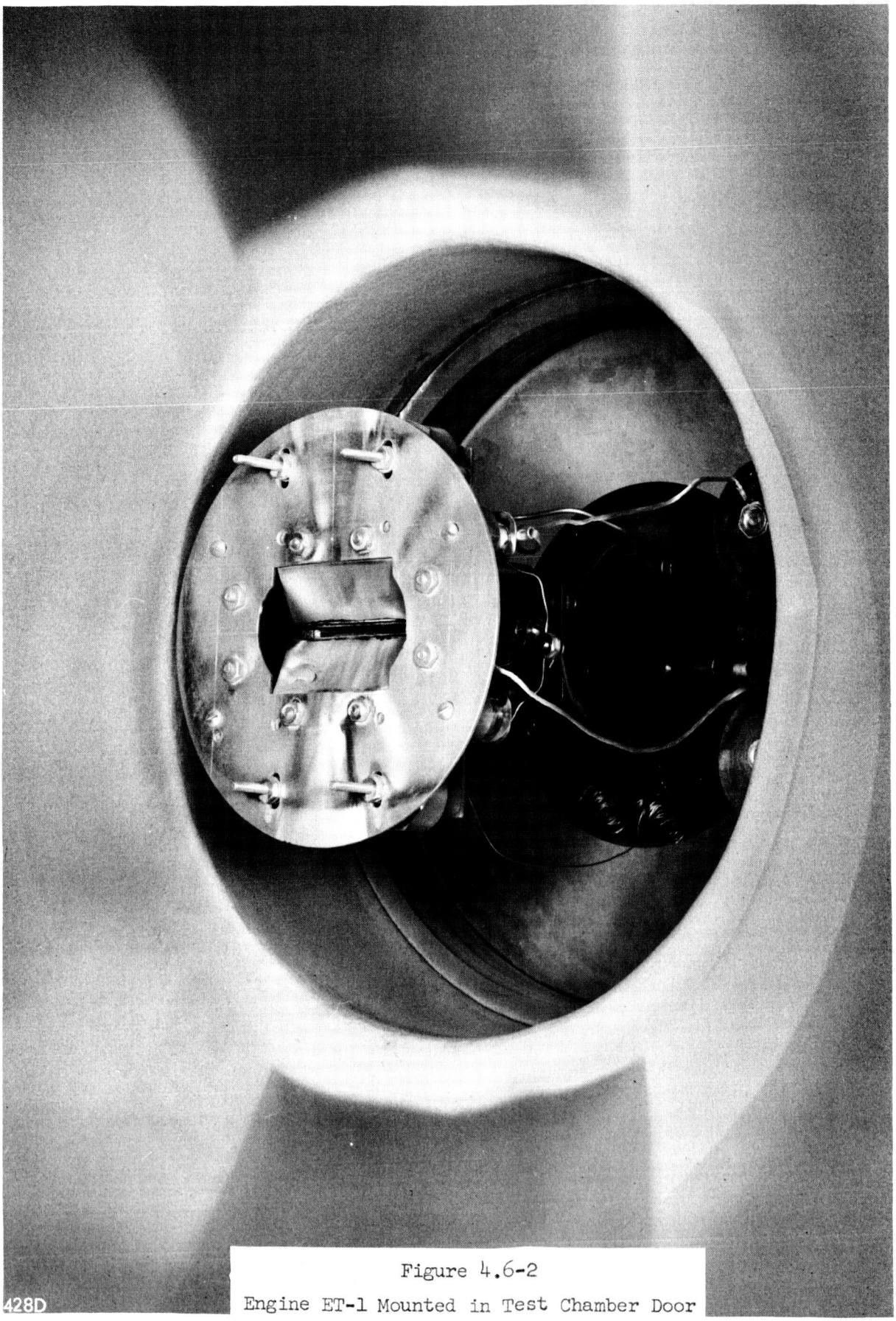

Figure 4.6-2

Engine ET-1 Mounted in Test Chamber Door

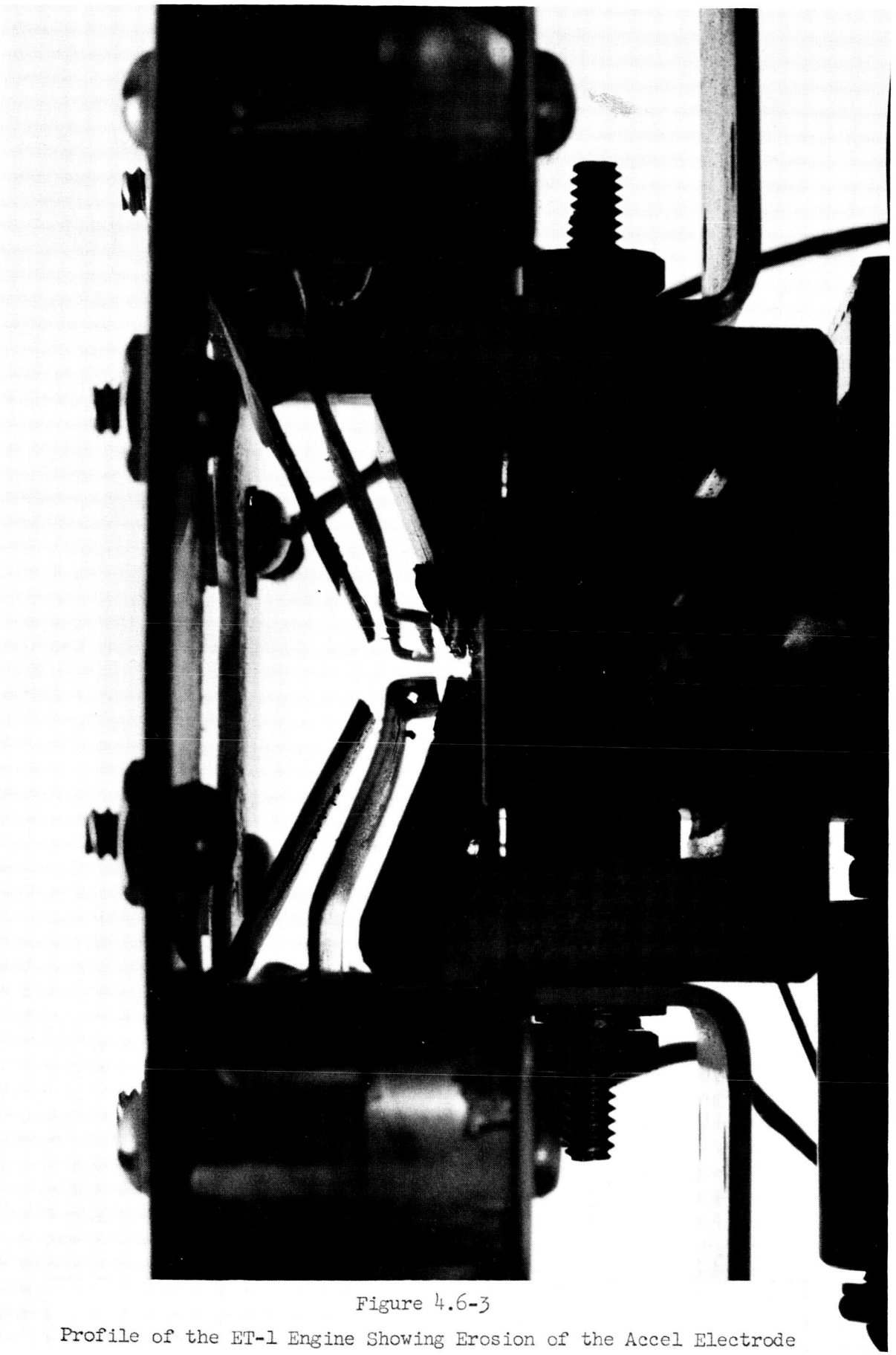

Figure 4.6-3

Profile of the ET-1 Engine Showing Erosion of the Accel Electrode

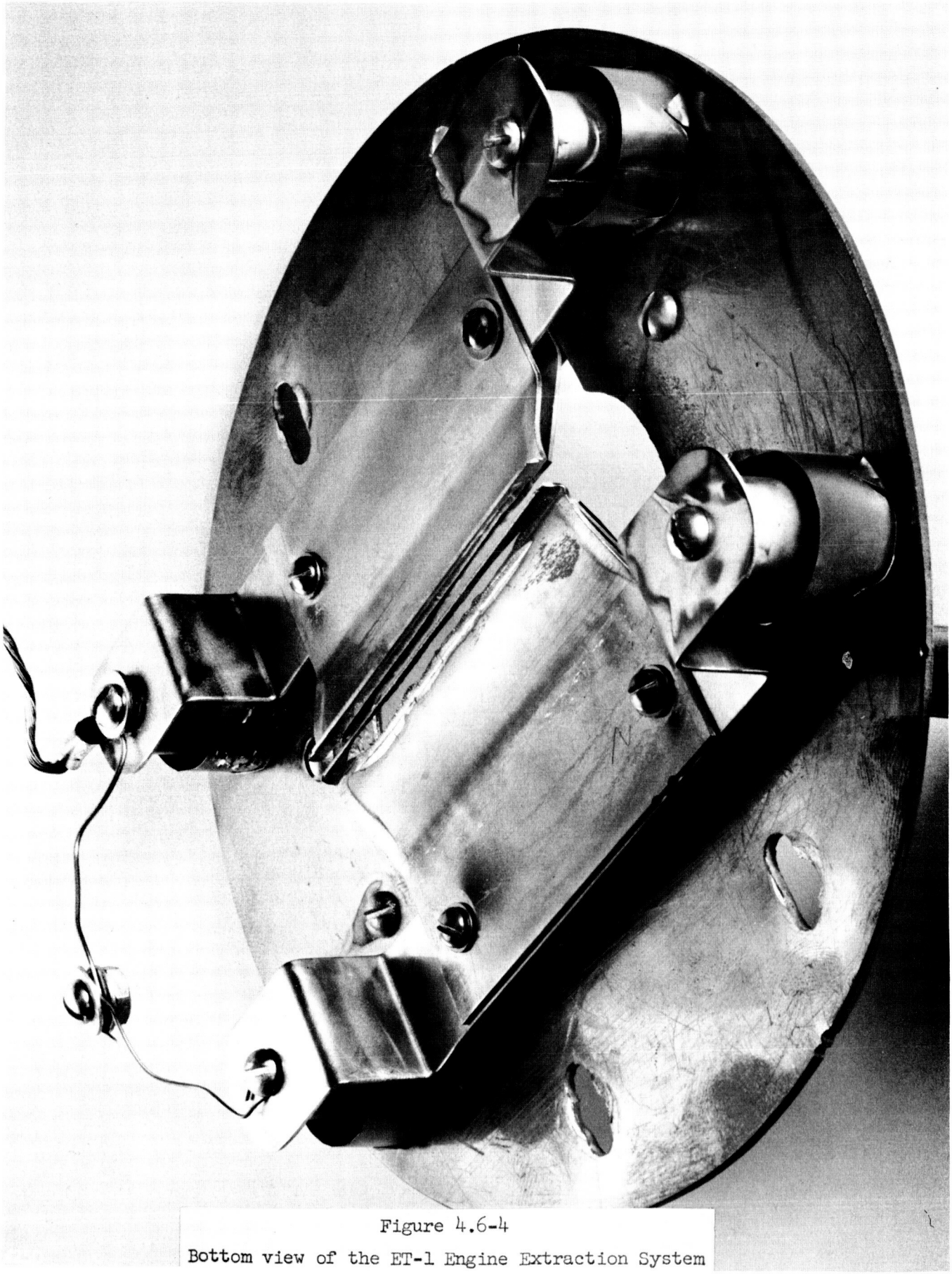

Figure 4.6-4

Bottom view of the ET-1 Engine Extraction System

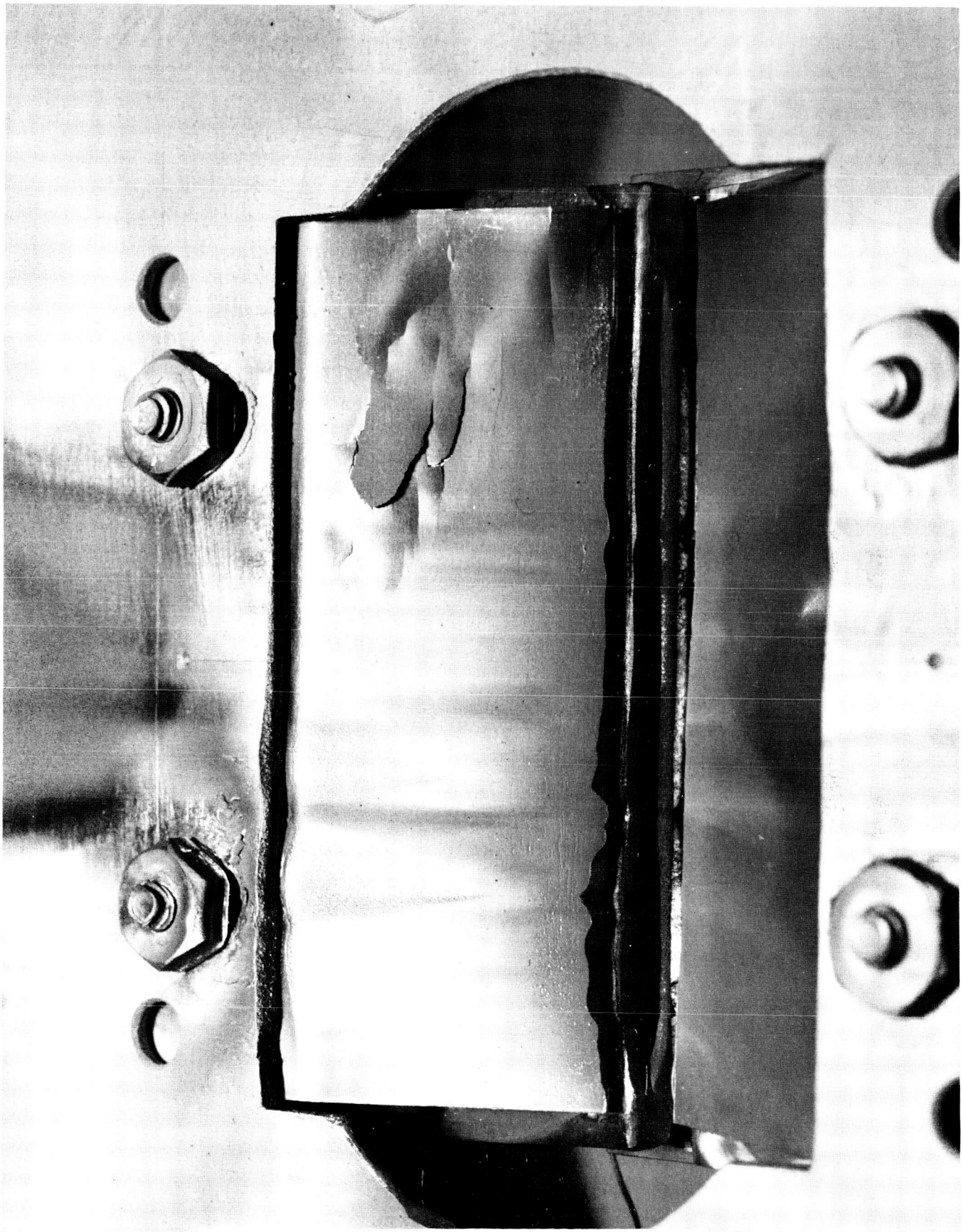

Figure 4.6-5

Top View of the ET-1 Engine Extraction System

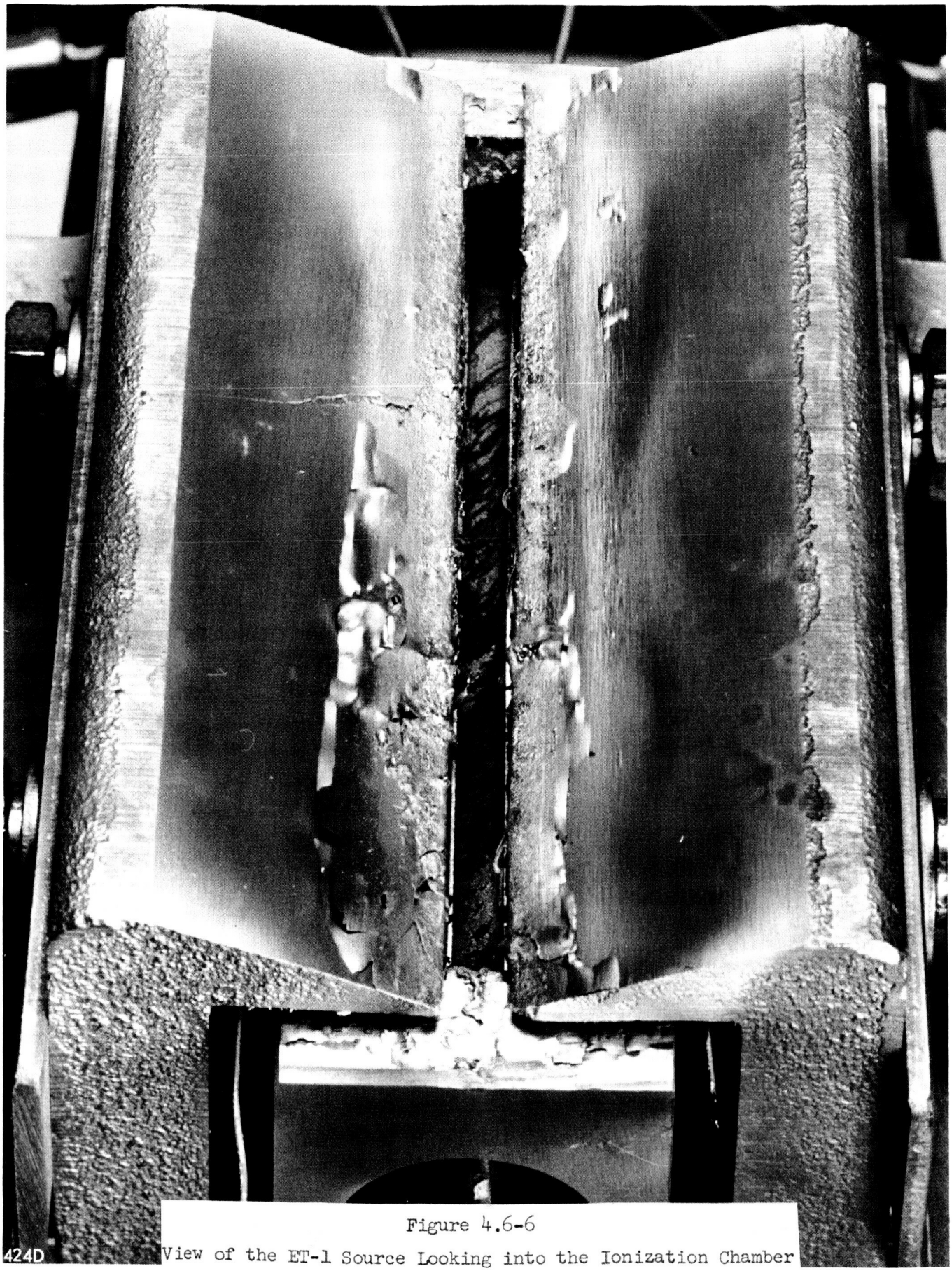

Figure 4.6-6
View of the ET-1 Source Looking into the Ionization Chamber

where T is the lifetime in hours and I_{Acc} is the accel electrode current expressed in milliamperes.

Using the ET-1 test representative values; I_T = 60 ma, η_M = 0.796, and I_{Acc} = 0.84; permits the evaluation of the constant in the relationship between accel interception, propellant utilization, and target current yielding the expression:

$$I_{Acc} = (8.98 \times 10^{-4}) \left(\frac{1 - \eta_M}{\eta_M} \right) I_T^{-2} . \qquad (4.6\text{-}2)$$

Combining Equations (4.6-1) and (4.6-2) yields

$$T = 906 \times 10^3 \left(\frac{\eta_M}{1 - \eta_M} \right) \frac{1}{I_T^2} \qquad (4.6\text{-}3)$$

representing the extraction system lifetime in terms of the propellant utilization and the beam current.

A second extended test ET-2 was initiated making use of the ET-2 engine. For this test the utilization was held at approximately 90 per cent, the arc voltage at approximately 36 volts, and the specific impulse at approximately 9000 seconds. Throughout this test very frequent extraction system shorting was encountered. The cause of the shorting was found to be due to the build up and subsequent flaking off of aluminum deposited onto an annular plate attached to the beam entrance end of the target. The size of the annulus was such that the engine passed through it and extended approximately one inch inside the inclosed region. As the aluminum flakes dropped off they fell onto the extraction system. Because of the highly frequent occurrence of the shorting, it was decided after 100 hours of intermittent operation to open the vacuum system to eliminate the cause of the trouble. By appropriately shielding the engine from the dropping aluminum flakes it was possible to resume testing. At this time, however, vacuum system difficulties were encountered. Before remedial action could be taken the period of work performance expired.

The typical performance parameters obtained during the ET-2 extended test are given in Table 4.6-3.

Table 4.6-3

Typical Performance Parameters During Extended Test ET-2

Date	10/20/64	10/26/64	10/29/64
Time of Day	9:15	16:45	14:35
Run Time, hrs.	0	49.4	93.8
Chamber Pressure (10^{-6} torr)	20	5.0	2.7
Cathode Voltage (volts)	6.0	7.2	7.4
Cathode Current (amperes)	4.4	5.0	5.0
Cathode Power (watts)	26.4	36.0	37.0
Cathode Temperature (°C)	915	965	985
Mercury Feed Rate (Equiv. ma.)	74.7	75.6	75.6
Source Current (ma)	67	67	66
Propellant Utilization (%)	89.5	88.5	87.2
Arc Voltage (volts)	36.8	36	35
Arc Current (amperes)	0.72	0.82	0.73
Arc Power (watts)	36.8	29.5	25.6
η_A (ev/ion)	559	440	387
η_C (ev/ion)	394	536	561
$\eta_A + \eta_C$ (ev/ion)	953	976	948
Magnet Power	0	0	0
Accel Voltage (kv)	13.9	12.8	13.6
Accel Current (ma)	0.7	0.40	0.40
Accel Power (watts)	9.7	5.1	5.5
Decel Voltage (kv)	8.0	8.2	8.1
Decel Current (ma)	0.2	0.28	0.10
Decel Power (watts)	1.6	2.2	0.8
Specific Impulse (sec.)	8950	9050	9000
Beam Power (watts)	529	544	530
Total Power (watts)	603.5	615.8	598.9
Power Efficiency (%)	87.6	88.3	88.3
Rocket Efficiency (%)	78.5	78.1	77.0

Measurement of the accel electrode weight loss yielded a loss of 0.689 grams for an integrated incident current of 0.0621 ampere-hours. The erosion rate, therefore, becomes 11.1 grams per ampere-hour. Using the previously assumed critical mass of 6.62 grams for tantalum electrodes yields the relationship

$$T = 597/I_{Acc} \quad . \tag{4.6-4}$$

Using the ET-2 test representative values, I_T = 67 ma, η_M = 88.5, I_{Acc} = 0.40 ma, yields the relationship

$$I_{Acc} = 6.86 \times 10^{-4} \left(\frac{1 - \eta_M}{\eta_M} \right) I_T^{-2} \tag{4.6-5}$$

Combining Equations (4.6-4) and (4.6-5) yields

$$T = 870 \times 10^3 \left(\frac{\eta_M}{1 - \eta_M} \right) \frac{1}{I_T^2} \tag{4.6-6}$$

which compares favorably with Equation (4.6-3).

4.7 Results and Conclusions

The combined results of the extended tests ET-1 and ET-2 may be expressed in the equation form:

$$T = (766 \pm 64)/I_{Acc} \tag{4.7-1}$$

and

$$T \times 10^{-3} = (898 \pm 10) \left[\eta_M/(1 - \eta_M) \right] I_T^{-2} \tag{4.7-2}$$

where the values of the constants are the weighted mean values, the weighting factors being the time duration of each test, and the indicated uncertainties are the standard deviations of the weighted mean values. Thus, there is a 68 per cent chance that the extraction system lifetime predicted by the above equations falls within the range indicated.

The conclusions, therefore, that can be drawn from the results of this work are that at a beam current of 60 ma, an extraction system lifetime of (1120 ± 13)

hours can be predicted for a propellant utilization of 80 per cent, at 90 per cent utilization the predicted lifetime is (2520 ± 28) hours, and at 95 per cent utilization the predicted lifetime is (5220 ± 59) hours. These lifetime predictions are for the extraction system only.

The lifetime determining mechanism of the cathode is somewhat uncertain. The experimental result is that this cathode suffered performance degradation during 334 hours of operation in extended test ET-1. It is not known, however, whether the degradation was due to increasing thermal shorting, sputtering because of the 30 volt arc potential difference, or deposition of tantalum onto the cathode surface. Because of this uncertainty, no definite conclusion can be made concerning a cathode lifetime prediction.

5.0 SUMMARY AND CONCLUSIONS

The goals of the program were to develop an ion engine of high performance and to determine the durability of the developed engine by performing extended testing. The utilization of a variable geometry source early in the program resulted in the development of a high performance ion engine. It was discovered, however, that the conditions for high performance were somewhat inconsistent with the requirements for cathode lifetime; that is, the arc voltage necessary to attain high propellant utilization was in excess of the cathode sputtering threshold. By making a compromise in performance, it was possible to reduce the necessary arc voltage to a level which was believed to have a high probability of permitting at least 500 hours of cathode lifetime. The arc voltage nonetheless was above the sputtering threshold and cathode degradation was observed during the extended testing. Using a permanent magnet engine, the design of which was determined from the results of the variable geometry source testing, extended testing was accomplished and from extraction system erosion measurements a prediction of the extraction system lifetime was made. Based on the results of the extended testing, no prediction of the cathode lifetime could be made.

In order to make the most accurate possible lifetime predictions the results of the present work have been combined with those obtained from previous extended testing. Table 5.0-1 presents the data obtained from four extended tests performed on the TRW engine. Taking the weighted mean of the quantities in the last two rows of Table 5.0-1 (the weighting factors are taken to be the time durations of the individual tests, thus long tests are weighted more than short tests) yields the following two expressions for the extraction system lifetime prediction in terms of accel interception current and in terms of total beam current and propellant utilization:

$$T = (787 \pm 45)/I_{Acc}, \qquad (5.0\text{-}1)$$

$$T = (907 \pm 11) \times 10^{3} \left(\frac{\eta_M}{1 - \eta_M} \right) I_T^{-2} . \qquad (5.0\text{-}2)$$

Table 5.0-1

Extended Testing Data

Test	1	2	3	4
Date	1/2/64-1/5/64	1/9/64-1/17/64	9/17/64-10/11/64	10/20/64-11/12/64
Contract No.	NAS3-2522	NAS3-2522	NAS3-5745	NAS3-5745
Time Duration, hrs	70	103	403.9	116
Beam Current (ma)	49	51	60	67
Nominal Power Efficiency (%)	75	75	80	90
Utilization (%)	68	71	79.6	89.2
Specific Impulse (sec)	7750	7400	7400	9000
Integrated Accel Current (amp-hr)	55.3×10^{-3}	100.9×10^{-3}	337×10^{-3}	62.2×10^{-3}
Accel Electrode Weight Loss (gm)	.477	.8104	2.732	.689
Erosion Rate (gm/amp-hr)	8.65	7.43	8.11	11.1
$T\ I_{Acc}$ (ma-hr)	765	890	815	597
$T(1 - \eta_M)\eta_M^{-1} I_T^2$ $((ma)^2\ hr)$	930×10^3	945×10^3	906×10^3	870×10^3

The indicated uncertainties are the approximate values of the standard deviation of the mean value.

Equation (5.0-2) is plotted in Figure 5.0-1 which shows the predicted extraction system lifetime as a function of propellant utilization for several values of beam current.

The conclusion that can be drawn from observation of Figure 5.0-1 is that in order to attain extraction system lifetimes in the useful range of 2000 to 10,000 hours for beam currents from 40 ma to 70 ma using the TRW engine of a two inch length, the propellant utilization must exceed 90 per cent. This high utilization, however, generally requires arc voltages in excess of the cathode sputtering threshold. The need for such high arc voltages, therefore, makes it improbable that the cathode lifetime will be as great as the extraction system lifetime. As a result, it is anticipated that the lifetime of the TRW ion engine is limited by the cathode lifetime while extraction system lifetimes from 2000 to 10,000 hours can be attained.

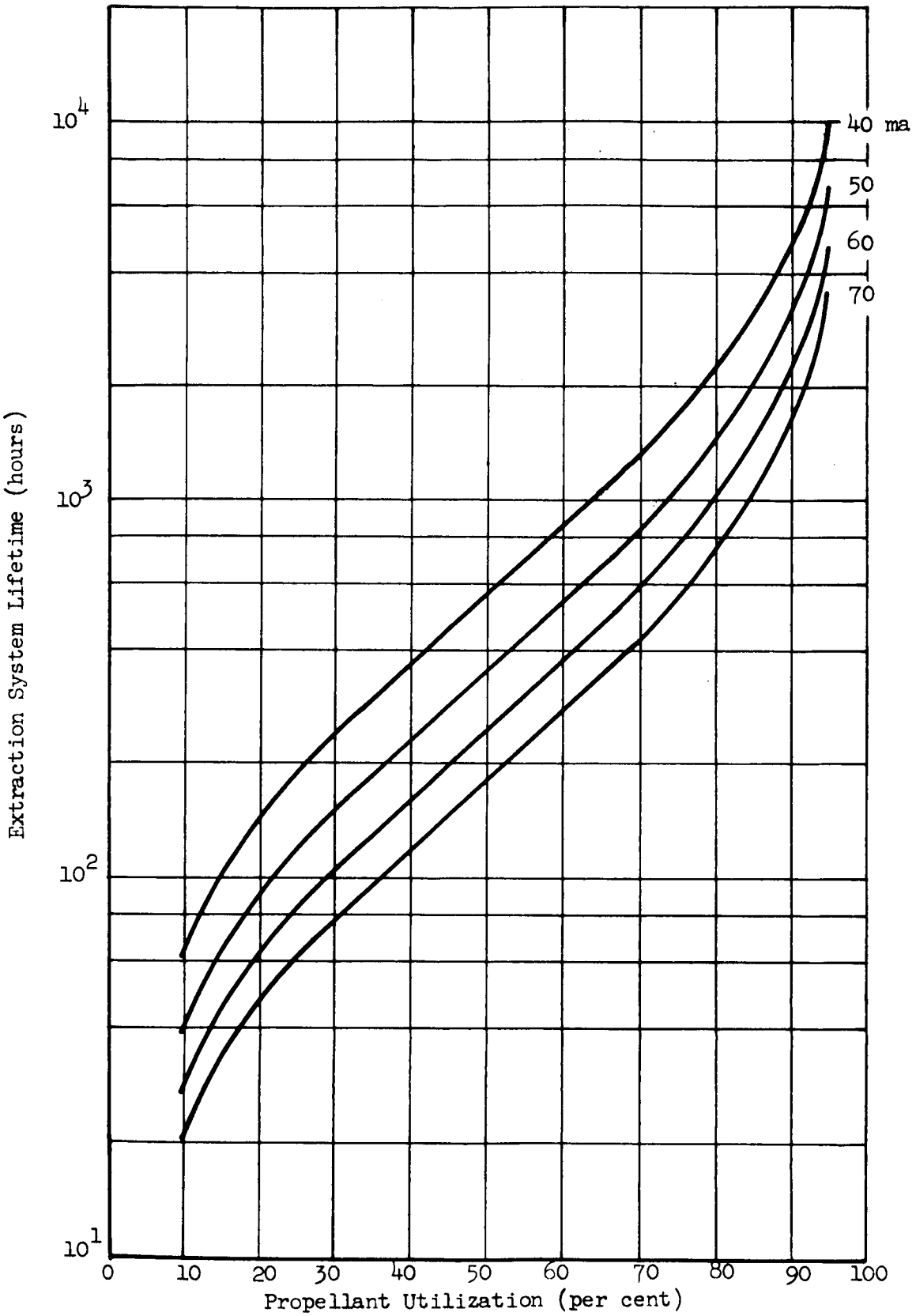

Figure 5.0-1
Predicted Extraction System Lifetime

REFERENCES

1. TRW Ion Engine Staff, "Summary Report on Bombardment Ion Engine Development", (Final Report on Contract NAS8-42), TRW ER-5180, October 1963.

2. Eckert, A. C., et al, "Summary Report on Electron Bombardment Ion Engine Development", (Final Report on Contract NAS3-2522), NASA CR-54082, February 1964.

3. Milder, N. L., "Comparative Measurements of Singly and Doubly Ionized Mercury Produced by Electron-Bombardment Ion Engine", NASA TN-D-1219, July 1962.

4. Hadley, C. P., Rudy, W. G., and Stoeckert, A. J., "A Study of the Molded Nickel Cathode", Journal of Electrochemical Society, 105, 395-398, July 1958.

5. Private communication with Samuel Nablo, May 13, 1964.

APPENDIX A

FAILURE REPORTING AND DATA RECORDING

The project management and reliability functions of the program included provisions for the reporting and analysis of failures and performance degradations which occurred during the extended testing phases. In addition, test specifications and equipment logs were prepared and maintained in a complete, current, and unified data recording system.

Failure Reporting and Analysis. Failure reporting was accomplished with the aid of two separate formats, the "Failure Report" and the "Failure Analysis" (see samples). The former, as the name implies, was used to report any "failures" and malfunctions which occurred during the extended testing phase of the program. The same format, moreover, could be employed to document and report any gradual degradation in performance or anticipated problem area likely to result in a "failure". The next step in the failure reporting process was the completion of the "Failure Analysis". Copies of both formats were supplied to NASA-Lewis as required.

Data Recording. A separate data recording function was maintained for each major testing area (i.e., source studies, cathode tests, extended tests). These records were complete in themselves and included all test specifications and data, test conditions, test facility data, in addition to a complete and current set of all design and fabrication drawings portinent to both the facility and item(s) under test. Thus the "test specifications" and "facility logs" were records associated with the particular test item rather than with any individual investigator. To assure that these records and logs were kept complete and current, all personnel engaged in the program were instructed in the desired manner of data recording (see Data Recording Instructions). These records were reviewed by the TRW project manager at regular intervals to verify their currency and completeness.

FAILURE REPORT

Instructions

This report is to be completed in the event of any failure or malfunction of engine system, engine components, facility (vacuum, power supplies, etc.), feed system, etc. during the course of extended testing. This report will also be prepared if any degradation in performance or potential failure becomes apparent; for example, a gradual long-time rise in arc voltage or decrease in cathode emission shall constitute sufficient cause for the preparation of this report.

The preparation of this report will be the responsibility of the engineer in charge of testing at the time the "failure" occurs. All entries should be complete, so as to facilitate the subsequent failure analysis.

The TRW project manager shall be notified of the failure as soon as possible. He will determine if notification of the NASA project manager is necessary.

Following the completion of this form, a "Failure Analysis" will be made in cooperation with the TRW project manager.

1. Failure Report No. _____
2. Date and Time of Failure _____
3. Test No. _____
4. Purpose of Test _____

_____

_____

5. History and Conditions of Test. Include pertinent temperatures, pressures, voltages, currents, flow rates, etc., and names of test personnel in attendance.

_____

_____

_____

_____

_____

_____

_____

_____

6. Failure Symptoms. Describe system behavior immediately prior to failure. If not a "failure" but rather a "degradation", describe such behavior. _____

_____

_____

_____

Failure Report

(Page 2)

6. Failure Symptoms. (continued) _____

_____

_____

_____

7. Nature of Failure. Describe (in chronological order, if possible) the sequence of events which constituted the "failure". _____

_____

_____

_____

_____

_____

8. Was failure in component, subsystem, facility, other? Describe. _____

_____

_____

_____

9. Was failure attributable to test procedure or human error? _____ Describe in detail. _____

_____

_____

_____

10. Was failure minor, severe? _____ Was failure such as to invalidate or render doubtful previous test results? _____

_____

_____

11. Has failure been noted in test records? _____

12. Did failure result in component or subsystem damage? Describe _____

_____

_____

13. Need component or subsystem be replaced? _____ Redesigned? _____

14. Describe effect of failure on ion engine system performance. (Was failure sufficiently severe to force stoppage of test?) _____

_____

_____

_____

_____

_____

15. Did failure result in damage to test equipment? _____
(Vacuum system, power supplies, instrumentation, other). Describe _____

_____

_____

_____

_____

16. Has equipment been tested to determine extent of additional possible damage?

_____

17. Recommended changes in design. _____

_____

_____

_____

18. General corrective action recommended. _____

_____

_____

_____

_____

_____

Signature _____

Title _____

Date _____

FAILURE ANALYSIS

Failure Analysis No. _____ Date _____

Ref: Failure Report No. _____ Failure Date _____

I. Background Information. (Review circumstances and nature of failure).

_____

_____

_____

_____

_____

_____

_____

_____

_____

_____

II. Severity. (Describe condition of, and extent of damage to, engine system and/or components. Discuss effect of failure on ion engine system performance. Did the failure force testing to stop? Was venting of vacuum system required? Was NASA Project Manager notified? Describe damage, if any, to accessory equipment, facilities, instrumentation). _____

_____

_____

_____

_____

_____

_____

_____

_____

_____

_____

_____

_____

_____

III. Cause. (Determine, to the extent possible, the specific cause of the failure. Indicate the reasoning behind the conclusion reached. If more than one cause is possible, discuss both, giving the logic, and indicate the more likely cause).

IV. Corrective Action. (Describe corrective action recommended. Indicate any recommended changes in system or component design, system or component replacements, or changes in testing procedure. List any desired changes or replacements of accessory equipment, facilities, or instrumentation. Indicate the extent to which corrective action has been initiated. If testing has been resumed, discuss the apparent effect of the corrective action taken).

Failure Analysis

(Page 3)

IV. Corrective Action. (continued) _____

_____

_____

_____

_____

_____

_____

_____

Signature _____
(Test Engineer)

Title _____

Date _____

Signature _____
(TRW Project Manager)

Title _____

Date _____

DATA RECORDING INSTRUCTIONS

I. All data pertinent to testing of a specific nature (i.e., cathode testing, source testing, etc.) will be consolidated from the outset and maintained in a single file for the particular test facility. For example, the source testing progress will be documented in every detail and the records kept in the "Progress File - Source Studies". The purpose of these records will be the assurance that a complete, unified, and current documentation of all work done is available at all times, so that meaningful performance comparisons and analyses may be made.

II. Included in the progress files for the major areas of effort will be the following:

A. A complete, up-to-date set of all design and fabrication drawings pertinent to both the facility and item(s) under test. (Any modifications made subsequent to the initial fabrication shall be so indicated. All drawings and modifications shall be appropriately numbered for easy reference.)

B. A record of all test data. (This record will include data obtained in testing, plus any and all data pertinent to the test facility itself, i.e., pumping characteristics, wiring diagrams, etc.).

C. A record, chronological insofar as practicable, of the testing effort. (This will include such information as the type of work done (testing or fabrication), the names of personnel involved, periodic summaries and conclusions, future plans, etc.).

III. To insure completeness and accuracy under II-B above test data sheets will be utilized. Their exact format will, of course, depend upon the item or property to be tested, but will be sufficiently detailed so as to completely specify the conditions of test. Described on these data sheets will be the test conditions, facilities used, and data obtained (measured and/or calculated). Included also will be an adequate description of the system or component under test, referenced to the appropriate numbered drawing(s) to be found elsewhere in the file.

IV. The chronological record referred to in II-C above will be maintained for the purpose of further documenting the testing of engine components and assemblies. Provided here will be a current record of items tested, the purpose of the tests, test parameters, the reason for test termination, and test personnel. Cross-references to drawings and test data sheets will be provided. Included also will be periodic summaries of test results, conclusions reached, and future plans.

DISTRIBUTION LIST FOR FINAL REPORT

CONTRACT NAS3-5745

National Aeronautics and Space Administration
Lewis Research Center
Spacecraft Technology Procurement Section
21000 Brookpark Road
Cleveland, Ohio 44135
Attention: John H. DeFord

National Aeronautics and Space Administration
Lewis Research Center
Technology Utilization Office
21000 Brookpark Road
Cleveland, Ohio 44135
Attention: John Weber

National Aeronautics and Space Administration
George C. Marshall Space Flight Center
Huntsville, Alabama 35812
Attention: M-RP-DIR/Dr. E. Stuhlinger

National Aeronautics and Space Administration
Lewis Research Center
21000 Brookpark Road — 2 copies
Cleveland, Ohio 44135
Attention: Library

NASA Headquarters
FOB-10B
600 Independence Avenue, S.W. — 2 copies
Washington, D. C. 20546
Attention: RNT/J. Lazar

Commander
Aeronautical Systems Division
Wright-Patterson Air Force Base, Ohio
Attention: AFAPL (APIE)/Lt. Robert Supp

Jet Propulsion Laboratory
4800 Oak Grove Drive
Pasadena, California 91102
Attention: J. J. Paulson

Electro-Optical Systems, Inc.
125 North Vinedo Avenue
Pasadena, California 91102
Attention: R. C. Speiser

General Electric Company
Flight Propulsion Lab.
Cincinnati, Ohio 45215
Attention: M. L. Bromberg

Ion Physics Corporation
Burlington, Massachusetts
Attention: Dr. S. V. Nablo

Space Technology Laboratories
8433 Fallbrook Avenue
Canoga Park, California
Attention: Dr. D. Langmuir

North American Aviation, Inc.
12214 Lakewood Avenue
Downey, California
Attention: Technical Information Office
Department 4096-314

Aerojet-General
Nucleonics Division
San Ramon, California
Attention: Mr. J. S. Luce

Hughes Research Laboratories
Malibu Canyon Road
Malibu, California
Attention: Dr. G. R. Brewer

National Aeronautics and Space Administration
Lewis Research Center
Spacecraft Technology Division
21000 Brookpark Road
Cleveland, Ohio 44135
Attention: J. H. Childs

2 copies

National Aeronautics and Space Administration
Lewis Research Center
Spacecraft Technology Division
21000 Brookpark Road
Cleveland, Ohio 44135
Attention: D. L. Lockwood

National Aeronautics and Space Administration
Lewis Research Center
Spacecraft Technology Division
21000 Brookpark Road
Cleveland, Ohio 44135
Attention: R. D. Shattuck

National Aeronautics and Space Administration
Lewis Research Center
Spacecraft Technology Division
21000 Brookpark Road
Cleveland, Ohio 44135
Attention: J. A. Wolters

National Aeronautics and Space Administration
Lewis Research Center
Spacecraft Technology Division
21000 Brookpark Road
Cleveland, Ohio 44135
Attention: S. G. Jones

7 copies

United Aircraft Corporation
Research Department
East Hartford, Connecticut
Attention: Dr. R. G. Meyerand, Jr.

National Aeronautics and Space Administration
Lewis Research Center
Electromagnetic Propulsion Division
21000 Brookpark Road
Cleveland, Ohio 44135
Attention: W. Moeckel

Westinghouse Astronuclear Laboratories
Pittsburgh, Pennsylvania 15234
Attention: Electric Propulsion Laboratory
Mr. W. H. Szymanowski

NASA Scientific and Technical Information Facility
Box 5700
Bethesda, Maryland 20014
Attention: NASA Representative RQT-2448

6 copies

AFWL
WLPC/Capt. C. F. Ellis
Kirtland Air Force Base
New Mexico

National Aeronautics and Space Administration
Lewis Research Center
21000 Brookpark Road
Cleveland, Ohio 44135
Attention: Reports Control Office

Aerospace Corporation
P. O. Box 95085
Los Angeles, California 90045
Attention: Library Technical Documents Group